AD-A032 820 HUGHES RESEARCH LABS MALIBU CALIF F/G 7/4
MOLECULAR BASIS FOR LIQUID CRYSTAL FIELD EFFECTS.(U)
OCT 76 J D MARGERUM F44620-72-C-0075
UNCLASSIFIED AFOSR-TR-76-1181 NL

1 OF 2
AD A032820

MOLECULAR BASIS FOR LIQUID CRYSTAL FIELD EFFECTS

J. David Margerum

Hughes Research Laboratories
3011 Malibu Canyon Road
Malibu, CA 90265

October 1976

Contract F44620-72-C-0075
Final Technical Report
For period 1 May 1972 through 20 June 1976

Prepared For
DIRECTORATE OF CHEMICAL SCIENCES
AIR FORCE OFFICE OF SCIENTIFIC RESEARCH
Bolling Air Force Base, Washington DC 20332

AIR FORCE OFFICE OF SCIENTIFIC RESEARCH (AFSC)
NOTICE OF TRANSMITTAL TO DDC
This technical report has been reviewed and is approved for public release IAW AFR 190-12 (7b).
Distribution is unlimited.
A. D. BLOSE
Technical Information Officer

UNCLASSIFIED

SECURITY CLASSIFICATION OF THIS PAGE (When Data Entered)

(19) REPORT DOCUMENTATION PAGE	READ INSTRUCTIONS BEFORE COMPLETING FORM
(18) 1. REPORT NUMBER AFOSR-TR-76-1181 2. GOVT ACCESSION NO.	3. RECIPIENT'S CATALOG NUMBER
4. TITLE (and Subtitle) (6) MOLECULAR BASIS FOR LIQUID CRYSTAL FIELD EFFECTS.	5. TYPE OF REPORT & PERIOD COVERED 1 May 72 - 30 June 76 Final
	6. PERFORMING ORG. REPORT NUMBER
7. AUTHOR(s) (10) J. David Margerum	8. CONTRACT OR GRANT NUMBER(s) (15) F44620-72-C-0075
9. PERFORMING ORGANIZATION NAME AND ADDRESS Hughes Research Laboratories 3011 Malibu Canyon Road Malibu, California 90265	10. PROGRAM ELEMENT, PROJECT, TASK AREA & WORK UNIT NUMBERS (16) 9536-01 61102F, 681303 (17)
11. CONTROLLING OFFICE NAME AND ADDRESS AF Office of Scientific Research/NC Bolling AFB, Bldg. 410 Washington, DC 20332	12. REPORT DATE (11) Oct 76 13. NUMBER OF PAGES 140
14. MONITORING AGENCY NAME & ADDRESS(if different from Controlling Office) (12) 137 p.	15. SECURITY CLASS. (of this report) Unclassified
	15a. DECLASSIFICATION DOWNGRADING SCHEDULE

16. DISTRIBUTION STATEMENT (of this Report)

Approved for public release; distribution unlimited.

(9) Final rept. 1 May 72-30 Jun 76,

17. DISTRIBUTION STATEMENT (of the abstract entered in Block 20, if different from Report)

18. SUPPLEMENTARY NOTES

19. KEY WORDS (Continue on reverse side if necessary and identify by block number)

Nematic Liquid Crystals	Dynamic Scattering Mode
Phenyl Benzoate Structures	Surface Alignment Effects
Conductivity Dopants	Conductivity Anisotropy
Electro-Optical Applications	Redox and Salt Dopants

20. ABSTRACT (Continue on reverse side if necessary and identify by block number)

The relationships between the molecular structure of liquid crystal (LC) components and dopants are studied in regard to the dynamic scattering (DS) electro-optical effects of nematic liquid crystals. Redox dopants which undergo electrochemically reversible reactions at lower potentials than the irreversible reactions of LC's are used to improve the dc-DS performance and stability. Two years of continuous dc-DS at 20 V is achieved by using such redox dopants in phenyl benzoate LC's. These

next page

DD FORM 1 JAN 73 1473 EDITION OF 1 NOV 65 IS OBSOLETE

UNCLASSIFIED

SECURITY CLASSIFICATION OF THIS PAGE (When Data Entered)

172 600

cont

redox dopants also give the LC lower threshold voltages (V_{th}) and higher scattering levels for dc-DS than are obtained with organic salt dopants. The mechanism of dc-DS is shown to be basically a unipolar charge injection process with space charge induced flow of LC. With redox dopants the turbulent LC flow that produces light scattering in dc-DS is first localized at the opposite electrode from which the charge injection occurs. Both ac-DS and dc-DS characteristics are highly dependent on the conductivity anisotropy ratio (R_σ) of doped LC's. The R_σ values depend upon the concentration and structure of the conductivity dopant as well as the LC structure. In a given LC, the V_{th} of ac-DS decreases markedly with increasing R_σ for different dopants, in agreement with the Carr-Helfrich theory. The initial surface alignment of the LC in a cell also affects the V_{th} of ac-DS. The V_{th} increases linearly with decreasing values of $\cos\bar{\theta}$, where $\bar{\theta}$ is the average tilt angle of the LC off the cell surfaces. Among the many electro-optical applications of LC's, dynamic scattering is particularly useful for flat panel, TV-rate, matrix displays and for electronically addressed telescope reticles.

TABLE OF CONTENTS

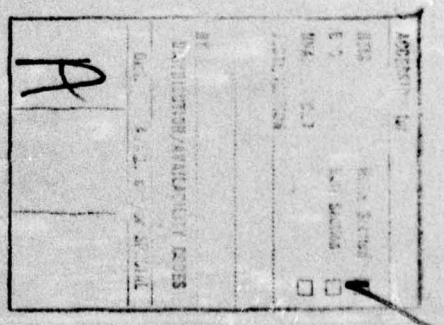

TABLE OF CONTENTS (cont)

LIST OF FIGURES

LIST OF FIGURES (contd)

LIST OF TABLES

SECTION I

INTRODUCTION AND SUMMARY

A. BACKGROUND AND OBJECTIVES

The unique properties of thermotropic liquid crystals have led to the development of many new electro-optical devices, particularly for applications in displays and in optical data processing systems. The applications are based on the resulting advantages of one or more factors made possible by the liquid crystal properties and field effects, including such factors as flat panel cells, low operational voltage, low power consumption, portability, viewability in high ambient light, good resolution capability, rapid response times, image storage, and stability. An application area of particular interest to the Air Force is a flat panel TV rate matrix display that can be viewed in the high ambient lighting conditions of airplane cockpits. This type of system has the potential of replacing many cathode ray displays, by providing better viewability and performance while taking up less space. Another area of great interest is that of real-time optical data processing with photo-activated liquid crystal light valves. These devices can be used to convert non-coherent light into high resolution coherent images at TV rates for very rapid parallel processing of optical information.

The performance of the liquid crystal electro-optical devices is to some extent limited by the properties of the liquid crystal materials and our understanding of their electro-optical behavior. The objective of this program has been to study relationships between the molecular structures of liquid crystal materials (including dopants) and the optical effects induced in them by electrical fields. The goals are to provide a better understanding of the molecular and ionic interactions in liquid crystal electro-optic effects, as an aid in the development of new materials for displays. Because of the Air Force interest in flat panel cockpit displays, most of our research studies have been related to the "dynamic scattering" electro-optical effect that is utilized in pictorial matrix

displays. We have emphasized studies on the structural effects of conductivity dopants on the mechanism of dynamic scattering in phenyl benzoate nematic liquid crystals. This has helped define major improvements in the performance characteristics and the operational lifetime of dynamic scattering displays.

B. SUMMARY OF ACCOMPLISHMENTS

The major accomplishments of this program are presented in the six reprints and preprints which make up the appendices of this report. These results and some other unpublished results are discussed in the next section. The following is a brief summary of these accomplishments:

- Electrochemical studies in solvents showed that while liquid crystals undergo irreversible oxidation and reduction reactions, selected redox dopants undergo reversible electrochemical reactions at much lower potentials. This indicates that, in principle, these redox dopants could be used in liquid crystals to improve the stability of dc dynamic scattering displays.

- Studies of a redox dopant pair in nematic ester liquid crystals showed long-term operational lifetimes (two years of continuous operation at 20 V dc) for dc dynamic scattering in test cells. These dopants are di-n-butylferrocene and (2,4,7-trinitro-9-fluorenylidene)malononitrile. They also improved performance by decreasing the dc threshold for scattering to ~2 V and by giving high scattering levels in the 10 to 20 V range.

- The mechanism of dc dynamic scattering in an ester liquid crystal was shown to depend upon the structure of the dopants. Organic salts, electron donors, electron acceptors, and mixtures of donors and acceptors all showed differences which were observed by microscopic flow patterns in the liquid crystal. These results showed that unipolar charge injection and space charge flow occur with a single redox dopant (donor or acceptor) and that the dynamic scattering turbulence occurs mainly at the opposite electrode from the charge injection reaction.

- The concentration dependence of resistivity in an ester liquid crystal shows that even ionic salt dopants are partially associated. Both the ac and the dc threshold voltages for dynamic scattering are concentration-dependent with salt dopants, but the dc threshold changes only slightly with the concentration of redox dopants.

- The conductivity anisotropy of liquid crystals is shown to be highly dependent on the structure of the conductivity dopants as well as the structure of the liquid crystals to which they are added. The threshold voltage for ac dynamic scattering in a given liquid crystal decreases with increasing values of the conductivity anisotropy ratio ($\sigma_{\parallel}/\sigma_{\perp}$) in general agreement with the Carr-Helfrich theory. The optical density of scattering at 30 V rms is directly proportional to $\sigma_{\parallel}/\sigma_{\perp}$. Thus the dynamic scattering characteristics of a display cell are highly dependent upon the structure and conductivity anisotropy of the dopants.

- The ac dynamic scattering threshold voltage, response times, and turbulent flow patterns are highly dependent on the surface alignment of the liquid crystal. The threshold voltage increases linearly with decreasing values of $\cos\bar{\theta}$, where $\bar{\theta}$ is the average tilt angle of the liquid crystal off the two electrode surfaces of a thin transparent cell. This is not in complete accord with existing theories. The response times are fastest for surface-parallel alignment ($\bar{\theta} = 0°$). The scattering versus voltage curves indicate that surface-parallel alignment is best for gray scale displays with fast response times, while surface-perpendicular alignment ($\bar{\theta} = 90°$) is best for two-level multiplexed displays with slow decay times.

- A review paper was prepared in which the basic properties of liquid crystals are discussed in regard to their electro-optical applications. Many references are given to pertinent literature. Three different types of displays are discussed in more detail as examples of these applications.

C. SUMMARY OF RELATED HUGHES STUDIES

Related research and development on liquid crystal devices for military applications have been carried out at the Hughes Research Laboratories and at several other divisions of Hughes Aircraft Company. The work on flat panel matrix displays and on reticles are closely related to this AFOSR contract because the dynamic scattering mode is used in these liquid crystal devices. The following is a brief summary of the major accomplishments on these other studies:

- Small flat panel TV-rate displays have been made using liquid crystals on a matrix of semiconductor activated reflective electrode elements. Defect-free 10,000 element displays (1" x 1") have been made which show a 15:1 constrast ratio and about seven shades of gray at television rates using

dc dynamic scattering of redox-doped ester liquid crystals. A larger (2" x 2") display was made by combining four of the one-inch modules. Such displays will be suitable for airplane cockpit usage because they are readily viewable in bright light, including direct sunlight. Our tests indicate that long dc operational lifetimes should be feasible in sealed cells. Future materials work should be directed toward the use of cells warmed to about 35° to 40° in order to optimize the liquid crystal resistivity and operational stability.

- An electronic telescope reticle for tank fire control systems was made using a liquid crystal sandwiched between windows with 1000 x 1000 horizontal and vertical transparent electrode lines. This cell provides an electronically selected crosshair by dc activation of dynamic scattering, using redox-doped ester liquid crystals. Liquid crystal reticle systems will provide faster response times, better resolution, and simpler (space-saving) controls than present mechanical systems.

- A variety of photoactivated liquid crystal light valves have been developed for applications such as large screen command and control displays and optical data processing systems. The former include color symbology projection display cells and black and white TV display cells. The latter include cells with laser readout for coherent optical data processing at real-time rates. In each case a weak input light activates the photoconductor layer side of the cell, which in turn transforms the image into a birefringent modulation of the liquid crystal on the reflective side of the cell. High birefringent, low viscosity liquid crystals are required for these devices and in the projection systems they must also have photochemical and surface tilt stability at intense light exposures.

- Improved liquid crystal eutectic mixtures have been formulated by synthesis of new components and application of differential scanning calorimetry analysis data. From these studies a new ester eutectic mixture was developed for dc dynamic scattering and it is being used for the pictorial matrix display and for the electronic reticle device.

SECTION II

RESEARCH PROGRAM*

A. TECHNICAL APPROACH

The general objective of this program has been to establish relationships between the molecular structures of nematic liquid crystal (LC) materials (including dopants) and the optical effects induced in them by electrical fields. The goals have been to provide a better understanding of ionic and molecular interactions in liquid crystal electro-optical effects, as an aid in the development of improved devices. Our main approach has been the study of conductivity dopant structures and the mechanism of dynamic scattering (DS) in nematic liquid crystals. Dynamic scattering involves a combination of surface, field and conduction effects in a LC to produce a turbulent motion which scatters light.[A3] It has been used in many device applications, including photoactivated light valves,[B1,4,5,7] pictorial matrix displays,[B6,9,15,16] and an electronic reticle device.[B12] The matrix displays are of particular interest to the Air Force (AF Avionics Laboratory, Wright-Patterson Air Force Base, Ohio) for uses such as direct view displays and heads-up displays in airplane cockpits.

Since the dynamic scattering matrix displays, which are being developed for the Air Force by the Hughes Aircraft Company, utilize a direct current (dc) activation of the liquid, we have been especially interested in fundamental aspects of dc-DS effects. One related key question was whether or not dopants and LC's can be developed which would provide reasonably long operational lifetimes (e.g., greater than a year) for such displays. Many other research groups had already abandoned the use of dc-DS displays due to rapid deterioration effects. We had some prior evidence that careful selection of dopants could be used to maintain

---

*The footnotes used refer to the bibliography listed in Section V. References to related work of other authors are given in these papers, such as in the six reprints and preprints in the Appendices.

electrochemical reversibility of LC materials in dc-DS cells. Thus, a large part of the present contract effort was devoted to studies of the electrochemical properties of dopants, the mechanism of dc dynamic scattering in doped nematic LC's, and factors related to dc-DS performance and lifetime.[A1,2,6]

Two properties which strongly affect dynamic scattering are anisotropy of charge conduction in nematic LC's, and the type of initial alignment of the LC on the cell surfaces. We carried out studies in each of these areas, using both dc and ac activation of materials. We found that the ac results were more consistent and better suited than dc activation for mechanistic interpretations. Thus we examined the effect of dopant structure on the conductivity anisotropy and ac-DS of two different types of liquid crystals.[A4] We also studied surface alignment effects on ac-DS with two differently doped liquid crystals.[A5] The basic results are generally applicable to dc as well as ac activation, but the dc cells are complicated by charge injection and space charge flow effects. We hope to clarify these differences in the future.

We had also planned other studies regarding molecular structure effects of LC's and dopants on the dielectric anisotropy and viscosity of nematics, but instead most of our work remained focused on the DS factors mentioned above, namely: dc mechanisms, dc stability, conductivity anisotropy, and surface alignment. Nevertheless, these other areas are important and we would like to continue these studies in the future, especially the molecular structure effects on viscosity and viscosity anisotropies of liquid crystals.

B. STRUCTURAL EFFECTS ON ELECTROCHEMICAL PROPERTIES

Many of the early studies of dc-DS reported in the literature appear to be based on the use of slightly impure LC's such as p-azoxyanisole or Schiff Bases. This observation is based on the fact that no mention was made of adding dopants and highly purified samples are not conductive enough to show dynamic scattering. Schiff bases such as N-(p-methoxybenzylidene)-p-butylaniline (MBBA) are easily hydrolyzed to an aldehyde

and an amine, which in turn can be air-oxidized to give ionic species such as carboxylate and anilinium ions. When conductivity dopants were added, ionic salts such as tetrabutylammonium bromide or perchlorate were often used. The dc activation of such LC's resulted in irreversible electrochemical oxidations and reductions of the liquid crystal itself, or of its ionic impurities (e.g., oxidation of carboxylate ions), causing degradation of the LC. In prior work we had used phenyl benzoate LC's (multicomponent, room temperature mixtures) because they were colorless, relatively stable to moisture, and could be prepared with high resistivity. By using cyclic voltammetry and polarographic techniques, we studied[A6] the electrochemical oxidation and reduction potentials of the ester compounds in solvents. They show irreversible anodic and cathodic reactions which occur at about 1.7 V (vs SCE) and -2.2 V, respectively. These compounds are less easily oxidized and reduced than Schiff bases or azoxybenzenes, but as a liquid crystal containing an inert salt dopant (such as tetrabutylammonium perchlorate) the esters as well as other LC's would be expected to decompose since they would probably have to react at the electrodes when a dc field is applied. (Alternatively, there would have to be a mechanism such as electron injection and transport without actual chemical reaction, and there is not strong evidence for such a process.) However, the addition of redox dopants, which readily undergo reversible reduction and oxidation reactions at lower potentials than the LC, can be used to control electrochemical reversibility of the system. Redox dopants such as (2,4,7-trinitro-9-fluorenylidene)malononitrile (TFM) and dibutylferrocene (DBF) show quite low formal reduction potentials (0.03 V for TFM and 0.32 V for DBF) for reversible reactions.[A1,2,6] Such dopants provide the basis for long lifetime dc-DS effects in LC displays.

C. DC DYNAMIC SCATTERING LIFETIMES

Substantial improvements in the dc-DS performance and lifetime were achieved by use of selected redox dopants in ester liquid crystals.[A1] The properties and composition of the ester mixture (designated as HRL-2N10) are shown in Figure 1. Comparisons with different dopants were

HRL–2N10 (ESTER LC)

5412-1

NEMATIC RANGE $\sim 20^{\circ}$ TO 54°; $\Delta\epsilon = -0.12$; $\Delta n = 0.14$

$\rho_{\perp}$ (UNDOPED) $> 10^{11}\ \Omega - cm$

4 – COMPONENT MIXTURE

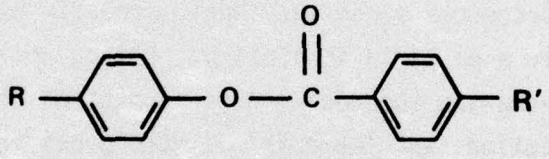

R	R′
C_4H_9	CH_3
C_4H_9O	OC_4H_9
C_4H_9O	OC_6H_{13}
C_4H_9O	OC_8H_{17}

Figure 1. Properties and components of the room temperature ester liquid crystal HRL-2N10. (The components are used in a 15:5:9:9 weight ratio in descending order.)

made of the scattering versus voltage curves and the long-term stability of dc-DS. (Structures and abbreviations for the salt and redox dopants used are shown in Figure 2.) We found that the DBF/TFM redox dopant gives lower threshold voltages and higher scattering levels than salt dopants such as TBAP and TBATMS. This is probably due to the ease of electrochemically generating charge injection with the redox dopants and also to their high conductivity anisotropy. Both of these factors are discussed below. We also showed[A1] that the LC ester with the DBF/TFM dopant system gave dc-DS lifetimes which were one to two orders of magnitude longer than those with the salt dopants. For example, under a continuous applied signal of 20 V dc the test cells with the redox dopants showed good dynamic scattering for about 400 to 800 days without generating serious defects, while the salt dopants showed poorer scattering quality all the time and only lasted about four to 20 days. These tests also showed that the redox-doped LC lasted longer when the unsealed cells were placed in a dry nitrogen atmosphere. Oxygen or moisture (or both) reduce the operational lifetimes, but this should not be a practical problem in display devices since they would normally be sealed anyway. The important result established by this work is the fact that long dc-DS operational lifetimes are in fact feasible by use of redox dopants in ester liquid crystals.

D. CHARGE INJECTION MECHANISM OF DC DYNAMIC SCATTERING

A corollary to the electrochemical reactions and long dc-DS lifetimes of redox-doped LC's is that the mechanism of dc-DS should be controlled by the types of redox dopants which are used. Our studies[A2,6] on the microscopic flow patterns in an ester LC containing various dopants show that redox dopants do indeed control the direction of charge injection and LC flow as we had expected, but also show an unexpected feature in that the scattering tends to be localized near the opposite electrode from where the charge injection occurs.

Salt-doped LC's showed thin flow lines (Williams domains) in each direction across the cells, corresponding to charge injection at each

4028-19 RI

SALT DOPANTS

$[(n\text{-}C_4H_9)_4N]\,ClO_4$ TBAP

$[(n\text{-}C_4H_9)_4N]\,CF_3SO_3$ TBATMS

4028-21

REDOX DOPANTS

4028-20

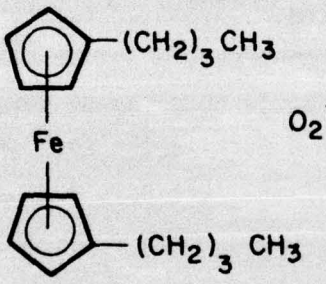

dibuFc

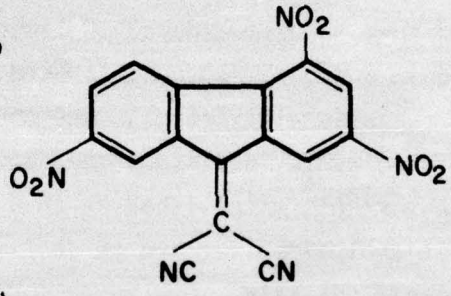

TFM

Figure 2. Dopants used in dc dynamic scattering lifetime studies of the ester liquid crystal HRL-2N10.

electrode and flow to the opposite electrode. If one measures the total scattering from a display cell using unpolarized light, then the threshold for dc-DS corresponds to the threshold for these Williams domains. Redox-doped LC's behave differently. If only a good electron donor such as DBF is used, then the LC flow is predominately from the anode to the cathode, corresponding to unipolar charge injection in which the dominant reactions are Eqs. (1) and (2):

$$\text{Anode:} \quad DBF = DBF^{+} + e^{-} \tag{1}$$

$$\text{Cathode:} \quad DBF + e^{-} = DBF \tag{2}$$

If only a good electron acceptor donor such as TFM is used, then the LC flow is from the cathode to the anode, corresponding to the following [Eqs. (3) and (4)] unipolar injection mechanism:

$$\text{Cathode:} \quad TFM + e^{-} = TFM^{-} \tag{3}$$

$$\text{Anode:} \quad TFM^{-} = TFM + e^{-} \tag{4}$$

The unexpected feature noted is that with a redox dopant turbulent flow patterns (not discrete lines) are formed at relatively low voltages near the opposite electrode from that at which the unipolar injection occurs. For example, charge injection occurs at the anode with DBF, but turbulence first occurs at the cathode. The opposite effect takes place with TFM. When both redox dopants are present, charge injection occurs at each electrode, and there is a mixture of flows and localized turbulence at each electrode. With widely spaced electrodes, Williams domains did not occur with either DBF, or TFM, or a mixture of them as dopants, although LC turbulence occurs at a lower voltage than with the Williams domains

produced by salt dopants such as TBAP or TBATMS. Thus not only do redox dopants control the charge injection and electrochemical processes in a LC, but they also alter the mechanism of the dc-DS that is produced.

E. DOPANT CONCENTRATION EFFECTS

The variation of ac conductivity with the concentration of three different dopants is shown in Figs. 3 and 4. The slopes of these log vs log plots indicate that the dopants are only partially dissociated into ions in this liquid crystal. In general, a simple dissociation equation can be represented by Eq. (5), in which the initial

$$\underset{(c^\circ - x)}{AB} = \underset{(x)}{A^+} + \underset{(x)}{B^-} \tag{5}$$

concentration (c°) of AB dissociates into (x) amounts of A^+ and B^- ions. Then the concentration of the conductive species (x) depends on the equilibrium constant K.

$$K = \frac{(x)^2}{(c^\circ - x)} \tag{6}$$

It follows from Eq. (6) that if K is very large, corresponding to complete dissociation, then $x = c^\circ$ and a plot of log σ vs log c° would have a slope = 1. On the other hand, if K is very small, then $x = \sqrt{Kc^\circ}$ and there would be a slope = 0.5. The slopes in Figs. 3 and 4 are in the 0.6 to 0.7 range, indicating that an appreciable amount of the dopants are dissociated into ions. Actually, the resultant quadratic expression [(Eq. (7)] would give

$$x = \frac{-K + \sqrt{K^2 + 4Kc^\circ}}{2} \tag{7}$$

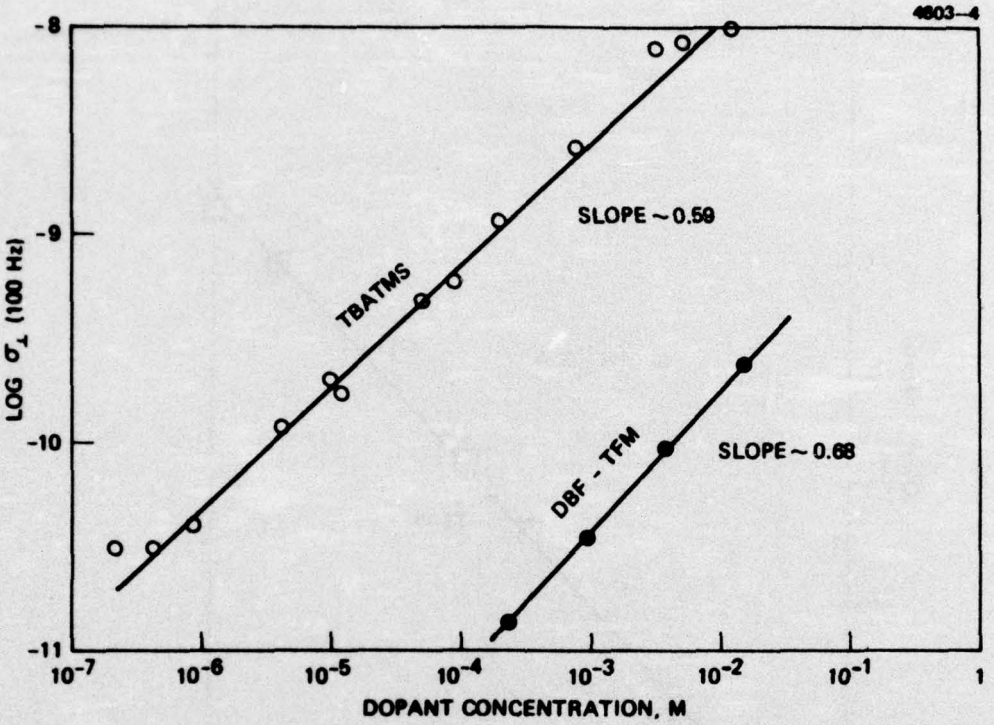

Fig. 3. Conductivity of HRL-2N10 as a function of dopant concentration for TBATMS and TFM-DBF.

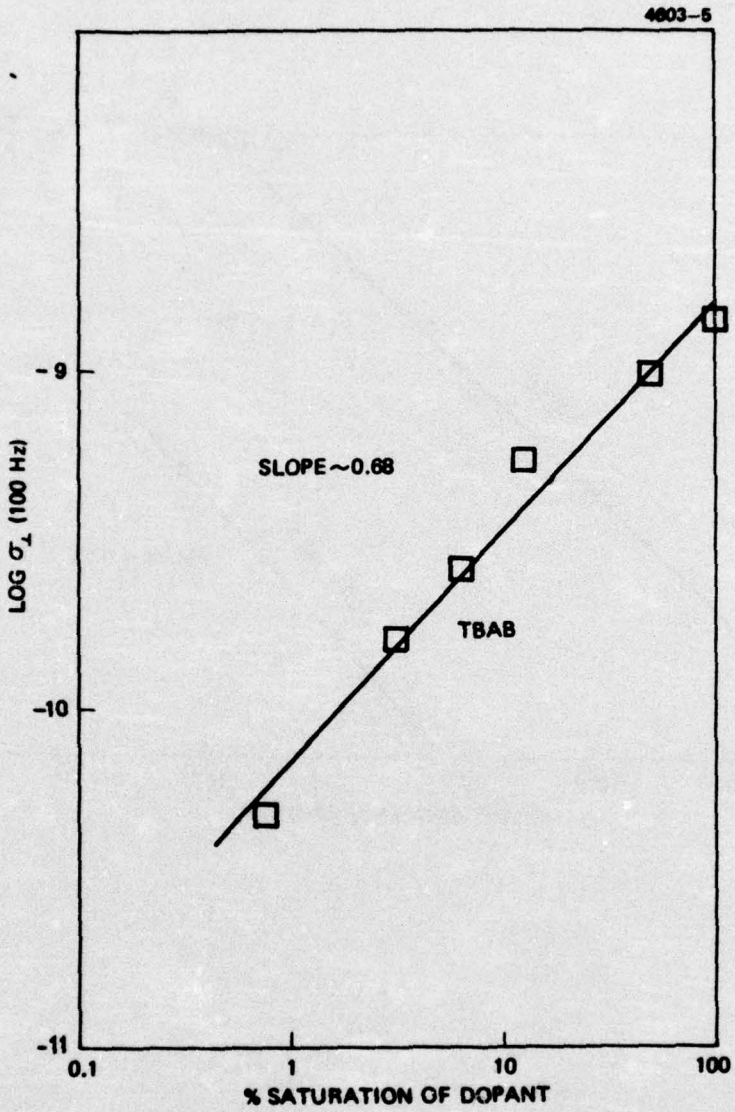

Fig. 4. Conductivity of HRL-2N10 as a function of the relative dopant concentration of TBAB.

only an approximate straight line over a limited portion of the log vs log plot. The slope for the TBATMS dopant in Fig. 3 indicates that a rough estimate for its dissociation constant in this liquid crystal is $K \sim 10^{-5}$. A computer fit of the data to Eq. (7) would give a more accurate estimate of this dissociation constant as well as the dissociation constant for DBF-TFM. As can be noted from Fig. 3, larger concentrations of the redox dopant pair are required than with TBATMS to obtain ac resistivities in the 10^9 to 10^{10} ohm-cm range. Presumably the ions are produced only by dissociation of a donor-acceptor complex, as indicated in Eq. (8).

$$D + A \rightleftarrows (DA) \rightleftarrows D^+ + A^- \qquad (8)$$

In general, the ac-DS behavior of the HRL-2N10 ester LC depends, as expected, upon variations of resistivity due to variations in dopant concentration. Our initial data are shown in Figs. 5, 6 and 7 for 13 μm thick cells with surface-parallel alignment. Figure 5 shows that the critical cut-off frequency decreases in direct proportion to the increase in ac resistivity for all dopants. (BF refers to butylferrocene, and TCNQ refers to 7,7',8,8'-tetracyanoquinodimethane.) An average line is shown in Fig. 5, but on close inspection it can be noted that one could actually correlate the data with two different lines — one for the TBAP and TBATMS salt dopants and another line (at higher frequencies) for the other redox dopants. As described below, this difference between these salt and redox dopants is related to their differences in conductivity anisotropy. Figure 6 shows that in a range of resistivities below the critical frequency the ac-DS threshold voltage (V_{th}) is approximately in direct proportion to the resistivity of the LC. The basis for this relationship is not obvious below $\rho = 10^9$ ohm-cm. Figure 7 shows that the scattering level at 30 V rms (100 Hz) decreases as expected as the resistivity increases toward the value of the critical frequency.

On the other hand, the effects of resistivity on dc-DS are quite different from the ac-DS effects, and also depend much more on the type of dopant that is used. This is indicated by our early data given in

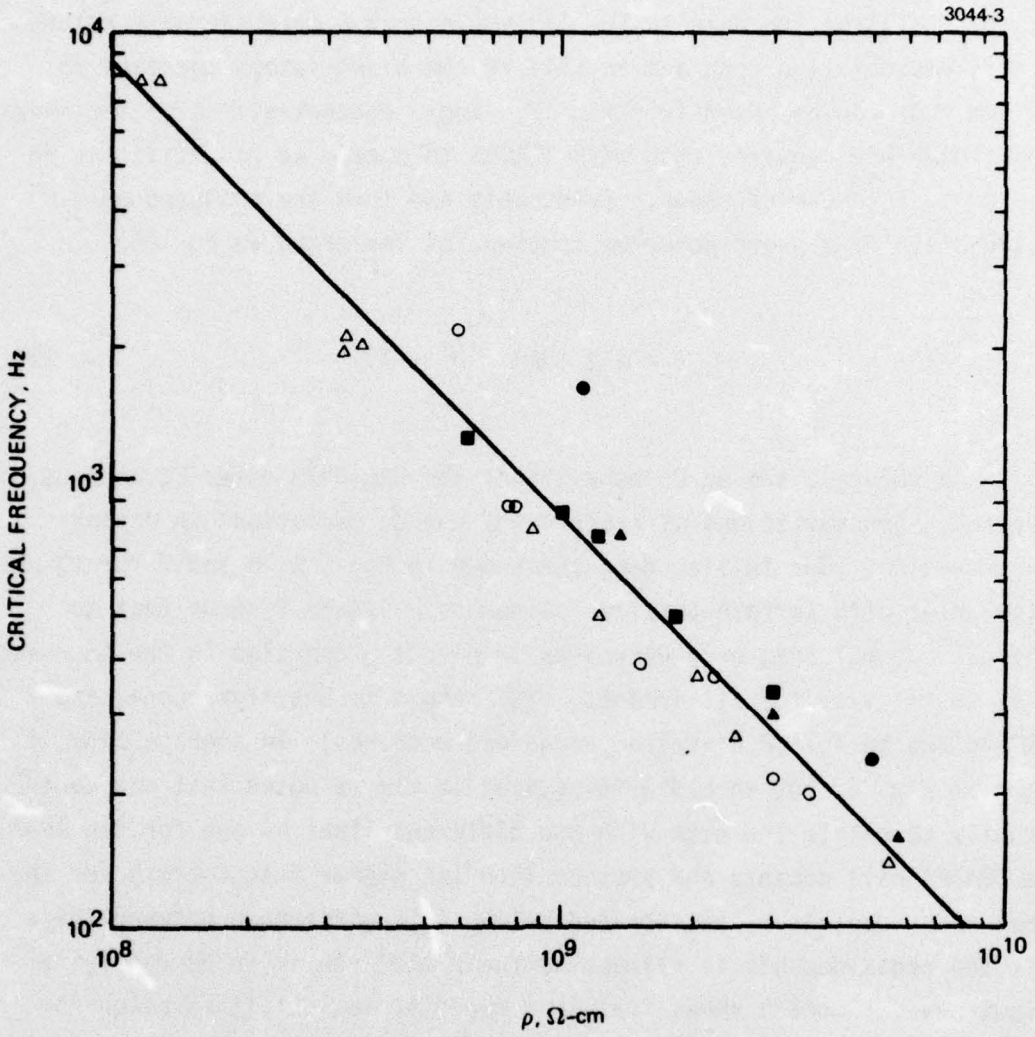

Figure 5. Critical cutoff frequencies for ac-DS as a function of the resistivity of the LC (HRL-2N10).

Dopants:
- ○ TBAP
- △ TBATMS
- ● TFM + DBF
- ▲ TFM + BF
- ■ TCNQ + DBF

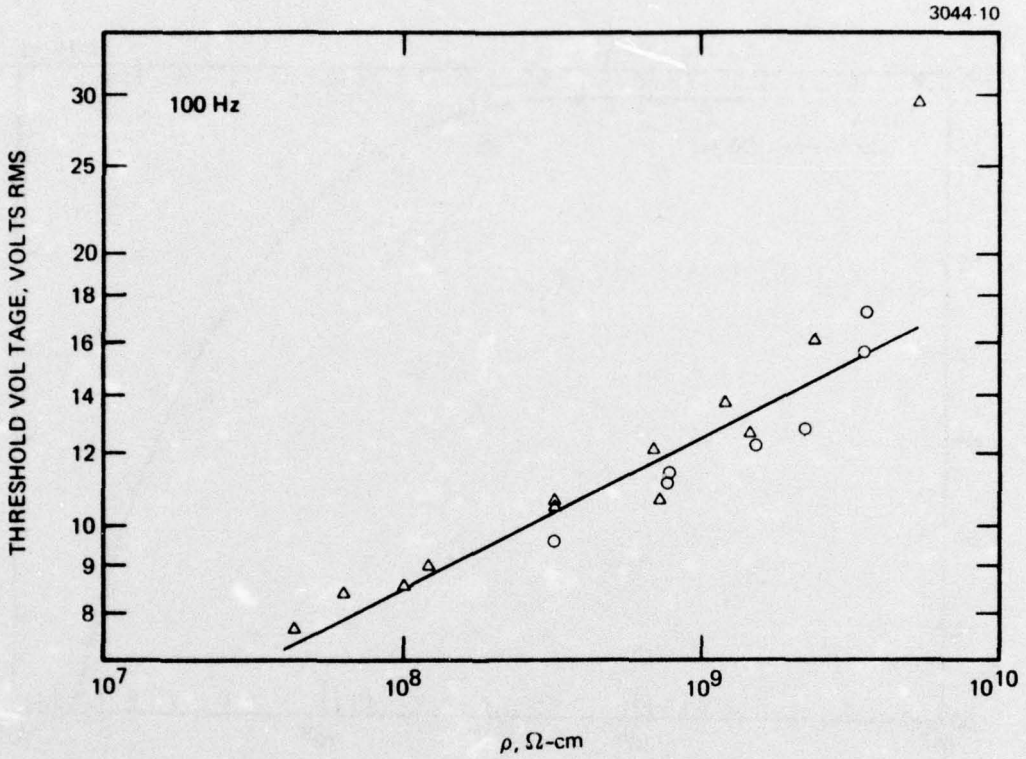

Figure 6. AC-DS threshold voltage (100 Hz) as a function of the resistivity. (LC and dopants as in Figure 5.)

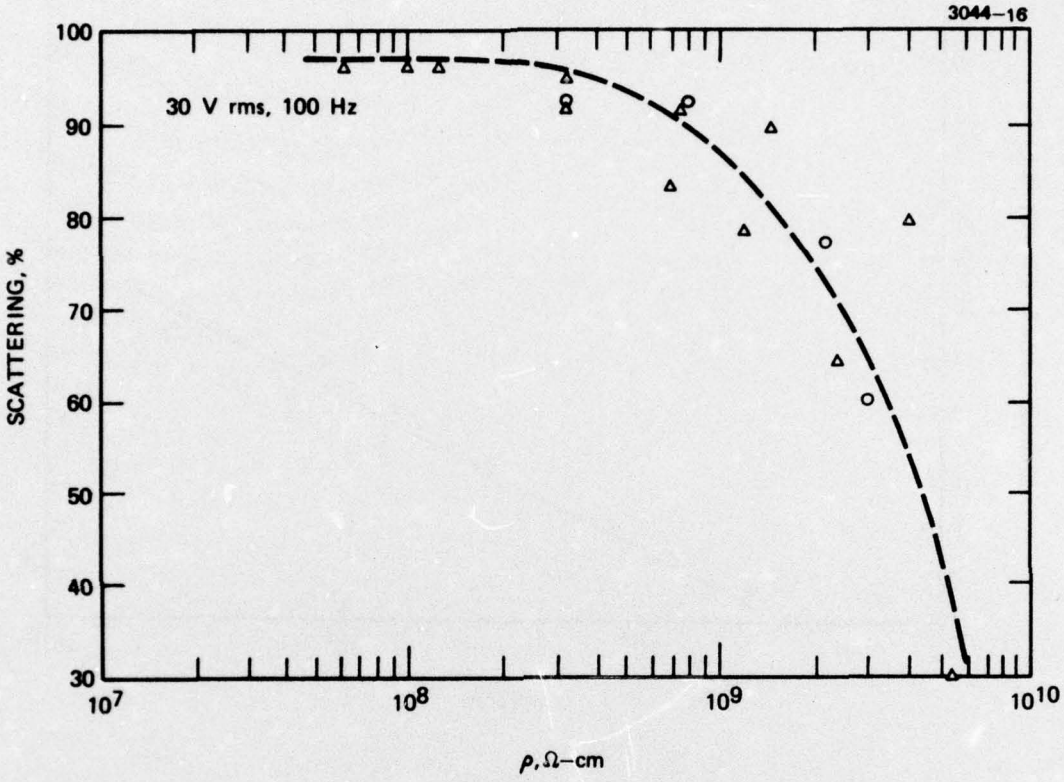

Figure 7. AC Scattering level, as a function of resistivity. (LC and dopants as in Figure 5).

Figs. 8, 9 and 10 for 13 μm thick cells with surface-parallel alignment. While the V_{th} for dc-DS decreases with increased resistivity of the salt-doped LC (Fig. 8), the V_{th} has lower and nearly constant values with resistivity changes for the redox dopants, as shown in Fig. 9. The scattering level at a fixed applied signal of 20 V dc also varies greatly with the type of dopant and its concentration, as indicated by the data in Fig. 10. The redox dopants show much higher scattering levels, which are constant with ρ; while the scattering level of the salt dopants decreases at lower ρ values, corresponding to the increase of V_{th} in the same region.

These initial results on the effects of dopant structure and concentration on the resistivity and on the dynamic scattering behavior led us to more detailed studies on the conductivity anisotropy effects with these various dopants, as discussed below.

F. CONDUCTIVITY ANISOTROPY

We began studies on the measurements of both ac and dc values of conductivity anisotropy and on their correlations with ac and dc dynamic scattering. We found that we could not obtain reproducible results for dc conductivity anisotropies due to space charge effects. By careful handling of doped LC samples we were able to obtain reliable values of the ac conductivity anisotropy ratio $R_\sigma = \sigma_\parallel/\sigma_\perp$, where $\sigma_\parallel$ is the conductivity parallel to the LC director and $\sigma_\perp$ is the conductivity perpendicular to the LC director. (The apparatus is described below in Section II-J.) We made R_σ measurements in our ester liquid crystal (HRL-2N10) and in MBBA for a number of different dopants as a function of their concentration. These results[A4] clearly show that R_σ is highly dependent upon the conductivity dopant structure and concentration as well as the LC composition. (This is in contrast to much of the earlier literature where it was tacitly assumed that R_σ is a physical constant of just the LC structure.) We found a surprisingly large effect of concentration on R_σ, and have suggested that multiple ion associations occur at higher concentrations. Contrary to other literature reports, we found no clear

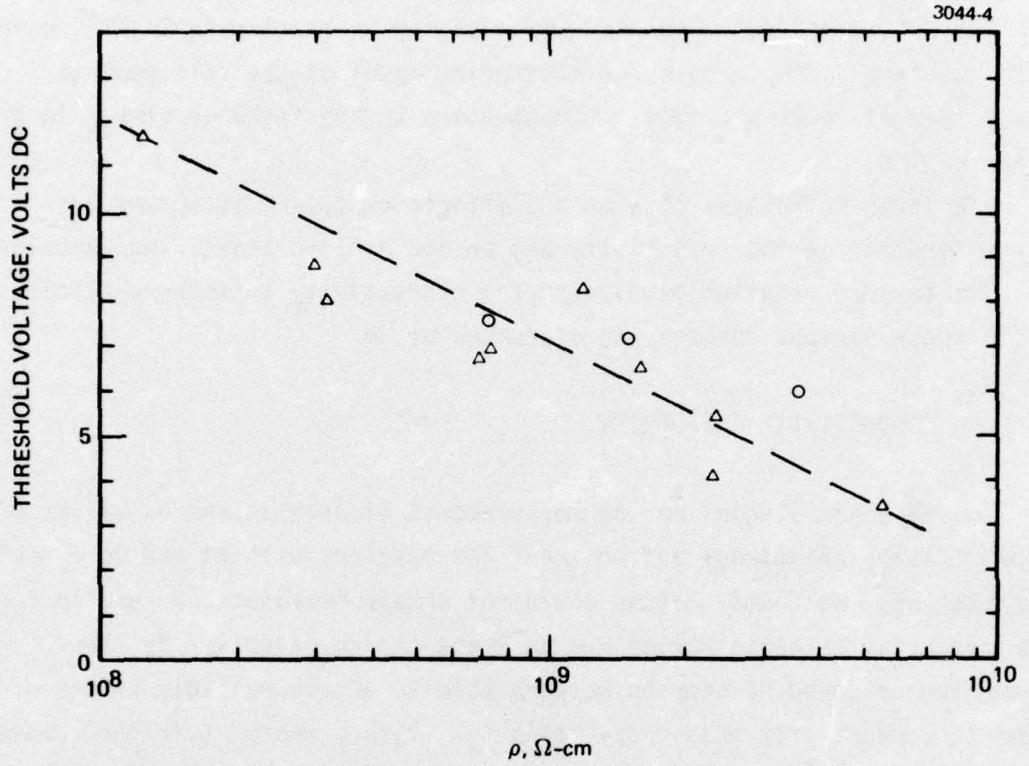

Figure 8. DC-DS threshold voltage as a function of resistivity with salt-type dopants in HRL-2N10.

Dopants: o TBAP, Δ TBATMS

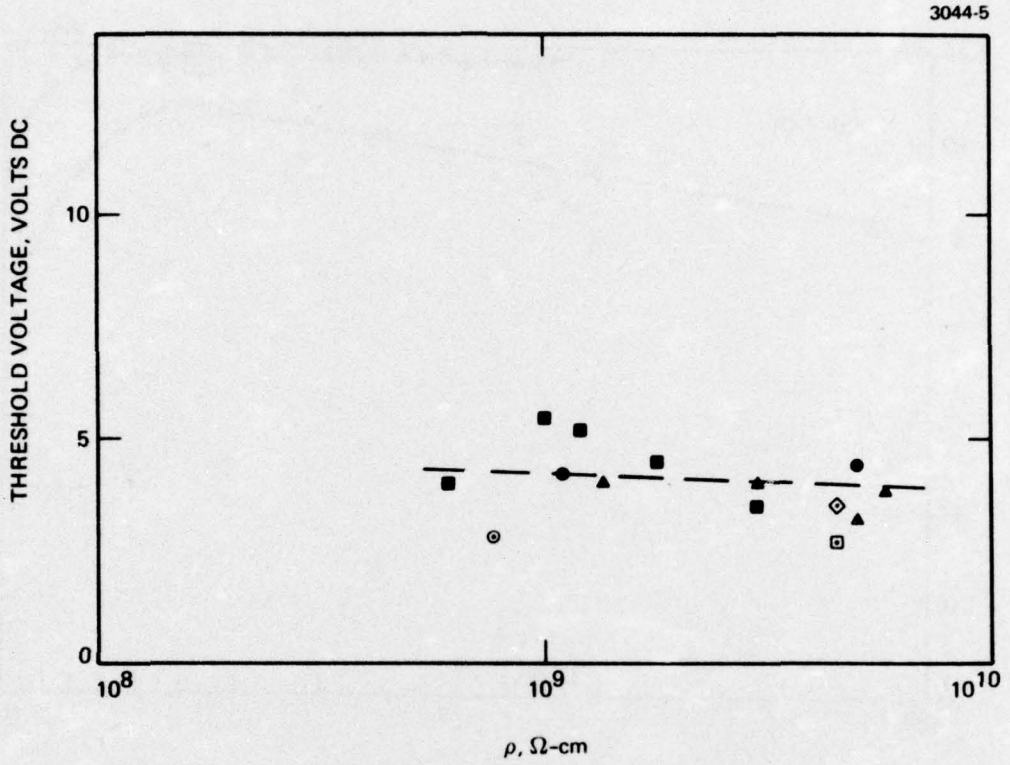

Figure 9. DC-DS threshold voltage as a function of resistivity, with redox-type dopants in HRL-2N10

Dopants:
- ● TFM + DBF
- ▲ TFM + BF
- ■ TCNQ + DBF
- ⊙ TFM
- ▲ BF
- ⊡ DBF
- ◇ HMF

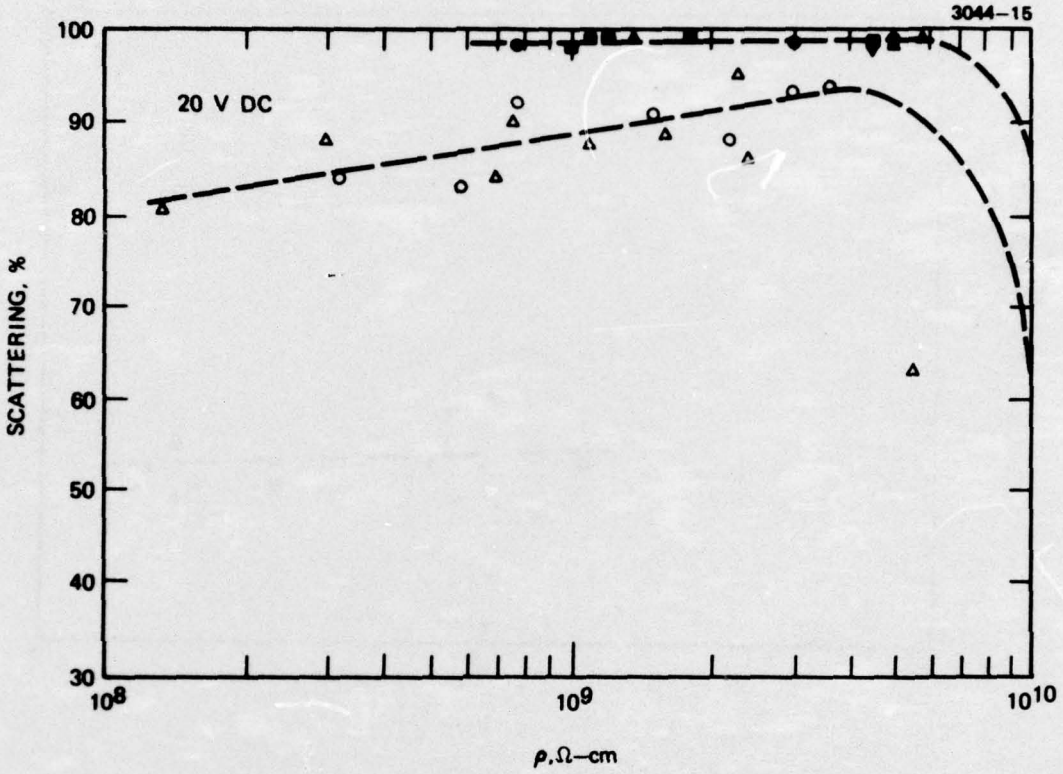

Figure 10. DC-DS scattering level as a function of resistivity and dopants in HRL 2N10. (Dopant symbols as indicated in Figures 8 and 9.)

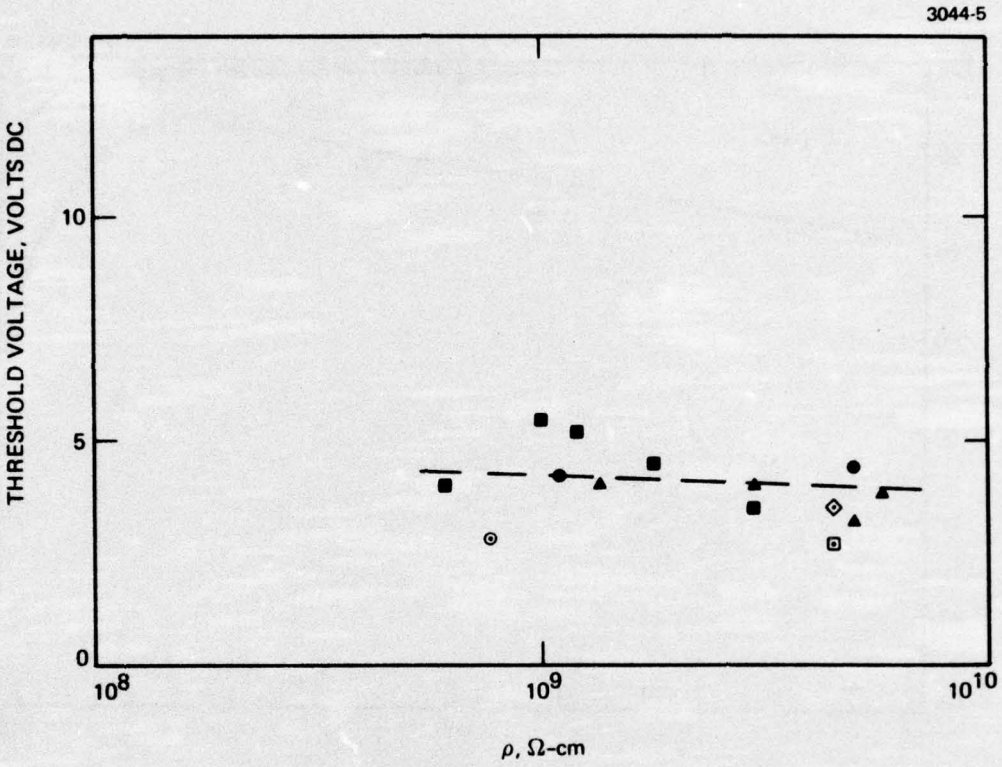

Figure 9. DC-DS threshold voltage as a function of resistivity, with redox-type dopants in HRL-2N10

Dopants:
- ● TFM + DBF
- ▲ TFM + BF
- ■ TCNQ + DBF
- ⊙ TFM
- ▲ BF
- ⊡ DBF
- ◈ HMF

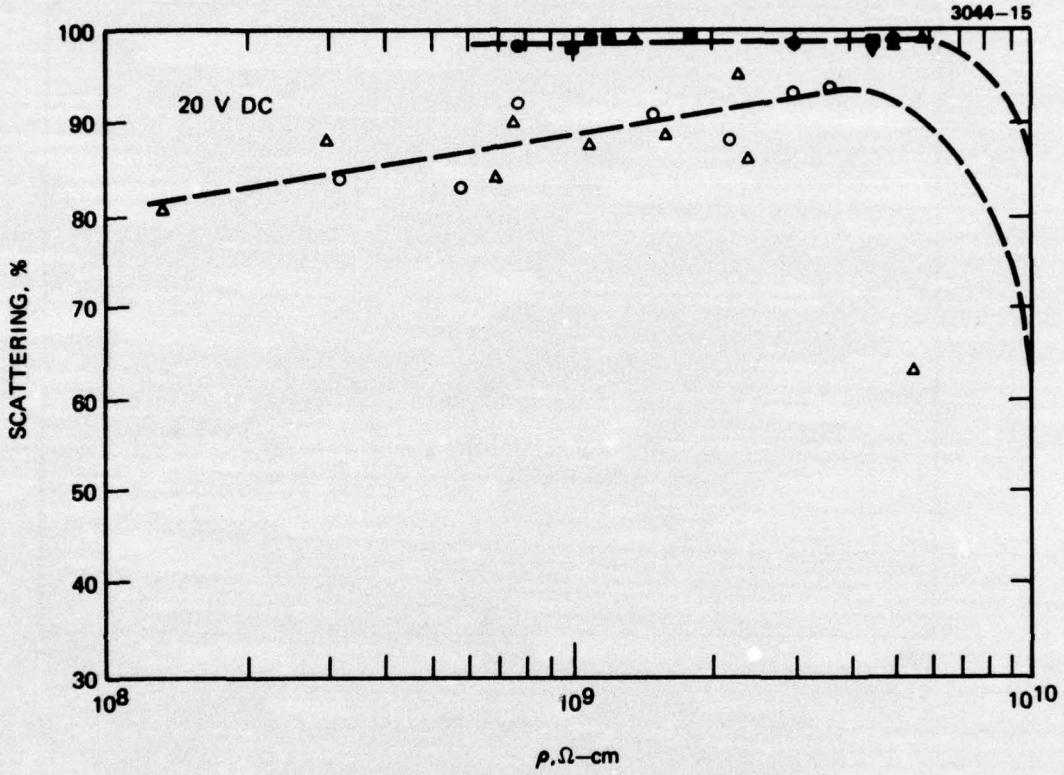

Figure 10. DC-DS scattering level as a function of resistivity and dopants in HRL 2N10. (Dopant symbols as indicated in Figures 8 and 9.)

correlation between R_σ and the size of spherically shaped anions in a series of tetrabutylammonium salts. However, large differences of R_σ do occur and we believe that the size, shape and structure of dopants do have large effects on R_σ. We plan to continue these studies with other materials using a larger selection of dopants.

We found that both dc-DS and ac-DS characteristics are highly dependent upon the conductivity anisotropy, with V_{th} decreasing as R_σ increases in a given LC. Because of electrochemical reactions and charge injection effects, the dc-DS results are more difficult to correlate; so for theoretical correlations we made ac-DS comparisons at resistivities of 10^9 ohm-cm with signals of 30 Hz. (This frequency is far enough below the DS cutoff frequencies so that in theory the ac and dc results should be the same.) Our results[A4] show that in a given LC with different dopants there is a linear relationship between V_{th}^{-2} and R_σ^{-1}, in good agreement with the Carr-Helfrich theory. We have also found that at a high applied voltage (e.g., 30 V rms) the optical density of scattering (i.e., negative logarithm of transmission of a beam passing normal through the cell) increases linearly as R_σ increases. Thus the ac-DS characteristics depend strongly on the conductivity anisotropy, which in turn is highly dependent on the structure of the conductivity dopant as well as the liquid crystal compounds.

G. SURFACE ALIGNMENTS

A careful series of studies on surface alignments and ac-DS characteristics show several new correlations for the effects of alignment.[A5] We used identical LC samples in cells with pretreated electrodes to obtain seven different tilt or twist angles for the LC alignment in the off-state. We found that the ac-DS threshold (V_{th}) increased linearly as the $\cos\bar{\theta}$ decreased, where $\bar{\theta}$ is the average tilt of the LC director off the two electrode surfaces. With our ester LC (HRL-2N10) the V_{th} is almost a factor of two larger in the surface-perpendicular ($\bar{\theta} = 90°$) than in the surface-parallel ($\bar{\theta} = 0°$) alignments. The difference is much smaller in MBBA but, contrary to theory, it is in the same direction (i.e., V_{th} is higher for surface-perpendicular alignments).

We also found[A5] that the domain structure of dynamic scattering and the response times are strongly dependent upon the initial surface alignments. Cells made in a twisted nematic configuration show particularly strong domain patterns up to twice their V/V_{th} ratios. This corresponds to a region of lower scattering efficiency at these higher voltages. The response times (especially the decay time) were longer for all cells with an alignment tilt off the surface ($\overline{\theta} > 0°$) than for various surface-parallel alignments ($\overline{\theta} = 0°$).

We also have pointed out the advantages of surface-parallel alignment displays in which gray scale and fast response times are desired, as well as the advantages of surface-perpendicular alignment for two-level displays with slow decay times such as multiplexed message boards.

H. ELECTRO-OPTICAL APPLICATIONS OF LIQUID CRYSTALS

We prepared a review paper[A3] on the electro-optical applications of thermotropic liquid crystals. It gives an extensive qualitative review of basic LC properties, alignments, and electro-optical effects. Three specific applications are discussed in more detail, namely a TV flat panel matrix display,[B6,9,15,16] a watch display, and a large screen projection display.[B10,14] A total of 157 references are provided as sources for more detailed information.

I. OTHER STUDIES

We carried out a few other studies on LC's in the areas of dielectric anisotropy, temperature effects, and the use of nonconductive dopants.

1. Dielectric Anisotropy

The dielectric anisotropy of our HRL-2N10 ester LC is essentially constant at $\Delta\varepsilon = -0.12$ over three orders of magnitude of resistivity (6×10^8 to 6×10^{11} ohm-cm) for many different dopants, as shown in Fig. 11. However, at high dopant concentrations of TBATMS (where

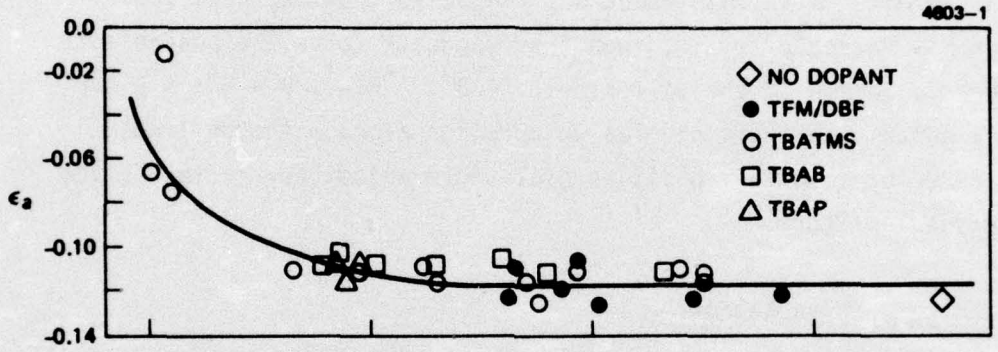

Figure 11. Dielectric anisotropies as a function of dopants in HRL-2N10 at ~25°C.

$\rho_{\perp} \sim 10^8$ ohm-cm) there is an apparent deviation of ε_a in the direction toward zero anisotropy. We are not quite certain that this deviation in dielectric anisotropy is actually real because of possible space charge effects in the measurements of the dielectric constant. We have noted such space charge effects at 100 Hz with the samples of ester liquid crystal that are highly doped (0.125 to 0.5%) with TBATMS. The ε_a values shown in Fig. a are taken in a frequency range where the ε_a is independent of frequency, which is a relatively narrow range of about 1,000 to 10,000 Hz for the high TBATMS concentrations. Normally, one would not expect space charge effects in this frequency range, so that the observed deviation may be real. If so, then this suggests to us the possibility that the association of the salt itself (A^+B^-, $A^+B^-A^+$, $B^-A^+B^-$, $A^+B^-A^+B^-$, etc.) may contribute ionic dipoles which align along with the liquid crystal director to give a positive dielectric anisotropy factor to the liquid crystal mixture.

2. Non-Conductive Dopants

We studied the effects of a number of non-conductive dopants on ac-DS with the idea that DS characteristics of a liquid crystal might be changed in the presence of a dopant that has a different molecular shape from that of the LC molecules. The molecules of the non-conductive dopant might act as centers of disorder, which might facilitate the setting up of the turbulent flow of the liquid crystal for DS.

Dopants studied include 2-tert-butylanthraquinone (TBA), 9-anthracene-carbonitrile (AC), 3-acetylphenanthrene (3-AP), 9-acetylphenanthrene (9-AP), 2,9-dimethyl-4,7-diphenyl-1,10-phenathroline (DDP), and p-butoxyphenyl p-hexyloxybenzoate (BPHB). The structures for these compounds are shown in Fig. 12. In each case (except DDP) 1% of the dopant was added to the HRL-2N10 ester liquid crystal along with the 0.1% tetrabutylammonium trifluoromethane sulfonate (TBATMS) as a conductivity dopant. The solubility of DDP was too low for a 1% solution, so it was used as a saturated solution.

The ac-DS characteristics of the liquid crystal with various dopants are compared in Table I. The cells were made with 13 μm spacers,

4603-9

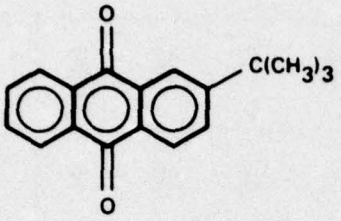

TBA

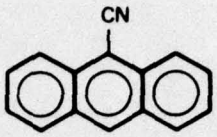

AC

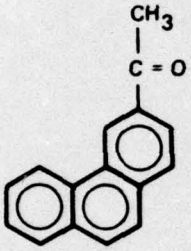

3-AP

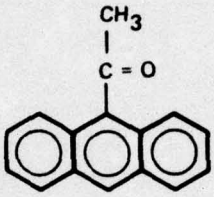

9-AP

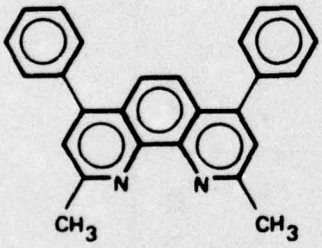

DDP

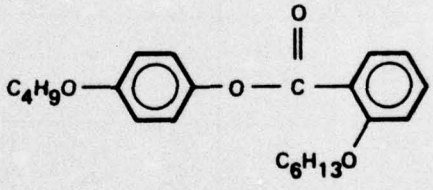

BPHB

Figure 12. Non-conductive dopants for liquid crystals.

TABLE I. Effects of Non-Conductive Dopants on ac-DSM
(13 μm Thick Cells, Using HRL-2N10 with 0.1% TBATMS).

Non-Conductive Dopant	Nematic Clearpoint °C	Resistivity Ω-cm	V_{th}, V rms	Scattering @ 30 V rms %	Response Times (0-20 V), msec			Response Times (0-30 V), msec		
					Delay	Rise	Decay	Delay	Rise	Decay
None	55°-57°	2.4×10^8	9.4	96	45	120	900	14	56	900
1% TBA	53°-55°	2.5×10^8	9.4	95.2	45	120	900	15	60	900
1% AC	53°-56°	1.6×10^8	9.1	96.0	35	85	600	10	40	600
1% 3-AP	54°-55°	2.2×10^8	9.1	95	42	115	900	15	65	900
1% 9-AP	53°-55°	1.8×10^8	9.4	96.5	45	60	500	10	35	500
Sat. DDP	54°-57°	2.2×10^8	9.4	96	40	90	700	15	35	700
1% BPHB	53°-56°	2.4×10^8	9.4	95.0	60	140	1200	20	60	1200

using conductive glass electrodes (indium tin oxide) coated with shallow angle (5°) deposited SiO to provide surface-parallel alignment in the off-state. The resistivities of the liquid crystals are all in the range of 1.6×10^8 to 2.5×10^8 ohm-cm, and the clearpoints are only slightly changed so the order parameter is approximately constant. There is no significant difference in the scattering levels attained, but there appears to be a slight lowering of the threshold voltage for the AC and 3-AP dopants. (These dopants may contribute a negative dielectric anisotropy component to the liquid crystal.) The response times appear to be affected by some of the dopants, with somewhat shorter response times for the AC and 9-AP dopants and substantially longer decay times for the ortho ester dopant BPHB. These response time effects should be confirmed by running a number of different cells to obtain average values of cell thickness and the surface alignment quality.

3. Temperature Effects

The rise and decay times of ac-DS are strongly temperature-dependent, as indicated in Fig. 13. Increasing the temperature from 22° to 48° decreases the decay time by a factor of four, from 200 ms to 50 ms. The straight line relationship shown in Fig. 13 between log (response time) and 1/T indicates that the response times are probably proportional to one or more of the LC viscosities, which might be expected to vary similarly with temperature.

J. APPARATUS FOR DIELECTRIC AND CONDUCTIVITY ANISOTROPIES

Since there is no standard apparatus for the measurements of dielectric anisotropy and conductivity anisotropy in LC's, we have included here a brief description of our instrumentation. Hughes company funds were used to fabricate and assemble the apparatus and to buy all of the associated instrumentation. A picture of the overall equipment is shown in Fig. 14, where the probe head is shown mounted in the magnet. A schematic diagram of the associated electronic instrumentation is given in Fig. 15. Accurate measurements are made over a frequency range of 1 Hz

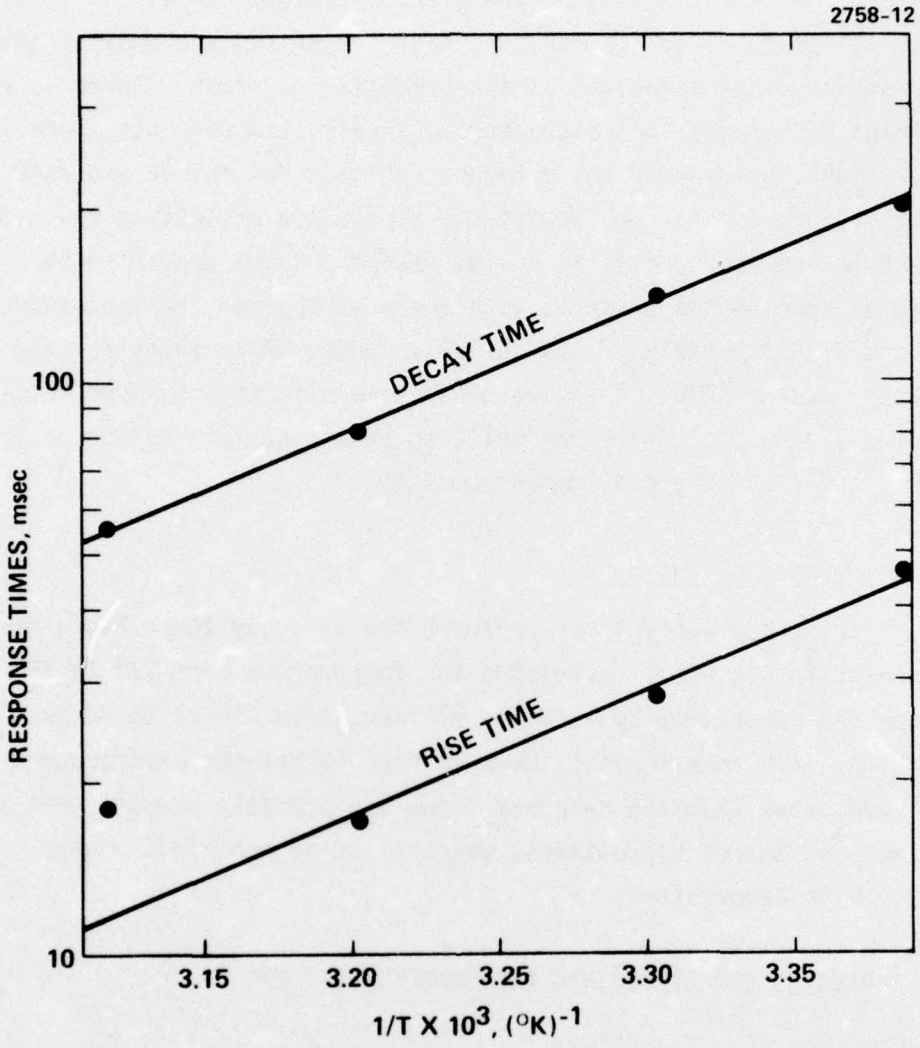

Figure 13. Effect of temperature on rise and decay times of ac-DS (TBATMS doped HRL-2N10, 13 μm cell, surface-parallel alignment.)

M10180

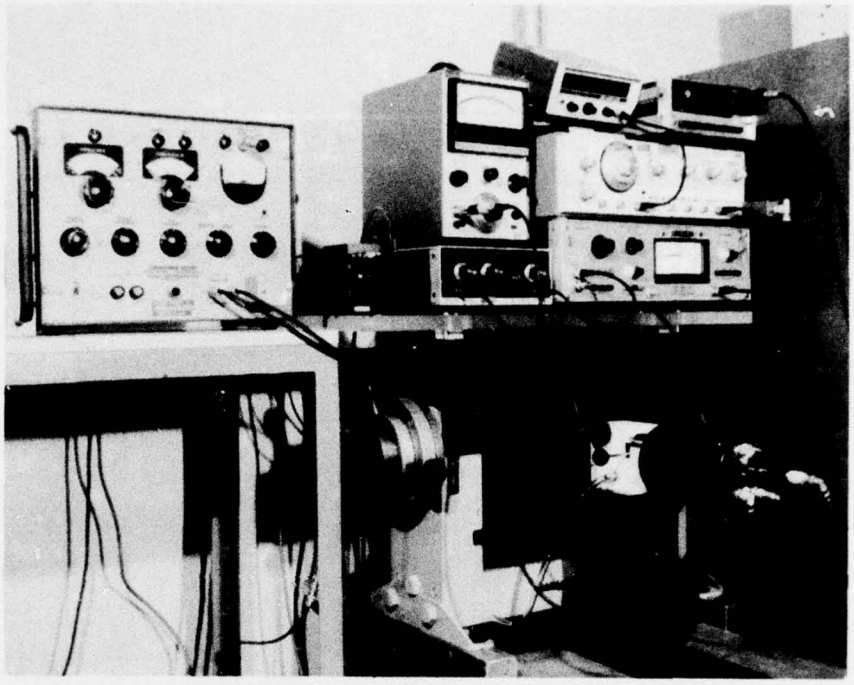

Figure 14. Apparatus for dielectric anistropy measurments.

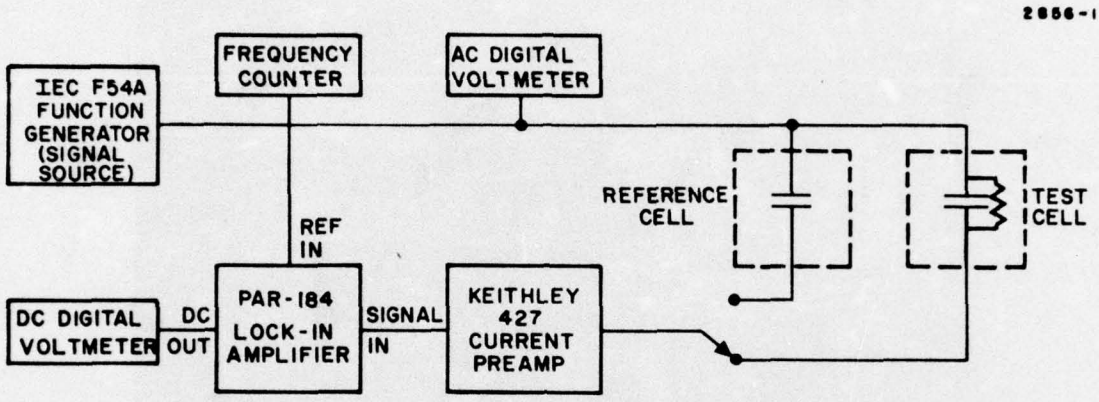

Figure 15. Electrical schematic diagram for the anisotropy instrument.

to 100 kHz. Two test cells are used, one as a reference cell and the other for the sample being tested. These are mounted between two epoxy fiberglass booms which in turn suspend the cells between the pole faces of a 7 kG (at 1 1/2 inch spacing) varian magnet. The mounted cells, pulled out of the magnetic field, are shown in Fig. 16. A cylindrical metal housing, into which the support booms are mounted, provides both electrical and thermal isolation. The sample temperature is monitored with a 500-ohm platinum resistance thermometer that is attached to the test cell. We plan to build a temperature-controlling system for future work.

Each test cell consists of two one-inch diameter, non-magnetic, stainless steel electrodes, separated by a 100 μm quartz spacer, and mounted in a Teflon^{R} canister to form a parallel-plate capacitor. Two test cells are shown in Fig. 17, where one is assembled and one is disassembled. The sample is introduced through the portholes of an assembled cell.

The entire assembly of test and reference cells can be rotated through an angle of 90°, which allows the cells to be oriented so that the electrical field and magnetic field are either parallel or perpendicular with respect to each other. Because the nematic liquid crystals are diamagnetic, they align so that their long molecular axes are parallel to the applied magnetic field ($\vec{H}$). The test cells are thick enough to avoid serious surface orientation effects in the bulk of the sample, and only small electrical signals are used. Measurements are made of the capacitance and conductivity in each direction of magnetic field alignment, and the dielectric constants are calculated using capacitance measurements of the reference (air-filled) cell.

M10179

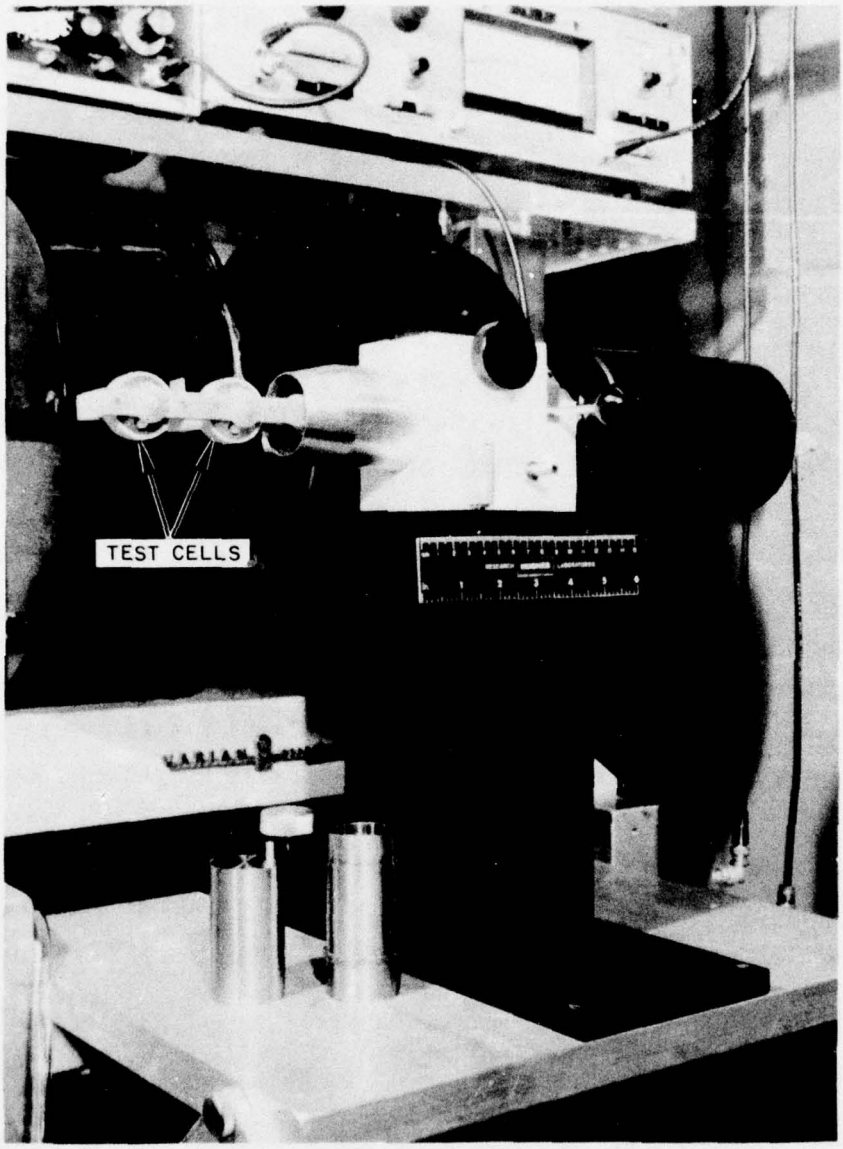

Figure 16. Mounted Test Cells Used for Dielectric Anisotropy Measurements.

M10149

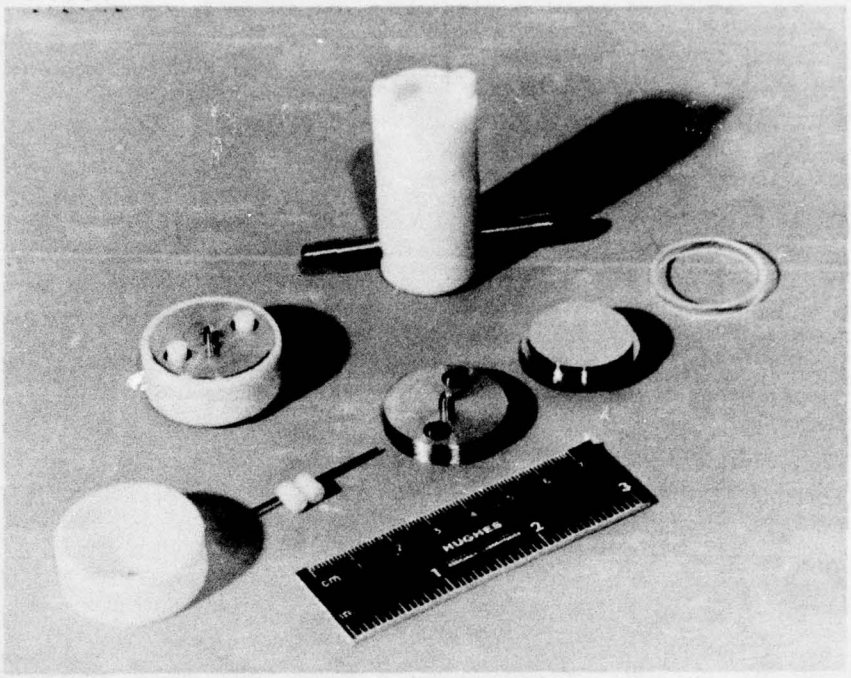

Figure 17. Assembled and Disassembled Test Cells for Dielectric Anisotropy Measurements.

SECTION III

RELATED STUDIES AT HUGHES*

A. PICTORIAL MATRIX DISPLAYS

A flat panel liquid crystal display[B6,9,15,16,A3] has been developed at Hughes with the aid of contracts from the Air Force Avionics Laboratory. It has an electronically driven semiconductor substrate matrix and it utilizes dc dynamic scattering (DS) to obtain TV display rates. It is viewable in high ambient light (direct sunlight) and is of interest for airplane cockpit display applications. It uses silicon wafer modules with 10,000 display elements per square inch, and each element is addressed every 1/30 second. Associated with each picture element is a transistor switch and a capacitor which can be charged to various levels in a microsecond by an incoming video signal pulse. The capacitor holds the dc signal on the liquid crystal for the milliseconds required to activate dynamic scattering. This pulse-stretching circuit makes it possible to build a real-time display using the comparatively slow response of liquid crystals because the overall light scattering picture from many elements is developed in nearly a parallel mode. The one-inch square display modules have 10,000 individual reflective metal electrodes (100 rows by 100 columns), each of which covers its own circuit element on a common silicon chip. The module is mounted on a glass plate and is used as the activating substrate for a reflective liquid crystal cell. The first defect-free 10,000 element display was made in June 1975. More recently, 2" x 2" displays with 40,000 elements have been made by combining four of the one-inch modules.[B15,16] Our AFOSR research studies are pertinent to these displays and we have used ester liquid crystals with redox dopants (DBF/TFM) to obtain favorable dc-DS operation.

---

*The footnotes used refer to the bibliography listed in Section V.

The capacitance of each display element is such that the liquid crystal must have a dc resistivity of $>10^9$ ohm-cm in order to activate the LC without discharging too rapidly as compared to the frame time of the input signal. This requires not only the use of purified liquid crystals and redox dopants, but also the avoidance of any contamination from other sources in the assembled display cell. Our studies on the change of LC resistivity with temperature are shown in Fig. 18. These results indicate that display cells should be thermostated to control the resistivity within the range desired. (This should probably be done by using less dopant and heating the cell slightly so that it would always be at least about 35°C during operation.) The exponential dependence of the dc resistivity shown in Fig. 18 indicates that the main effect of temperature is probably due to changes in the viscosities of the LC.

Tests on the continuous dc-DS of redox-doped ester liquid crystal in reflective mode cells have also shown the feasibility of obtaining long operational lifetimes with a reflective metal electrode, as indicated by the results in Fig. 19. The two samples shown in Fig. 19 were run continuously between conductive glass and silver electrodes and they showed good scattering for 612 days before becoming too resistive to show good dc-DS. In this test period the resistivity of the samples during good scattering varied from as low as 2.4×10^9 to as high as 3.3×10^{10}. This is consistent with the range desired for the operation of the TV matrix display system.

B. ELECTRONIC RETICLE

Another liquid crystal device which utilizes the dynamic scattering effect is an electronically addressed reticle device[B12] which Hughes is developing for fire-control systems in Army tanks. The 1000 x 1000 lines of the LC cell are transparent but a given set of lines can be addressed to give a crosshair which is viewable under a wide range of conditions. The computer-driven reticle can provide many corrections automatically while the viewer sights at a target. The laboratory demonstration models of this device have also used redox-doped ester liquid crystals for dc activation of dynamic scattering.

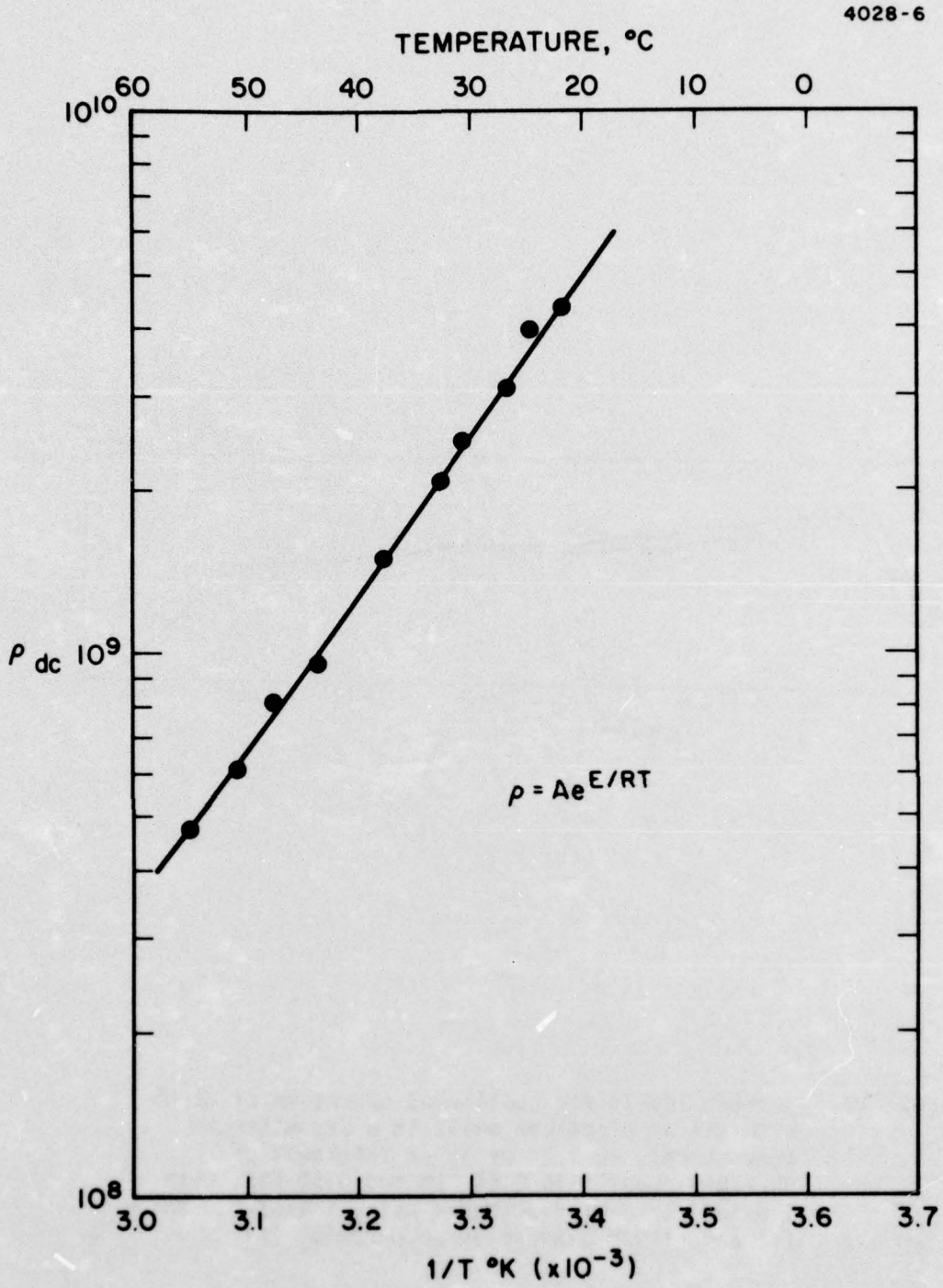

Figure 18. Effect of temperature on apparent dc resistivity of liquid crystal (redox-doped HRL-2N10, 12.5 μm cell, 20 V dc).

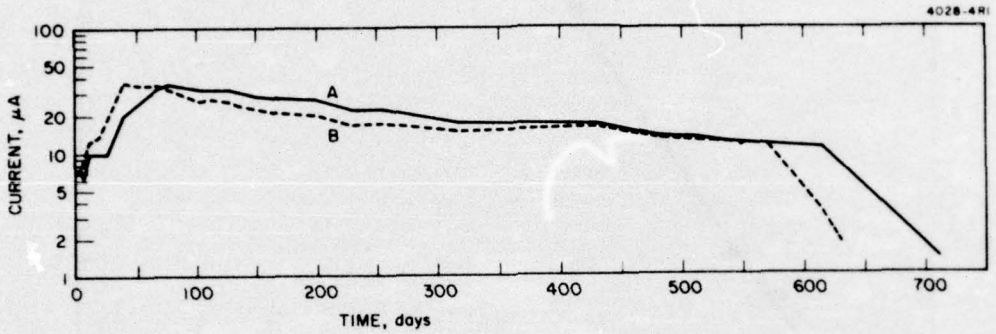

Figure 19. Current levels for continuous operation of dc-DS with silver electrode cells in a dry nitrogen atmosphere: 20 V dc on 13 μm thickness of HRL-2N10 doped with 0.5% TFM and 0.5% DBF, with 1.0 in.^{2} area of electrodes using indium-tin oxide (+) and silver evaporated on chromium (-).

C. PHOTOACTIVATED LIGHT VALVES

We have pioneered the development of light valves[B1,2,4] in which a photoconductor layer is sandwiched with a liquid crystal, which acts as a reversible recording medium to allow light amplification (or processing) of images received by the photoconductor. Many of the early Hughes dc light valves used dynamic scattering effects,[B1,4,7] as did our first ac light valve.[B5] However, the need for a dark off-state as well as fast response times led to the use of various types of liquid crystal birefringent field effect light valves for color symbology projection displays,[B10] for TV projection displays,[B14] and for real-time optical data processing devices.[B11,13] These devices use the same type of substrate with a photoactive layer (CdS), light-blocking layer (CdTe), thin layer mirror (multilayer dielectric) and an overcoating (SiO_2). In each case the counter electrode is an overcoated (SiO_2) transparent conductive glass coating on glass. These reflective mode LC cells are all operated in the ac mode with light activation on the CdS side opposite (away from) the LC. The differences in these devices are all related to differences in the properties, surface alignment, and thickness of the liquid crystal. Another type of light valve is used to convert visible images into infrared images. Its design is essentially the same as the others except that it does not use a mirror and is used in the transmission mode instead of the reflection mode. The main features of the liquid crystal and optical designs used for these various light valves are summarized in Table II.

Most of these light valves utilize the birefringent characteristics of the liquid crystal, although in somewhat different ways. In the projection light valves it is very important to have photochemically stable liquid crystals which have as high as possible a birefringence so that thin cells can be used to obtain fast response times. For the same reason, low viscosity materials are desired. It is also important to have strongly negative dielectric anisotropies so that relatively low voltages can be used across the cell, thus extending the lifetime of the photosensitive substrate. Because of these requirements, new liquid crystal materials and mixtures are being studied as a means of increasing the birefringence

TABLE II. Summary of Various Light Valve Design Features for Optical Modulation Devices.

Light Valve Device	Surface Alignment Configuration	Liquid Crystal Material		Typical Cell Thickness	Operational Mode (LC Effect)	Polarizer Positions
		ε_a	Structure Type			
Symbology Projection (B&W)	Perpendicular Tilted	Negative	Phenyl benzoate	4-6 μm	Reflection (birefringence)	Crossed
Color Symbology Projection	Perpendicular Tilted	Negative	Schiff Base	4-6 μm	Reflection (birefringence)	Crossed
TV Projection (B&W)	Perpendicular Tilted	Negative	Phenyl benzoate	2 μm	Reflection (birefringence)	Crossed
Optical Data Processing	Parallel 45° Twist	Positive	Cyano-biphenyl	2 μm	Reflection (birefringence)	Crossed
Vis to IR Converter	Parallel 90° Twist	Positive	Cyano-biphenyl	6 μm	Transmission (polarization)	Parallel

without extending the liquid crystal light absorption into the visible range. It is also important to have a stable pre-tilted surface alignment[A3] for the color symbology[B10] and TV[B14] projection light valves.

D. FORMULATION OF LIQUID CRYSTALS

We have synthesized a wide variety of liquid crystal materials, and have been particularly interested in the formulation of phenyl benzoate mixtures for use in dc-activated dynamic scattering displays. By carefully purifying the LC compounds synthesized and then using DSC (differential scanning calorimetry) analyses, we found that we could successfully apply the Schroeder-van Laar equation for the calculation of eutectic mixtures. Earlier we had obtained many useful results with the HRL-2N10 and HRL-2N12 ester mixtures, but they are not eutectic mixtures and sometimes crystals would form after long periods of standing in a cool room. However, these mixtures did have the advantage of not being too viscous. On the theory that low viscosity in a phenyl benzoate LC mixture is related to short para-substituted end groups (i.e., shorter molecular length), we calculated a large number of possible ester combinations which should be eutectic mixtures and still have relatively short molecular lengths. This has led to the development of a new six-component liquid crystal eutectic mixture designated as HRL-2N40. This is now being tested in pictorial matrix and reticle displays. Its characteristics are compared with those of the earlier mixtures in Table III.

TABLE III. Properties of Ester LC Mixtures

Property	HRL-2N10	HRL-2N12	HRL-2N40
Number of Components	4	5	6
Eutectic Mixture	No	No	Yes
Nematic Temperature Range	~20° to 55°	~21° to 55°	(13°)[a] to 58°
Dielectric Anisotropy (100 Hz)	-0.12	-0.26	-0.27
Calculated Average Length	24.6 Å	24.5 Å	24.0 Å

[a]Calc. mp = 13°, but this has not been observed due to supercooling and glass formation. HRL-2N40 shows a glass transition at -60°.

SECTION IV

RESEARCH PERSONNEL AND FACILITIES

A. PERSONNEL

The principal investigator for this contract was Dr. J. D. Margerum. Other major participants in these liquid crystal studies were Dr. H. S. Lim on the electrochemical and dopant studies. Mr. P. O. Braatz and Mrs. A. M. Lackner on the conductivity and dielectric anisotropy studies, and Mr. M. J. Little on the effects of surface alignment.

The following personnel of the Exploratory Studies Department of the Hughes Research Laboratories participated in this project:

Mr. Paul O. Braatz (Member of the Technical Staff; MS in Electrical Engineering).

Mr. Andrejs Graube (Member of the Technical Staff; BS in Chemical Engineering).

Mr. John E. Jensen (Member of the Technical Staff; BS in Chemistry).

Mrs. Anna M. Lackner (Member of the Technical Staff; BS in Chemistry).

Dr. Hong Sup Lim (Member of the Technical Staff; PhD in Electrochemistry).

Mr. Michael J. Little (Member of the Technical Staff; BS in Physics).

Dr. J. David Margerum (Head, Chemistry Section; PhD in Physical Chemistry).

Mr. James T. Marx (Senior Research Assistant).

Dr. Leroy J. Miller (Staff Engineer and Member of the Technical Staff; PhD in Organic Chemistry).

Mrs. Deborah S. Smythe (Associate Engineer; BS in Biology).

Dr. Shi-Yin Wong (Consultant; PhD in Organic Chemistry and MD).

B. FACILITIES

The facilities used in this contract were primarily those available in the Chemistry Section, Exploratory Studies Department, of the Hughes Research Laboratories in Malibu, California. Extensive capital equipment and all of the materials used in these studies were provided by the Hughes Aircraft Company without direct charge to the contract.

Other related liquid crystal studies were carried out in various Hughes Aircraft Company divisions, including the Hughes Research Laboratories (Malibu, California), the Aerospace Groups (Culver City, California) and the Industrial Products Division (Carlsbad, California).

SECTION V

CHRONOLOGICAL PUBLICATION BIBLIOGRAPHY

A. PAPERS FROM THIS CONTRACT*

1. H. S. Lim and J. D. Margerum, "Improved DC Dynamic Scattering with Redox Dopants in Ester Liquid Crystals," Appl. Phys. Lett. 28, 478-480 (1976).

2. H. S. Lim and J. D. Margerum, "Dopant Effects on DC Dynamic Scattering in a Liquid Crystal: Microscopic Pattern Studies," J. Electrochem. Soc. 123, 837-838 (1976).

3. J. D. Margerum and L. J. Miller, "Electro-optical Applications of Liquid Crystals," J. Colloid and Interface Sci. (in press, Vol. 58, 1977). This review will also appear as a chapter in a book consisting of the Plenary and Invited lectures given at the 50th International Conference on Colloids and Surfaces in San Juan, Puerto, Rico in June 1976.

4. J. D. Margerum, H. S. Lim, P. O. Braatz and A. M. Lackner, "Effect of Dopants on the Conductivity Anisotropy and AC Dynamic Scattering of Liquid Crystals" (submitted to Mol. Cryst. Liq. Cryst.). Presented at Sixth International Liquid Crystal Conference, Kent, Ohio, August 1976.

5. M. J. Little, H. S. Lim and J. D. Margerum, "Alignment Effects on the Dynamic Scattering Characteristics of an Ester Liquid Crystal" (submitted to Mol. Cryst. Liq. Cryst.). Presented at Sixth International Liquid Crystal Conference, Kent, Ohio, August 1976.

6. H. S. Lim, J. D. Margerum and A. Graube, "Electrochemical Properties of Dopants and the DC Dynamic Scattering of a Nematic Liquid Crystal" (submitted to J. Electrochem. Soc). To be presented at 150th Electrochemical Society Meeting, Las Vegas, Nevada, October 1976.

B. OTHER RELATED HUGHES PUBLICATIONS

1. J. D. Margerum, J. Nimoy and S.-Y. Wong, "Reversible Ultraviolet Imaging with Liquid Crystals," Appl. Phys. Lett. 17, 51-53 (1970).

*See Appendices A to F for copies of these papers.

2. J. D. Margerum, T. D. Beard, W. P. Bleha, Jr., and S.-Y. Wong, "Transparent Phase Images in Photoactivated Liquid Crystals," Appl. Phys. Lett. 19, 216-218 (1971).

3. J. D. Margerum, "Organic Based Imaging Systems," in "Symposium III, Unconventional Photographic Systems," Society of Photographic Scientists and Engineers, October 1971, pp. 54-64 (a review paper).

4. T. D. Beard, W. P. Bleha, Jr., M. Braunstein, A. D. Jacobson, J. D. Margerum and S.-Y. Wong, "Real-Time and Reversible Stored-Image Displays Using Photoactivated Liquid Crystals" (in preparation), initially presented at SPSE Symposium III on Unconventional Photographic Systems, Washington, D.C., October 1971.

5. T. D. Beard, W. P. Bleha and S.-Y. Wong, "AC Liquid Crystal Light Valve," Appl. Phys. Lett. 22, 90-92 (1973).

6. M. N. Ernstoff, A. M. Leupp, M. J. Little and H. T. Peterson, "Liquid Crystal Pictorial Display," presented at IEEE Electron Device Meeting, Washington, D.C., December 1973.

7. A. D. Jacobson, T. D. Beard, W. P. Bleha, J. D. Margerum and S.-Y. Wong, "The Liquid Crystal Light Valve, an Optical to Optical Interface Device," Pattern Recognition 5, 13-19 (1973).

8. J. D. Margerum, J. M. Little and P. O. Braatz, "Pyroelectric Film/Liquid Crystal Detector for 10.6 μm Region," Final Technical Report AFML-TR-74-268 of Contract F33615-73-C-5129 (November 1974).

9. M. N. Ernstoff, "Liquid Crystal Pictorial Display," presented at 1975 Digital Avionics Systems Conference, April 4, 1975.

10. J. Grinberg, W. P. Bleha, A. D. Jacobson, A. M. Lackner, G. D. Myer, L. J. Miller, J. D. Margerum and L. M. Fraas, "Photoactivated Birefringent Liquid Crystal Light Valve for Color Symbology Display," IEEE Trans. Elec. Devices ED-22, 775-783 (1975).

11. J. Grinberg, A. D. Jacobson, W. P. Bleha, L. J. Miller, L. M. Fraas, D. Boswell and G. D. Myer, "A New Real-time Non-Coherent to Coherent Light Image Converter. The Hybrid Field Effect Liquid Crystal Light Valve," Optical Engineering 14, 217-225 (1975).

12. R. P. Farnsworth, L. W. Hill and S.-Y. Wong, "Liquid Crystal Digital Reticle," U. S. Patent 3,885,861 (May 27, 1975).

13. A. D. Jacobson, J. Grinberg, W. P. Bleha, L. J. Miller, L. M. Fraas, G. D. Myer and D. Boswell, "A Real-Time Optical Data Processing Device," Information Display 12, 17-22 (September 1975).

14. A. D. Jacobson, J. Grinberg, W. P. Bleha, L. J. Miller, L. M. Fraas and D. D. Boswell, "A New Television Projection Light Valve," SID Digest of Technical Papers, pp. 26-27 (April 1975).

15. C. R. Stephens and L. T. Lipton, "A Multichip MOS Video Rate Liquid Crystal Display," SID Digest of Technical Papers, pp. 44-45 (May 1976).

16. Hughes Technical Staff, "Liquid Crystal Video Display," Electro-Optical Systems Design, pp. 38-40 (September 1976).

APPENDIX A

Reprint

"Improved DC Dynamic Scattering with
Redox Dopants in Ester Liquid Crystals"

by Hong Sup Lim and J. David Margerum

Applied Physics Letters 28, 478-480 (1976)

Improved dc dynamic scattering with redox dopants in ester liquid crystals

Hong Sup Lim and J. David Margerum

Hughes Research Laboratories, Malibu, California 90265
(Received 9 January 1976)

Redox dopants are used to improve the dc dynamic scattering (DS) characteristics of phenyl benzoate liquid crystals as compared to the use of salt-type conductive dopants. The redox dopants are selected by their electrochemical properties so that they react preferentially and reversibly at the electrodes, thus providing the current carriers for the dc-DS effect. Low-threshold voltages (~2 V), high scattering efficiency (99% at 20 V), and long dc-DS lifetimes (up to 18000 h) are obtained with an ester liquid crystal containing a redox dopant pair consisting of di-*n*-butylferrocene and (2,4,7-trinitro-9-fluorenylidene)malononitrile.

PACS numbers: 81.55.+x, 61.30.+w, 82.45.+z, 72.80.Ph

We have used selected redox dopants to improve the lifetime, threshold voltage, and scattering characteristics of the dc dynamic scattering[1] (DS) of nematic liquid crystals (LC) with phenyl benzoate structures. Results with new redox dopants are compared with those with salt-type dopants. We define redox dopants as donors or acceptors (or both) that readily undergo reversible electrochemical reactions, and which do so at lower voltages than the electrochemical reactions of the LC components. The redox dopants are thus designed to carry the dc current in LC cells. Salt-type dopants are defined as electrochemically inactive ionic compounds. In related studies, Baise *et al.*[2] reported that acceptor dopants which form charge-transfer complexes with an azoxybenzene LC lower its dc-DS threshold voltage. Ohnishi and Ozutsumi[3] used a hydroquinone-quinone

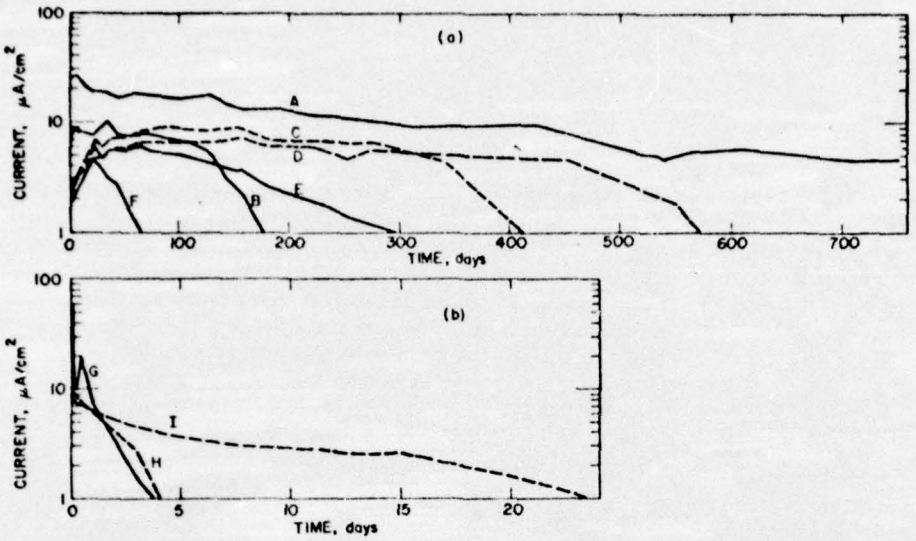

FIG. 1. DS life tests at 20 V dc with 13-μm thickness of HRL-2N10 in unsealed cells between ITO electrodes: (a) Redox dopants (DBF/TFM): A, 0.5% (N_2 atm); B, C, and D, 0.05% (N_2 atm); E and F, 0.005% (in air). (b) Salt dopants (N_2 atm): G, 0.1% TBATMS; H, 0.025M TBATMS. I, saturated TBAP.

dopant system to extend the dc-DS lifetime of Schiff-base LC's. p-Benzoquinone falls into our category of redox dopants, but hydroquinone undergoes irreversible electrochemical oxidation in aprotic solvents.[4] They reported[3] long dc-DS lifetime for p-methoxybenzylidene–p-n-butylaniline (MBBA) with this dopant pair added. However, their data showed rather poor scattering levels, with a best value of only about 65% scattering at 20 V in a 25-μm-thick cell.

We have found several different mixtures of p-p', disubstituted phenyl benzoates which show comparable behavior with regard to the effect of dopants on their dc-DS. A four-component ester LC designated as HRL-2N10 is used in the present study.[5] It has a nematic range of about 18–55°, a negative dielectric anisotropy of $\epsilon_a = -0.12$ (25°C, 500 Hz), and a birefringence of $\Delta n = 0.14$ (25°C, 545 nm). The undoped LC has a high resistivity ($\rho_\perp = 3.8\times10^{11}$ Ω cm at 100 Hz) and does not show DS effects until conductivity dopants are added. The dopants used include electrochemically inactive salts such as tetrabutylammonium perchlorate (TBAP) and tetrabutylammonium trifluoromethanesulfonate (TBATMS); electron acceptors such as (2,4,7-trinitro-9-fluorenylidene)malononitrile (TFM); and electron donors such as di-n-butylferrocene (DBF).

Electrochemical studies[6] in solvents containing 0.1M TBAP show that decomposition potentials (vs saturated calomel electrode) for the irreversible reactions of the LC components occur at about +1.7 V (in acetonitrile) for oxidation and −2.2 V (in dimethylformamide) for reduction. On the other hand, the formal reduction potentials (in acetonitrile vs SCE) for the reversible electrode process of the redox dopants are quite low, e.g., 0.03 V for TFM and 0.32 V for DBF. Thus, in the presence of such acceptor (A) and donor (D) redox dopants, the electrochemistry in the LC should be dominated by their reversible reactions: At the negative electrode, $A + e^- = A^-$ and $D^+ + e^- = D$, and at the positive electrode, $D = D^+ + e^-$ and $A^- = A + e^-$. Our studies[7] of the flow patterns of the redox-doped LC with dc activation are consistent with the following charge injection mechanism: Acceptor dopants react at the negative electrode to form anions which travel to the positive electrode and undergo the reverse reaction; donor dopants form cations at the positive electrode which move to the negative electrode and undergo the reverse reaction. When both redox dopants are present, bipolar injection of cations and anions takes place and the back reaction probably also occurs by disproportionation in the bulk: $A^- + D^+ = A + D$.

The redox-doped LC shows long dc-DS lifetimes with good scattering levels. Relatively stable current density is obtained in cells with indium tin oxide (ITO) electrodes, as shown in Fig. 1(a) for DBF/TFM dopants. No bubble defects were formed in any of these cells and the scattering remained good in the current range shown. Sample A (with 0.5% DBF/TFM) shows a lifetime >18 000 h and sample D (0.05% DBF/TFM) showed a 13 000 h lifetime. In general, longer dc-DS lifetimes

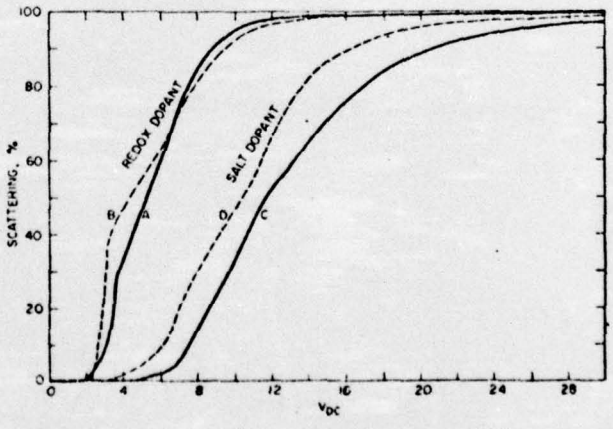

FIG. 2. Scattering vs voltage curves for 13-μm-thick transmission cell of HRL-2N10 with various dopants. Curves A and B: 0.5% and 0.1% each of TFM/DBF redox dopants. Curves C and D: 0.002% and 0.0005% TBATMS salt dopant. Resistivity of LC: A, 1.1×10^9; B, 2.8×10^9; C, 1.6×10^9; and D, 2.3×10^9 Ω cm. Alignment is surface parallel, by rubbing.

are obtained with higher concentrations of DBF/TFM when the unsealed cells are operated in an atmosphere flushed with dry N_2. These long dc-DS operating lifetimes indicate that the electrochemical reversibility is very good in the ester LC host, in agreement with the electrochemical properties of these dopants in other solvents.

The salt-doped LC shows very limited dc-DS lifetimes. At higher current levels, bubbles are formed in the LC cell. As indicated in Fig. 1(b), the current density decreases rapidly within a few days. In this time, the scattering becomes very poor and nonuniform, and the electrodes are darkened. (At 20 V dc the scattering with the salt dopants is never as good as with the redox dopants.) The irreversible reactions which occur in the LC and at the electrode surface are believed to be from reactions of radical cations and anions formed by electrochemical oxidation or reduction of the LC components.

Slow scan curves of dc-DS vs voltage are shown in Fig. 2 using similar sets of ac resistivities with the redox dopant pair DBF/TFM (curves A and B) as compared to the salt dopant TBATMS (curves C and D). These scattering curves (where $\%S = 100\% - \%T$) were obtained using the LC in flat sandwich cells with rubbed transparent (ITO) electrodes on glass. (Green light centered at 525 nm was used in an optical system with a resolution of 20 lp/mm.) The redox dopants show low dc-DS thresholds (2.0 and 2.1 V) as compared with the salt dopant ($V_{th} = 3$ and 5 V). The redox dopants give a much higher scattering level at a given applied voltage, which is an important consideration in display devices where limited driving voltages are available.

At least two factors appear to be involved in the lower threshold voltage and higher scattering level with the redox dopant than with the salt dopant. One is the low charge injection potential[6,7] due to the low redox potential of the redox dopant compared to those of the LC components. The other is the difference in the conductivity anisotropies of the redox and salt dopants. We find that the ac (100 Hz) conductivity anisotropy ratio ($R_\sigma = \sigma_\parallel/\sigma_\perp$) in this LC is higher for DBF/TFM ($R_\sigma = 1.34$) than for TBATMS ($R_\sigma = 1.12$). This may be due to the aromatic groups in the redox dopants and to the flat shape of TFM as compared to the nearly spherical shape of the ions from TBATMS. However, the dc conductivity anisotropy, which is more relevant to dc-DS, might be different from these values. Additional studies are planned for further understanding of the dc-DS behavior.

The authors are indebted to the Directorate of Chemical Sciences, Air Force Office of Scientific Research, Contract F44620-72-C-0075 for partial financial support of this research.

[1]F.G. Heilmeier, L.A. Zanoni, and L.A. Barton, Proc. IEEE 56, 1162 (1968).
[2]A.I. Baise, J. Teucher, and M.M. Labes, Appl. Phys. Lett. 21, 142 (1972).
[3]Y. Ohnishi and M. Ozutsumi, Appl. Phys. Lett. 24, 213 (1974).
[4]C.K. Mann and C.K. Barnes, *Electrochemical Reactions in Nonaqueous Systems* (Marcel Dekker, New York, 1970), pp. 190–196.
[5]A four-component mixture of *p*-butylphenyl *p*-toluate, *p*-butoxyphenyl *p*-butoxybenzoate, *p*-butoxyphenyl *p*-hexyloxybenzoate, and *p*-butoxyphenyl *p*-oxyloxybenzoate in a weight ratio of 15:5:9:9, respectively.
[6]H.S. Lim and J.D. Margerum (unpublished).
[7]H.S. Lim and J.D. Margermum, J. Electrochem. Soc. (to be published).

APPENDIX B

Reprint

"Dopant Effects on DC Dynamic Scattering in a Liquid Crystal: Microscopic Pattern Studies"

by Hong Sup Lim and J. David Margerum

Journal of the Electrochemical Society 123, 837-838 (1976)

Dopant Effects on D-C Dynamic Scattering in a Liquid Crystal: Microscopic Pattern Studies

Hong Sup Lim* and J. David Margerum

Hughes Research Laboratories, Malibu, California 90265

Our studies on the microscopic patterns of d-c dynamic scattering (DS) show that the electrochemical properties of dopants determine the dominant charge injection reaction, direction of liquid crystal (LC) flow, and location of the LC turbulence. This report compares different dopants (an electron acceptor, an electron donor, and a nonreactive salt) in an ester LC. These results differ substantially from earlier microscopic observations (1,2) of d-c DS in other LC's, but are consistent with our studies (3) showing that redox dopants (donors and acceptors which readily undergo reversible electrochemical reactions in the LC) give d-c DS at lower threshold voltages as well as giving higher scattering levels and much longer lifetimes than salt dopants.

A nematic LC (4) designated as HRL-2N10 is used. It has a nematic range of about 18°-55°, a dielectric anisotropy of $\epsilon_a = -0.12$ (25°C, 500 Hz) and a birefringency of $\Delta n = 0.14$ (25°, 545 nm). In the undoped state, it is highly resistive ($\rho_\perp = 3.8 \times 10^{11}$ ohm-cm at 100 Hz) and does not show DS effects. The salt dopant used is tetrabutylammonium trifluoromethanesulfonate (TBATMS); the acceptor is (2,4,7-trinitro-9-fluorenylidene)malononitrile (TFM); and the donor is di-*n*-butylferrocene (DBF).

Electrochemical studies (5) in solvents containing 0.1M tetrabutylammonium perchlorate show decomposition potentials (*vs.* saturated calomel electrode) of the LC components at about +1.7V (in acetonitrile) for oxidation and −2.2V (in dimethylformamide) for reduction. The formal reduction potentials (in acetonitrile *vs.* SCE) for the reversible electrode process of the redox dopants are quite low, *e.g.*, 0.03V for TFM and 0.32V for DBF. Thus when the LC contains TFM or DBF, the electrochemical reactions of these dopants should be a dominant factor in the passage of current through the LC (6). This is confirmed by using a polarizing microscope to observe the direction of LC flow between electrodes. Test cells (Fig. 1) are made by sandwiching the LC between a substrate containing two thin-film transparent electrodes and a glass cover plate with a 51 μm thick Mylar spacer. This cell geometry is chosen to allow space for the back flow of the LC outside the area of observation, *i.e.*, in the periphery of the cell where the field is low. The LC is aligned parallel to the surface of the glass and perpendicular to the electric field by a rubbing technique. With TFM added, the LC flow is predominately from the negative to the positive electrode, while with DBF added the predominant LC flow is from positive to negative. When equimolar mixtures are added, the LC flow in each direction is approximately balanced, which is also the case when the salt dopant is used. These flow patterns are observed by the movement of dust particles in the LC. The flow directions are also confirmed by studies in tubular cells with screen electrodes and sidearm capillaries to indicate the pressure effect of the LC flow.

The direction of the LC flow is consistent with a unipolar space charge injection followed by the propagation of the space charge under the influence of the applied electric field, as previously observed (2) or discussed (7) by others. Our results indicate that in the presence of TFM unipolar injection of negative ions is probably dominant (TFM + e^- = TFM$^-$), followed by the reverse reaction at the positive electrode. Similarly with DBF, unipolar injection of positive ions is probably dominant (DBF = DBF$^+$ + e^-) followed by the reverse reaction at the negative electrode. A simultaneous bipolar injection occurs when both redox dopants or when the salt is present. However, when the dopant is a nonreactive salt, LC radical ions (8,9) are probably formed at the electrodes.

Scattering patterns with the different dopants at various applied voltages are shown in Fig. 2. (No scattering was observed with the salt dopant at 40V.) With the salt dopant, the scattering pattern has a line structure which contains alternating lines originating from each electrode. Thin flow lines of LC are initiated from each electrode at the same time and propagate toward the opposite electrode. Dust particles move along the lines in the direction of the propagation, indicating that the lines are caused by LC flow. These effects are similar to Williams domains (10), in which the source of the LC hydrodynamic motion has been well analyzed (11-13). However, with a redox dopant the general appearance of the scattering pattern is quite different. Turbulent motions of LC are observed at lower voltages, without formation of a regular line structure. The turbulence is initiated from one electrode and propagates toward the other. Except at very high voltages, the turbulence does not reach the opposite electrode but remains localized near the electrode where it was initiated. The most interesting observation is that the turbulence is initiated from the negative electrode when the dopant is the donor and from the positive when the dopant is the acceptor, while the charge injection and the liquid crystal flow are in the opposite directions. Dust particles move from the rear of the nonturbulent electrode toward the turbulent electrode and travel across it.

When the redox dopant is a balanced mixture of the acceptor and donor, the turbulence occurs more randomly. At low voltages turbulence begins at both

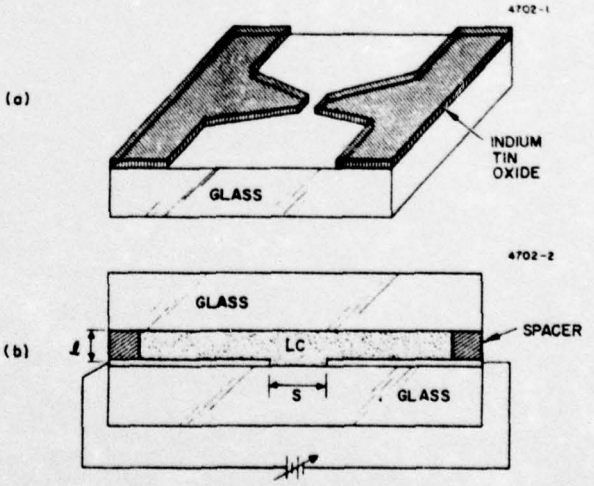

Fig. 1. Test cells for microscopic pattern studies of d-c DS. (a) Substrate with electrodes. (b) Cross section of assembled cell, with $S \sim 380$ μm and $l = 51$ μm. The microscope view is from the top, perpendicular to the applied field.

* Electrochemical Society Active Member.

Key words: redox dopant, salt dopant, charge injection, liquid crystal flow.

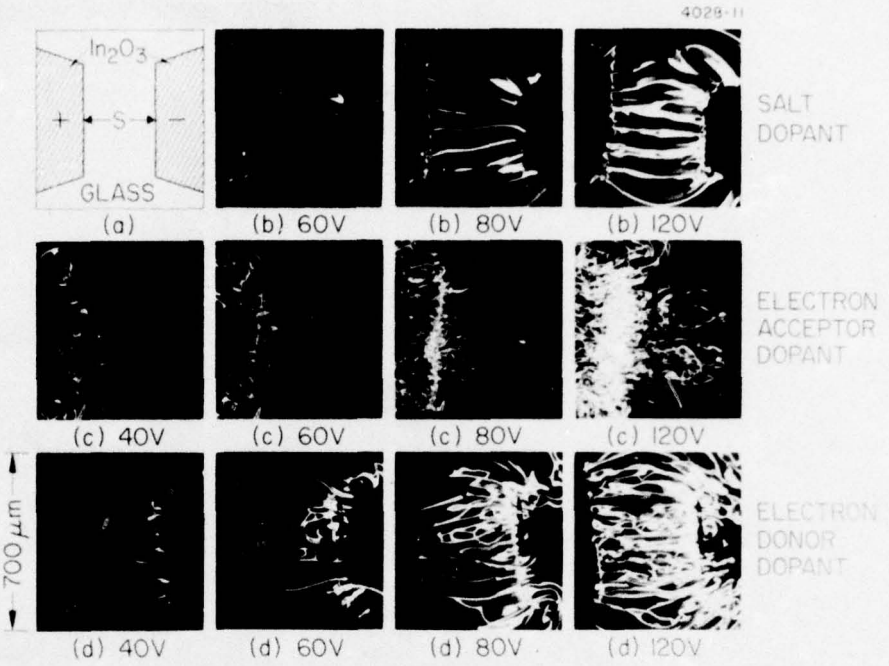

Fig. 2. Photographs of the microscopic patterns of DS. (a) Schematic view of the electrodes. (b) 0.0004% TBATMS ($\rho \sim 5 \times 10^9$ ohm-cm; $S = 350$ μm). (c) 0.5% TFM ($\rho \sim 5 \times 10^9$ ohm-cm; $S = 400$ μm). (d) 0.5% DBF ($\rho \sim 3 \times 10^{10}$ ohm-cm; $S = 375$ μm). The polarizers are crossed, with the analyzer perpendicular to the direction of the LC alignment.

electrodes and also between them, although to a lesser extent. Regions of flow may appear, but the over-all effect is more like a combination of pictures from the individual redox dopants than that of the salt dopant finger patterns. The onset of turbulence occurs at lower voltages with redox dopants (single or mixed) than with salt dopants, and the LC turbulence is greater at a given voltage. Similar results are observed with the same LC between transparent electrodes in conventional flat panel cells (3).

Acknowledgments

We are indebted to the Directorate of Chemical Sciences, Air Force Office of Scientific Research, contract F44620-72-C-0075 for partial financial support of this research.

Manuscript submitted Jan. 12, 1976; revised manuscript received Feb. 26, 1976.

Any discussion of this paper will appear in a Discussion Section to be published in the December 1976 JOURNAL. All discussions for the December 1976 Discussion Section should be submitted by Aug. 1, 1976.

Publication costs of this article were partially assisted by Hughes Research Laboratories.

REFERENCES

1. G. H. Heilmeier, L. A. Zanoni, and L. A. Barton, *Proc. IEEE*, **56**, 1162 (1968).
2. J. C. Lacroix and R. Tobazeon, *Appl. Phys. Letters*, **20**, 251 (1972).
3. H. S. Lim and J. D. Margerum, *ibid.*, **28**, 478 (1976).
4. A four-component mixture of p-butylphenyl p-toluate, p-butoxyphenyl p-butoxybenzoate, p-butoxyphenyl p-hexyloxybenzoate, and p-butoxyphenyl p-octyloxybenzoate in a weight ratio of 15:5:9:9, respectively.
5. Authors' unpublished results.
6. The current level in the experiments was much lower than the expected diffusion-limited current of the redox dopants.
7. F. Gaspard and R. Herino, *Appl. Phys. Letters*, **24**, 452 (1974).
8. A. Lomax, R. Hirasawa, and A. J. Bard, *This Journal*, **119**, 1679 (1972).
9. A. Denat and B. Gosse, *Chem. Phys. Letters*, **22**, 91 (1973).
10. R. Williams, *J. Chem. Phys.*, **39**, 384 (1963).
11. E. F. Carr, *Mol. Cryst. Liq. Cryst.*, **7**, 253 (1969).
12. W. Helfrich, *J. Chem. Phys.*, **39**, 384 (1969).
13. P. A. Penz, *Phys. Rev. Letters*, **24**, 1405 (1970).

Reprinted from JOURNAL OF THE ELECTROCHEMICAL SOCIETY
Vol. 123, No. 6, June 1976
Printed in U.S.A.

APPENDIX C

Partial Preprint

"Electro-Optical Applications of Liquid Crystals"

by J. David Margerum and Leroy J. Miller

Accepted for publication in

(1) The Journal of Colloid and Interface Science 58 (1977).

(2) A book of the Plenary and Invited Lectures at the 50th International Conference on Colloids and Surfaces.

(The full paper is a long review article, which is currently available as Hughes Research Laboratories Research Report #499, June 1976. On the following pages only the Abstract, Table of Contents, Introduction, Summary and Outlook, and Acknowledgment sections are shown.)

ELECTRO-OPTICAL APPLICATIONS OF LIQUID CRYSTALS

J. David Margerum and Leroy J. Miller
Hughes Research Laboratories
Malibu, California 90265

ABSTRACT

The unique properties of thermotropic liquid crystals have led to the development of many new electro-optical devices, particularly for display applications. Basic properties and surface alignments of liquid crystals are reviewed with regard to these applications. Electro-optical effects based on conductivity and field effect alignment are described for both nematic and cholesteric materials. Three applications of nematics are selected for more detailed discussion: a flat panel television display using dynamic scattering activated by a semiconductor matrix, a watch display using polarization modulation of twisted nematic cells on transparent segment electrodes, and a large screen projection system using tunable birefringence in a photoactivated light valve.

Presented as an invited lecture at the 50th International Conference on Colloids and Surfaces, San Juan, Puerto Rico, June 25, 1976.

TABLE OF CONTENTS

INTRODUCTION

The intermolecular forces responsible for the mesomorphic phases also lead to a cooperative behavior between large numbers of molecules in regard to their surface alignment, field alignment, and flow alignment phenomena. Because liquid crystals have highly anisotropic properties such as birefringence, conductivity anisotropy and dielectric anisotropy, large effects in thin cells can result from subtle surface pre-treatments combined with relatively low applied electrical fields and current levels. Liquid crystals are particularly attractive for display applications such as wrist watches, calculators, message boards, flat panel television, and large screen projection systems. Other devices include page composers, electronic reticles, real-time optical data processing systems, waveguide switches, and graphic arts duplicating devices. The applications are based on the resulting advantages of one or more factors, particularly: flat panel cells, low operational voltage, low power consumption, portability, viewability in high ambient light, good resolution capability, rapidity of response, image storage, and stability.

In this paper we summarize the liquid crystal and surface alignment properties most pertinent to display device applications and we review the general scope of electro-optic device effects. We also describe three distinctly different types of nematic liquid crystal display systems in more detail as illustrative of the broad range of applications being used. To avoid excessive length, we have limited this paper to description, without equations for

device characteristics. Readers seeking more information should find adequate leads in the references cited, and also should consult some of the recent reviews and books on electro-optical effects and applications of liquid crystals (1-6).

.
.
.

SUMMARY AND OUTLOOK

A great variety of interesting electro-optical devices result from the proper combinations of surface treatments, liquid crystal materials, addressing signals, and optical components. Liquid crystals are finding wide acceptance in digital watches, in which the display is on continuously and can be read in bright sunlight. New digital color displays may be made feasible by utilizing improved guest/host dyes (31). Advances in the control of surface effects, the development of liquid crystal materials tailored to specific device requirements, and improved addressing techniques are expected to result in the increased use of electro-optical devices. Multiplexing techniques are being applied to bar-graph (156) and alpha-numeric (131) displays for use in instrument panels, portable message boards, etc. Similarly, multiplex address of liquid crystal matrix systems is being developed for large area flat panel displays (136) and for real-time page-composer devices (157). Semiconductor matrix addressing circuits can be used to provide small flat panel, TV-rate, pictorial displays (143,144). Such

portable panels will have widespread military and commercial applications when economical manufacturing techniques are perfected. Photoactivated light valves, in which the liquid crystal acts as a high resolution medium for temporary image-storage, are expected to have widespread applications for large screen TV projection displays (43,151) and real-time optical data processing systems (56,90).

ACKNOWLEDGMENT

The authors are indebted to the Directorate of Chemical Sciences, Air Force Office of Scientific Research, Contract F44620-72-C-0075 for partial financial support of our research studies. We are also indebted to our many colleagues in the Hughes Aircraft Co. who have carried out advanced work on liquid crystal applications in watches, matrix displays, reticles, and light valves.

APPENDIX D

Preprint

"Effects of Dopants on the Conductivity Anisotropy and AC Dynamic Scattering of Liquid Crystals"

J. D. Margerum, H. S. Lim, P. O. Braatz and A. M. Lackner

Submitted for publication in Molecular Crystals and Liquid Crystals

(Presented at Sixth International Liquid Crystal Conference, Kent, Ohio, August 1976.)

EFFECT OF DOPANTS ON THE CONDUCTIVITY ANISOTROPY AND AC DYNAMIC SCATTERING OF LIQUID CRYSTALS*

J. David Margerum, Hong Sup Lim, Paul O. Braatz,
and Anna M. Lackner
Hughes Research Laboratories
Malibu, California 90265

Abstract

The dynamic scattering (DS) characteristics and the conductivity anisotropy ratio ($R_\sigma = \sigma_\parallel/\sigma_\perp$) are shown to depend upon the structure and concentration of conductivity dopants as well as upon the structure of two nematic liquid crystals. For both a phenyl benzoate liquid crystal and for MBBA the ac threshold voltage (V_{th}) decreases with increasing R_σ, and the optical density of scattering at 30 V rms is directly proportional to R_σ. In each liquid crystal there is a linear relationship between V_{th}^{-2} and R_σ^{-1}, in agreement with the Carr-Helfrich theory.

---

*Presented at the Sixth International Liquid Crystal Conference, Kent, Ohio, August 1976.

INTRODUCTION

The dynamic scattering[1] (DS) behavior of a nematic liquid crystal under an applied electrical field depends upon its alignment by the field and the conduction of current through it as well as on other factors. Purified liquid crystals, to which dopants have not been added, have high resistivities and do not show dynamic scattering.[2] Conductivity anisotropy has been assumed to be important in DS-type effects,[3-5] and in the Carr-Helfrich[6,7] model it is a key factor in the formation of Williams domain[8] patterns. Numerous conductivity dopants have been used to obtain DS effects, and there have been many reports on the conductivity anisotropy ratio[9] ($R_\sigma = \sigma_\parallel / \sigma_\perp$) of various nematic liquid crystals. Frequently, R_σ has been assumed to be simply a property of the liquid crystal, and the conductivity dopant was often an unknown impurity. Several authors[10-13] reported a variety of R_σ values for N-(p-methoxybenzylidene)-p-butylaniline (MBBA) containing different dopants but did not comment on the dopant effect. Chang[14] reported that the conductivity anisotropy of MBBA increases with decreasing radius of the halide ion in a series of three tetrapentylammonium halide dopants. He also observed that the maximum contrast ratio of DS obtainable with various dopants increased with the conductivity anisotropy. Barnik *et al.*[15,16] recently measured R_σ values and the threshold voltage (V_{th}) of electrohydrodynamic instability (Williams domains) for a number of dopants in different liquid crystals. They reported[16] that a two-dimensional

threshold analysis[17,18] for MBBA gave an excellent correlation between theory and the experiment for plots of V_{th} versus R_{σ}. Surprisingly, they found that the same theoretical calculations for MBBA also fit the experimental points for two other liquid crystals, namely a mixture of azoxy compounds and a mixture of MBBA with EBBA (p-ethoxybenzylidene-p-n-butylaniline).

In this work we examine the effect of dopant structure and concentration on the conductivity anisotropy as well as on the dynamic scattering properties of a phenyl benzoate liquid crystal in cells with surface-parallel alignment. Some similar studies on MBBA are carried out for comparison purposes regarding the effect of the liquid crystal (LC) on these factors.

EXPERIMENTAL

Both MBBA (clpt. 46.2°) and a phenyl benzoate mixture designated as HRL-2N10 are used in this study. The latter is a four-component mixture of p-butylphenyl p-toluate, p-butoxyphenyl p-butoxybenzoate, p-butoxyphenyl p-hexyloxybenzoate and p-butoxyphenyl p-octyloxybenzoate in a weight ratio of 15:5:9:9, respectively. HRL-2N10 has a nematic range of about 20° to 55°, a dielectric anisotropy of $\Delta\varepsilon = (5.14 - 5.26) = -0.12$ (25°C, 500 Hz) and a birefringence of $\Delta n = 0.14$ (25°, 545 nm). Before adding dopants, the LC's are highly resistive, with $\rho_{\perp} > 1 \times 10^{11}$ ohm-cm for MBBA and $\rho_{\perp} > 3 \times 10^{11}$ ohm-cm for HRL-2N10 at 100 Hz. The following conductivity dopants are used after purification and drying: (1) tetrabutylammonium trifluoromethanesulfonate

(TBATMS); (2) tetrabutylammonium tetrafluoroborate (TBATFB); (3) tetrabutylammonium perchlorate (TBAP); (4) tetrabutylammonium iodide (TBAI); (5) tetrabutylammonium chloride (TBAC); (6) tetraethylammonium bromide (TEAB); (7) tetrabutylammonium bromide (TBAB); (8) tetrabutylammonium tetraphenylboride (TBATPB); and (9) a redox dopant[19,20] mixture consisting of equimolar concentrations of the donor di-n-butylferrocene (DBF) and the acceptor (2,4,7-trinitro-9-fluorenylidene)malononitrile (TFM). The salt dopants were obtained commercially and are purified by standard techniques, except for TBATMS which is prepared[21] by reaction of trifluoromethanesulfonic acid and tetrabutylammonium bromide and is purified by recrystallization from water and drying. Commercial DBF and TFM were purified by vacuum distillation and recrystallization from acetonitrile, respectively.

The conductivity anisotropy is calculated from resistivity measurements at room temperature with a 100 μm thick cell in which the liquid crystal is aligned by a 7.5 kG magnetic field, using a readout with a lock-in amplifier (PAR-186) and a current-to-voltage converter (Keithley 427). The R_σ values are taken at 100 Hz, but the values are constant over a wide frequency range. Both the R_σ values and the DS behavior are compared at the same resistivity (e.g., $\rho_\perp = 1.0 \times 10^9$ ohm-cm) from data taken for several different concentrations of each dopant over a $\rho_\perp$ range of about 6×10^8 to 3×10^9 ohm-cm. The DS test cells are made with transparent electrodes (indium tin oxide

rubbed to give surface-parallel alignment) using 12.7 μm thick Mylar spacers. The transmission of DS is measured in an optical system with a resolution of 20 lp/mm using collimated green light (centered at 525 nm). The V_{th} for DS is obtained by extrapolating the steep decrease of transmission back to 100% T. This is essentially the same as the threshold voltage for the formation of Williams domains. The scattering curves (where %S = 100-%T) are obtained from slow scan increases of applied voltage at 30 Hz and 100 Hz (sinusoidal). The thresholds at 30 Hz are reported here because they are slightly lower for the samples with a resistivity of 1×10^9 ohm-cm.

RESULTS AND DISCUSSION

Effect of Dopants on Conductivity Anisotropy

Typical results are shown in Figures 1, 2 and 3. These clearly show that the conductivity anisotropy ratio (R_σ) for both the ester liquid crystal and MBBA is highly dependent upon the structure and concentration of the dopants. Comparisons made at a given resistivity also show that the R_σ for a given dopant is different in the ester than in MBBA. For example, at $\rho_\perp = 10^9$ ohm-cm TBATMS, TBAI, TBAC and TBAB all have lower R_σ values in the ester than in MBBA, despite the fact that the ester (clpt. 55°) might be expected to have a higher order parameter at 25° than MBBA (clpt. 46°). Our comparisons are made at the same liquid crystal resistivity rather than at the same dopant concentrations because the dissociation constants

of the various salts are not identical. The resistivity is an approximate measure of the concentration of ionic species present if the ionic mobilities of the different species are roughly the same.

Increased dopant concentration shows a rather large effect in some cases, particularly in the ester liquid crystal. The dopants with less solubility in the ester, such as TBAC and TBAB show the largest increases of R_σ at increased concentration (lower $\rho_\perp$). At high concentrations of 0.03 to 0.5% TBATMS shows a similar increase when $\rho_\perp < 10^9$ ohm-cm. Two of the more soluble dopants, TBATPB and DBF/TFM, show no significant variation of R_σ for the concentrations used. (Up to 0.5% of each redox dopant compound is used, and the conductive ions are presumably due to a small equilibrium concentration from: $DBF + TFM = DBF^+ + TFM^-$.) The salt dopants are more soluble in MBBA than in the ester, and as indicated in Figure 3 the R_σ values are less concentration-dependent. However, in MBBA they also show a general trend of higher R_σ values at increased dopant concentrations. We speculate that multiple ion association effects may occur as the salt concentrations approach saturation in the liquid crystal, where species such as ⊕⊖⊕, ⊖⊕⊖, etc., may be present and might contribute significantly to the conductivity anisotropy.

As noted by Chang,[14] the reproducibility of R_σ values is poor with different batches of MBBA, despite our method of handling the samples in a dry box flushed with nitrogen. The

ester shows better reproducibility, although some dopants such as TBAB give more variable results than the others. We suspect some sort of impurity effects probably are responsible for the large deviations of R_σ at low concentrations ($\rho_\perp > 10^{10}$) of TBAB and TBATMS. Nevertheless, the R_σ values around $\rho_\perp = 10^9$ are fairly reproducible and comparisons can be made on the general effects of dopant structure. Our initial result with TBATMS, TBATFB, TBAP, TBAI and TBAB in the ester seemed to support Chang's observations[14] that in MBBA smaller anions give larger R_σ values. However, this correlation does not hold up when we also consider the small Cl^- anion in TBAC and the large $(C_6H_5)_4B^-$ anion in TBATPB. Table I indicates that the R_σ data from Figures 1 and 2 do not correlate well with the crystallographic[22] sizes of anions. Other factors must be involved, such as ionic association, liquid crystal solvation, and the shape of the ions. For example, the flat shape and aromatic character of TFM^- anions may contribute to the large R_σ value of the DBF/TFM dopant. We plan to study such effects in more detail with other dopant and liquid crystal structures.

Effect of Conductivity Anisotropy on Dynamic Scattering (DS)

The DS behavior of a given liquid crystal is highly dependent upon the conductivity dopants used in it, as illustrated by the typical scattering versus voltage curves in Figure 4 for three different dopants in the HRL-2N10 ester liquid crystal. Scattering curves were taken for a total of eight dopants in the ester and for five dopants in MBBA. The

experimental results of the DS threshold voltage (V_{th}) versus the conductivity anisotropy ratio (also at $\rho_\perp = 10^9$ ohm-cm) are shown in curves (a) and (b) of Figure 5. (Similar results were obtained at other resistivities.) Our DS comparisons are made at the same sample resistivities so that approximately equal current levels occur at the same applied voltage. It is apparent that each of these liquid crystals shows a distinctly different V_{th} versus R_σ curve, showing that V_{th} depends on the liquid crystal as well as the dopants. Of course, this is as we expected since the dielectric anisotropy of the ester ($\Delta\varepsilon = -0.12$) is much less negative than that of MBBA ($\Delta\varepsilon = -0.53$), the conductivity anisotropy of a given dopant is smaller in the ester than in MBBA, and the other material constants are probably different for the two liquid crystals.

Helfrich[7] derived a one-dimensional expression for the dc threshold voltage of Williams domains in cells with surface-parallel alignment of liquid crystal. If the domain periodicity (λ) is included,[5] then the Helfrich equation is as follows:

$$V_{th} = \pi \left(\frac{2d}{\lambda}\right) \left[\frac{k_{33}/\varepsilon_o}{\frac{\kappa_1 \varepsilon_\parallel}{\eta_1}\left(\frac{\varepsilon_\perp}{\varepsilon_\parallel} - \frac{1}{R_\sigma}\right) + \frac{\Delta\varepsilon}{R_\sigma}} \right]^{1/2} \qquad (1)$$

The expression for threshold voltage with low frequency ac excitation[23-25] contains extra terms of frequency dependence. The frequency dependence terms, however, drop out if $\omega^2/\omega_c^2 << 1$, where ω is the frequency of the applied ac signal and ω_c is the

cut-off frequency, i.e., the space charge-limited dielectric relaxation frequency. This frequency is proportional to the conductivity of LC.[5] Since the cut-off frequencies of the LC's used in the present studies are about 700 Hz at $\rho_\perp = 1 \times 10^9$ ohm-cm, the condition $\omega^2/\omega_c^2 << 1$ is satisfied at 30 Hz. Equation (1) and recent[26] values of physical constants for MBBA ($k_{33} = 8.11 \times 10^{-7}$ dyne, $\kappa_1 = 79.5$ cp, $\eta_1 = 104.5$ cp, $\varepsilon_\parallel = 4.72$, $\varepsilon_\perp = 5.25$) and a reported[27] experimental value of $\lambda = 1.3\ d$ (where d = cell thickness) are used to calculate curve c in Figure 5 for various values of R_σ. The refined two-dimensional models[16-18] give more accurate computer-calculated results for MBBA, but it can be seen that our results for MBBA (curve a) and the ester (curve b) are qualitatively similar to curve c. This qualitative fit to the Helfrich equation is confirmed by the straight line relationships shown in Figure 6 for plots of V_{th}^{-2} versus R_σ^{-1}. Note that equation (1) can be rewritten as equation (2),

$$V_{th}^{-2} = A\left(R_\sigma^{-1}\right) + B \qquad (2)$$

in which A and B are constants for a particular liquid crystal if we assume that the conductivity dopant concentrations are too small to affect the other physical constants.

The data in Figure 7 show that the optical density of scattering (-log T) of each of the two liquid crystals at a high voltage (30 V) is directly proportional to its conductivity

anisotropy with a particular dopant. This is not surprising when one observes the long gray scale region of the scattering curves in Figure 4 and notes that the relationship of V_{th} versus R_σ in Figure 5 is not far from linear. In other words, it seems reasonable to us that the density of scattering is proportional to V/V_{th} and thus it is linear with R_σ, since we have found V_{th} to be approximately linear with R_σ.

ACKNOWLEDGMENT

We are indebted to the Directorate of Chemical Sciences, Air Force Office of Scientific Research, Contract F44620-72-C-0075 for partial financial support of this research, and to John E. Jensen and Deborah S. Smythe for assistance in preparing some of the samples.

References

1. Heilmeier, G. H., Zanoni, L. A., and Barton, L. A., Appl. Phys. Lett., 13, 46 (1968); Proc. IEEE, 56, 1162 (1968).
2. Heilmeier, G. H., Zanoni, L. A., and Barton, L. A., IEEE Trans. Elec. Dev., ED-17, 22 (1970).
3. Penz, P. A., Phys. Rev. Lett., 24, 1405 (1970).
4. De Gennes, P. G., Comments Solid State Phys., 3, 35 (1970).
5. Scheffer, T. J., and Gruler, H., "Electro-Optics of Liquid Crystals," in Molecular Electro-Optics, O'Konski, C. T., Ed. (Marcel Dekker, in press, 1976).
6. Carr, E. F., Mol. Cryst. Liq. Cryst., 7, 253 (1969).
7. Helfrich, W., J. Chem. Phys., 51, 4092 (1969).
8. Williams, R., J. Chem. Phys., 39, 384 (1963).
9. $R_\sigma = \sigma_\parallel / \sigma_\perp$, where $\sigma_\parallel$ and $\sigma_\perp$ are conductivities of the LC with its directors parallel and perpendicular to the electric field, respectively.
10. Rondelez, F., Diguet, D., and Durand, G., Mol. Cryst. Liq. Cryst., 15, 183 (1971).
11. Sprokel, G. J., Mol. Cryst. Liq. Cryst., 22, 249 (1973).
12. Sprokel, G. J., Mol. Cryst. Liq. Cryst., 26, 45 (1974).
13. Chang, R., and Richardson, J. M., Mol. Cryst. Liq. Cryst., 28, 189 (1974).
14. Chang, R., in Liquid Crystals and Ordered Fluids, Vol. 2, Johnson, J. F., and Porter, R. S., Eds. (Plenum Publishing Corp., 1974), p. 367.

15. Barnik, M. I., Blinov, L. M., Grebenkin, M. F., Pikin, S. A., and Chigrinov, V. G., Zh. Eksp. Teor. Fiz., 69, 1080 (1975).

16. Barnik, M. I., Blinov, L. M., Grebenkin, M. F., Pikin, S. A., and Chigrinov, V. G., Physics Lett., 51A, 175 (1975).

17. Pikin, S. A., Zh. Eksp. Teor. Fiz., 60, 1185 (1971); Sov. Phys.-JETP, 33, 641 (1971).

18. Penz, P. A., and Ford, G. W., Phys. Rev A, 6, 414 (1972).

19. Lim, H. S., and Margerum, J. D., Appl. Phys. Lett., 28, 478 (1976).

20. Lim, H. S., and Margerum, J. D., J. Electrochem. Soc., 123, 837 (1976).

21. Ronseau, K., Farrington, G. C., and Dolphin, D., J. Org. Chem., 37, 3968 (1972).

22. Stern, K. H., and Amis, E. S., Chem. Rev., 59, 164 (1959).

23. Orsay Liquid Crystal Group, Phys. Rev. Lett., 25, 1642 (1970).

24. Orsay Liquid Crystal Group, Mol. Cryst. Liq. Cryst., 12, 251 (1971).

25. Dubois-Violette, E., de Gennes, P. G., and Parodi, O., J. Physique, 32, 305 (1971).

26. van Doorn, C. Z., J. Appl. Phys., 46, 3738 (1975).

27. Meyerhofer, D., and Sussman, A., Appl. Phys. Lett., 20, 337 (1972).

Figure Captions

Fig. 1. Conductivity Anisotropy Ratio of an Ester Liquid Crystal Containing Different Dopant Structures and Concentrations, ∿25°C.

Fig. 2. Conductivity Anisotropy Ratio of an Ester Liquid Crystal Containing Different Dopant Structures and Concentrations, ∿25°C.

Fig. 3. Conductivity Anisotropy Ratio of MBBA Containing Different Dopant Structures and Concentrations, 25°C.

Fig. 4. Typical Dynamic Scattering Curves for Dopants in an Ester Liquid Crystal ($\rho_{\perp}$ = 1.0 x 10^9 ohm-cm, 12.7 μm thick cell spacers, surface-parallel alignment).

Fig. 5. Effect of Conductivity Anisotropy Ratio on Dynamic Scattering Thresholds ($\rho_{\perp}$ = 1.0 x 10^9 ohm-cm, 12.7 μm thick spacer, surface-parallel alignment). Curve a — experimental points for MBBA; curve b — experimental points for HRL-2N10; curve c — Helfrich equation calculation for MBBA. Dopants: 1 = TBATMS, 2 = TBATFB, 3 = TBAP, 4 = TBAI, 5 = TBAC, 6 = TEAB, 7 = TBAB, 8 = TBATPB, 9 = DBF/TFM.

Fig. 6. Helfrich Equation Plots for Dynamic Scattering Threshold (same data and conditions as in Fig. 5).

Fig. 7. Effect of Conductivity Anisotropy Ratio on the Optical Density of Scattering at 30 V rms (same conditions as in Fig. 5).

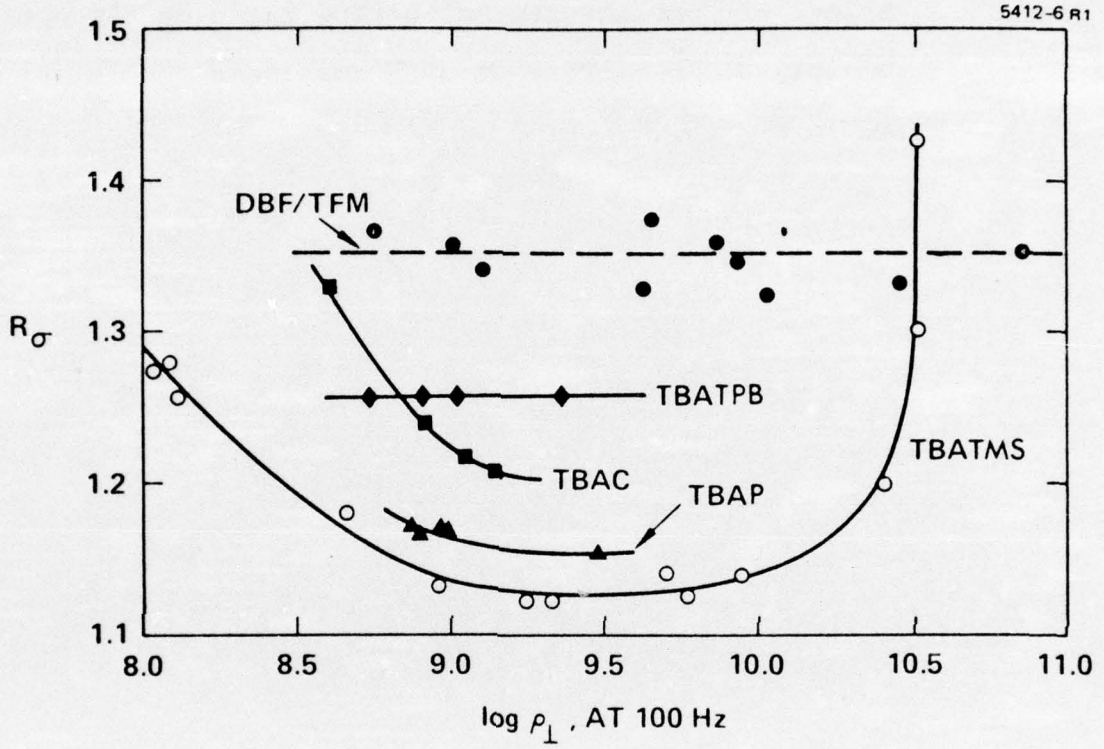

Fig. 1. Conductivity Anisotropy Ratio of an Ester Liquid Crystal Containing Different Dopant Structures and Concentrations, ∿25°C.

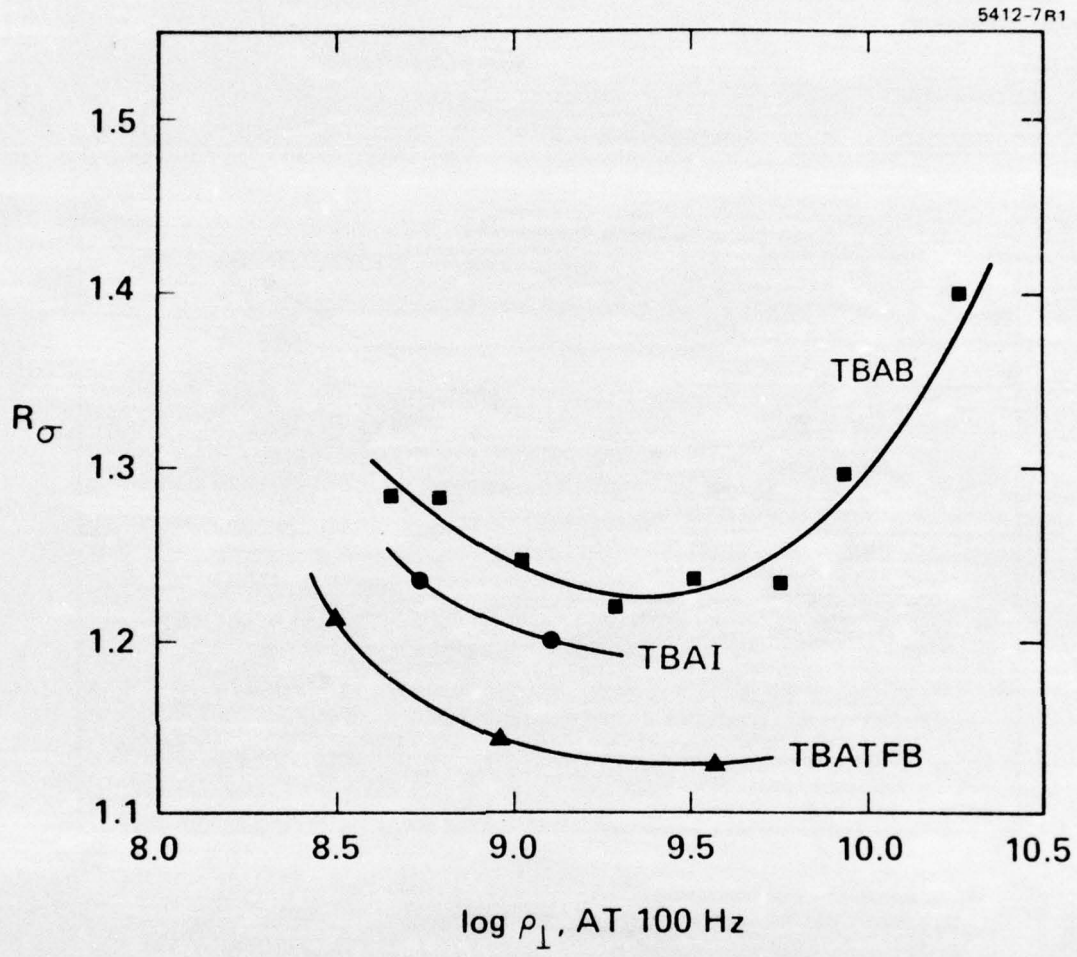

Fig. 2. Conductivity Anisotropy Ratio of an Ester Liquid Crystal Containing Different Dopant Structures and Concentrations, ∿25°C.

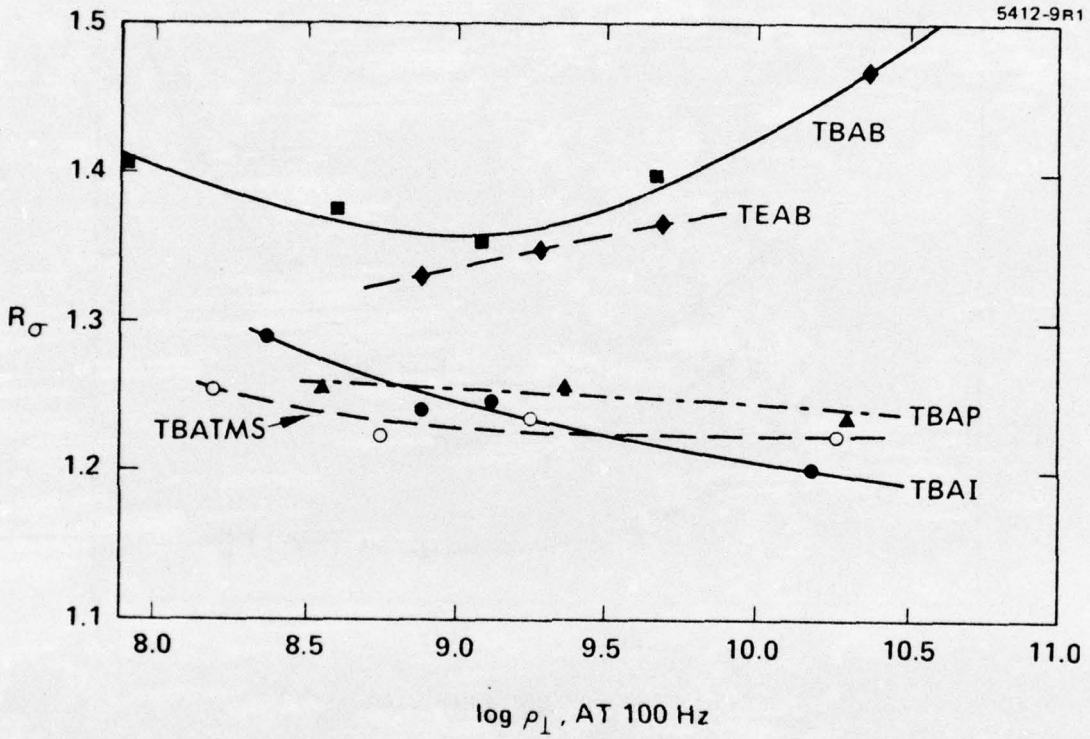

Fig. 3. Conductivity Anisotropy Ratio of MBBA Containing Different Dopant Structures and Concentrations, 25°C.

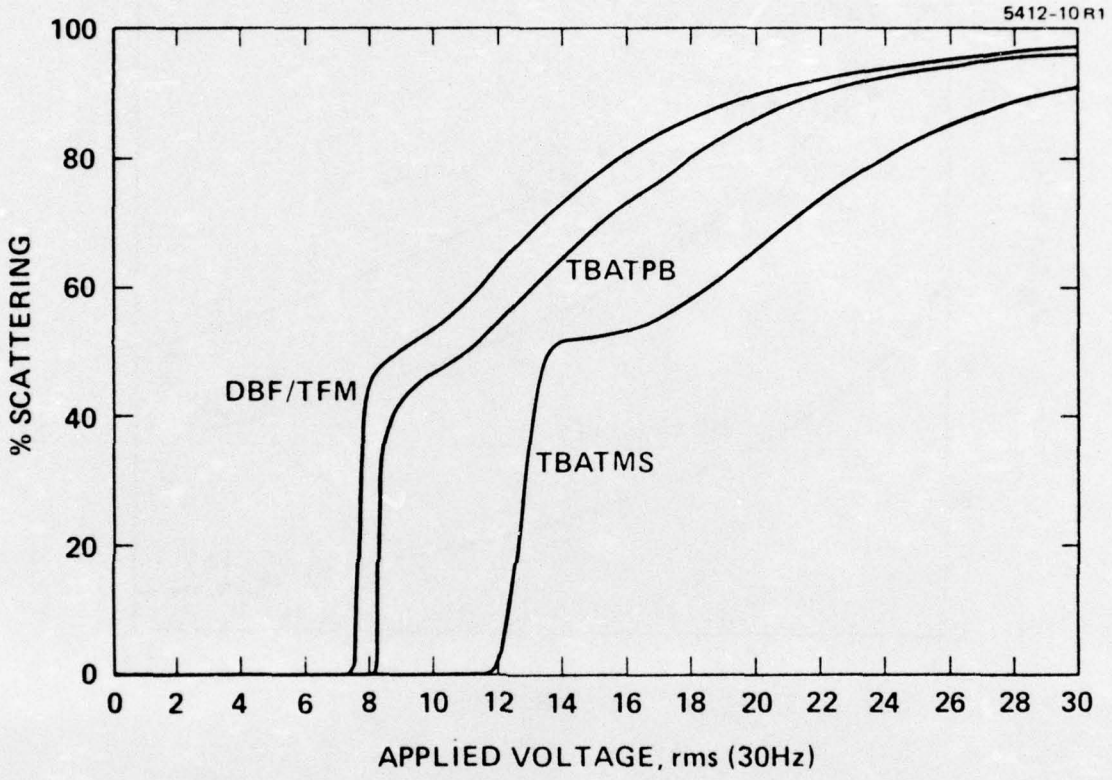

Fig. 4. Typical Dynamic Scattering Curves for Dopants in an Ester Liquid Crystal ($\rho_{\perp}$ = 1.0 x 10^9 ohm-cm, 12.7 μm thick cell spacers, surface-parallel alignment).

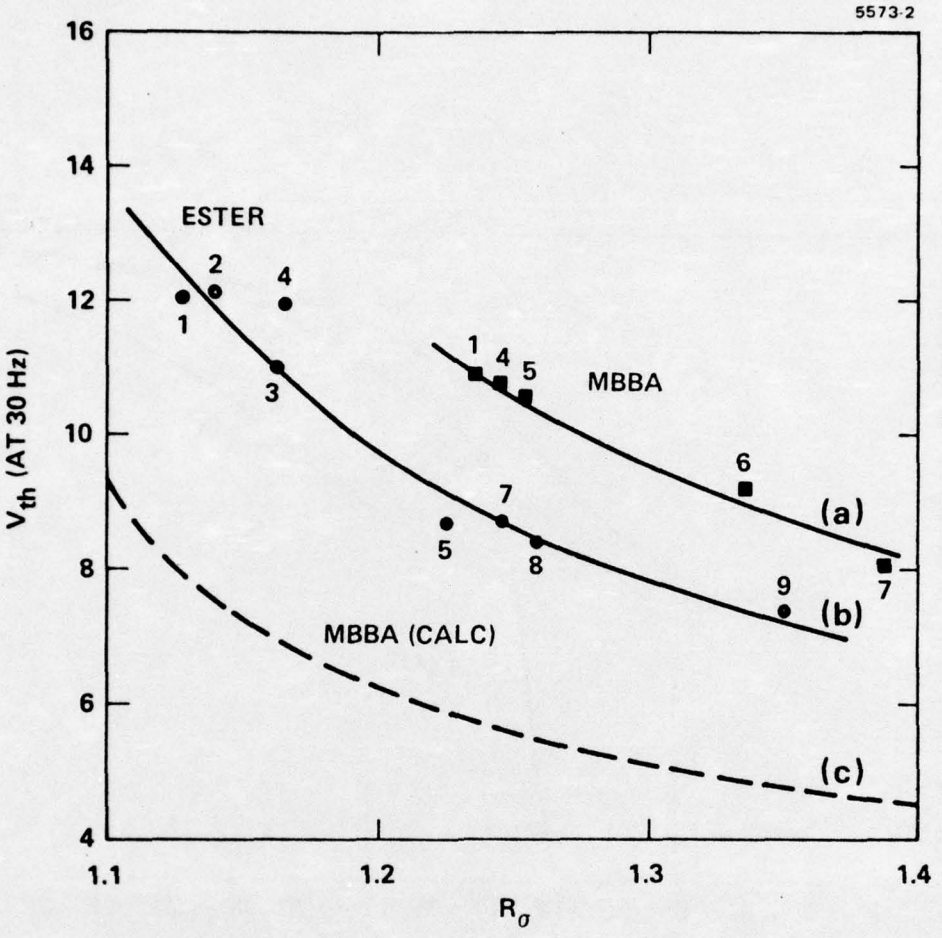

Fig. 5. Effect of Conductivity Anisotropy Ratio on Dynamic Schattering Thresholds ($\rho_\perp$ = 1.0 x 10^9 ohm-cm, 12.7 m thick spacer, surface-parallel alignment).
Curve a — experimental points for MBBA;
Curve b — experimental points for HRL-2N10;
Curve c — Helfrich equation calculation for MBBA.
Dopants: 1 = TBATMS
2 = TBATFB
3 = TBAP
4 = TBAI
5 = TBAC
6 = TEAB
7 = TBAB
8 = TBATPB
9 = DBF/TFM

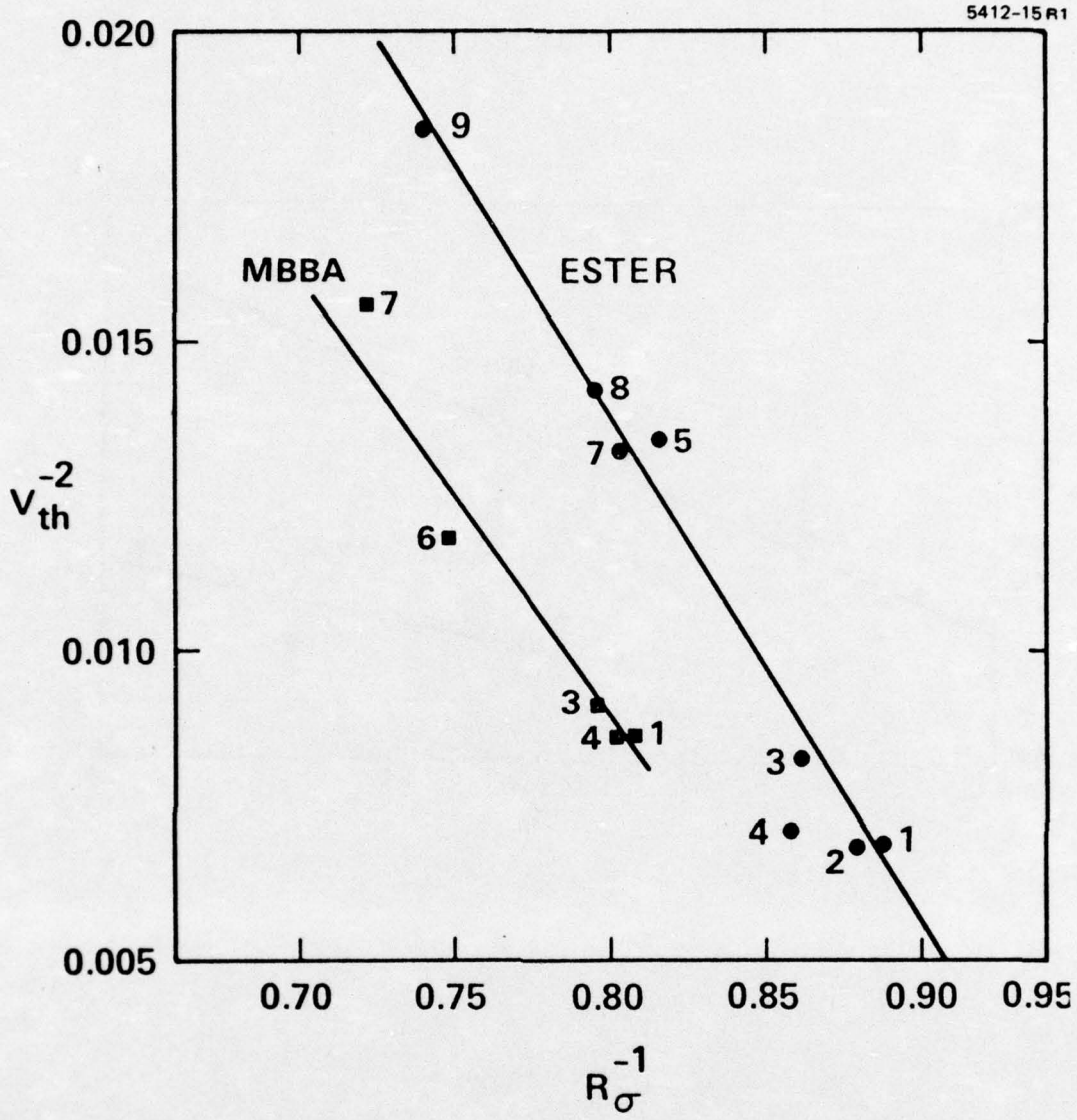

Fig. 6. Helfrich Equation Plots for Dynamic Scattering Threshold (same data and conditions as in Fig. 5).

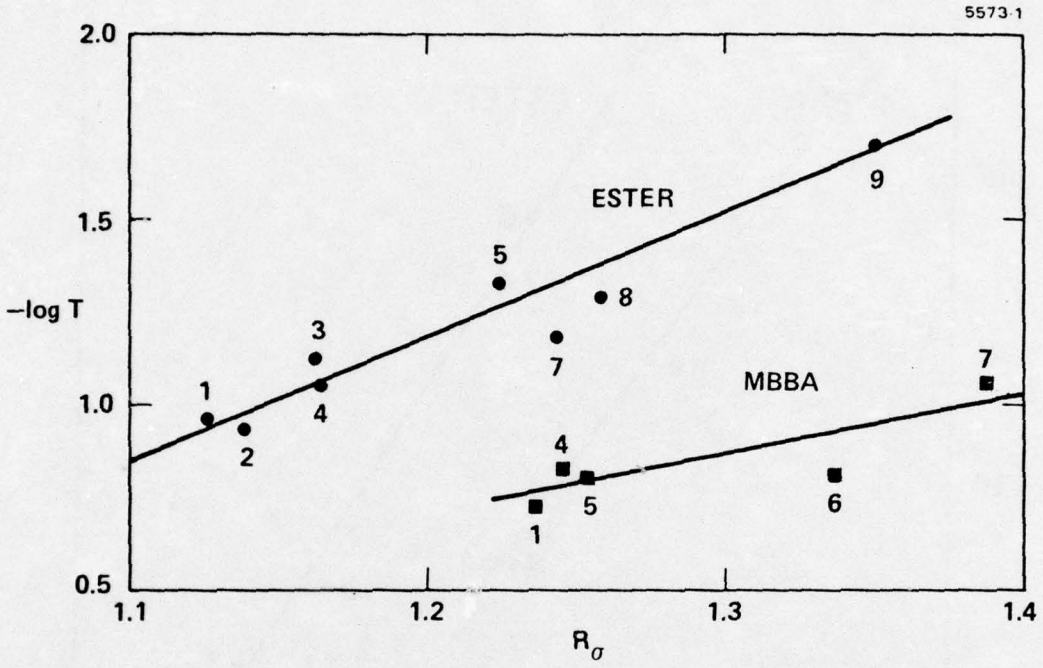

Fig. 7. Effect of Conductivity Anisotropy Ratio on the Optical Density of Scattering at 30 V rms (same conditions as in Fig. 5).

Table I. Comparison of Relative Anion Sizes and R_σ Values for TBA Salts in an Ester Liquid Crystal.

R_σ Value* (Increasing Magnitude)	Anion Size (Crystallographic) (Decreasing Magnitude)
$CF_3SO_3^-$	$(C_6H_5)_4B^-$
BF_4^-	$CF_3SO_3^-$
ClO_4^-	ClO_4^-
I^-	BF_4^-
Cl^-	I^-
Br^-	Br^-
$(C_6H_4)_4B^-$	Cl^-

*At $\sigma_\perp = 10^{-9}$ ohm^{-1} cm^{-1} in HRL-2N10.

APPENDIX E

Preprint

"Alignment Effects on the Dynamic Scattering Characteristics of an Ester Liquid Crystal"

by M. J. Little, H. S. Lim and J. D. Margerum

Submitted for publication in Molecular Crystals and Liquid Crystals

(Presented at Sixth International Liquid Crystal Conference, Kent, Ohio, August 1976.)

ALIGNMENT EFFECTS ON THE DYNAMIC SCATTERING CHARACTERISTICS OF AN ESTER LIQUID CRYSTAL*

M. J. Little, H. S. Lim, and J. D. Margerum
Hughes Research Laboratories
Malibu, California 90265

Abstract

The effects of surface alignment are studied on the ac dynamic scattering characteristics of a phenyl benzoate nematic liquid crystal. Seven different alignment modes are used with identical liquid crystal samples by pretreating the conductive glass surfaces to obtain the desired alignments. We find that the threshold voltage (V_{th}) increases with increasing initial average tilt angle ($\bar{\theta}$) between the liquid crystal director and the two electrode surfaces. The V_{th} increases linearly as the $\cos\bar{\theta}$ decreases. The surface-perpendicular alignment ($\bar{\theta} = 90°$) has almost twice the V_{th} of the surface-parallel alignment. The dynamic scattering decay times are considerably shorter when $\bar{\theta} = 0°$ than when $\bar{\theta} > 0°$. The scattering versus voltage curves and the microscopic domain patterns are highly dependent upon the initial alignment, even at 1.5 to 2.0 times V_{th}.

---

*Presented at the Sixth International Liquid Crystal Conference, Kent, Ohio, August 1976.

AD-A032 820 HUGHES RESEARCH LABS MALIBU CALIF F/G 7/4
MOLECULAR BASIS FOR LIQUID CRYSTAL FIELD EFFECTS.(U)
OCT 76 J D MARGERUM F44620-72-C-0075
UNCLASSIFIED AFOSR-TR-76-1181 NL

2 OF 2
AD A032820

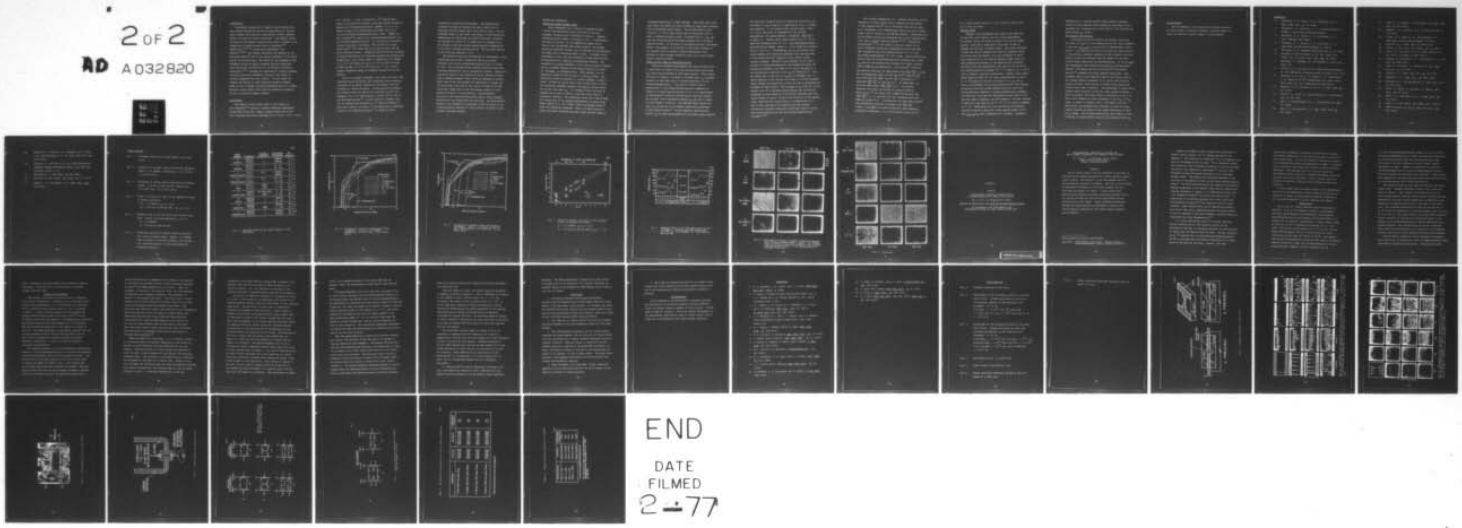

END

DATE
FILMED
2-77

INTRODUCTION

The dynamic scattering[1] of nematic liquid crystals has been studied extensively because of applications in electro-optic displays for electronic calculators, watches, message boards, and even flat panel television.[2] The display characteristics of the dynamic scattering are known to depend on the properties of liquid crystals such as viscosity,[3-6] conductivity,[3,4,7,8] conductivity anisotropy,[9] and dopants.[9,12-15] The dynamic scattering also depends on the electrode spacing[16] and on the surface alignment of the liquid crystal at the electrode. The effect of the alignment on the threshold voltage of domain formation has been predicted from theoretical calculations for two surface orientation conditions.[17-19] Although the importance of surface alignment has been recognized, systematic studies on the effect of various alignments have been lacking. In this report we compare the effects of seven different surface alignment modes on the ac dynamic scattering characteristics of a phenyl benzoate liquid crystal which contains conductivity dopants but has no surface alignment dopants.

EXPERIMENTAL

The nematic liquid crystal used in this study is a four-component[12,13] mixture of phenyl benzoates (designated as HRL-2N10) which has a nematic range of about 20° to 55°, and a negative dielectric anisotropy of $\Delta\varepsilon = (5.14 - 5.26) = -0.12$

(25°, 500 Hz). It has a resistivity 10^{11} ohm-cm before adding the conductivity dopants, which were either tetrabutylammonium trifluoromethanesulfonate (TBATMS), or a 1:1 (by weight) mixture of di-n-butylferrocene (DBF) and (2,4,7-trinitro-9-fluorenylidene)malononitrile (TFM). TBATMS is a salt prepared[20] by reaction of trifluoromethanesulfonic acid and tetrabutylammonium bromide. It is purified by recrystallization from water and drying. DBF and TFM are a redox dopant pair[12,13] in which DBF is an electron donor and TFM is an electron acceptor. Commercial DBF and TFM were purified by vacuum distillation and recrystallization from acetonitrile, respectively. The liquid crystal is doped with 0.1% TBATMS ($\rho_\perp \tilde{=} 2.0 \times 10^8$ ohm-cm and $\sigma_\parallel/\sigma_\perp \tilde{=} 1.23$) or with 0.5% each of DBF and TFM ($\rho_\perp \tilde{=} 1.8 \times 10^9$ and $\sigma_\parallel/\sigma_\perp \tilde{=} 1.34$), giving roughly comparable ranges of threshold voltage for the two samples.

Prior to alignment treatments, the indium tin oxide (ITO) conductive glass electrodes (PPG Industries) were cleaned by a sequence of scrubbing, degreasing and chromic acid etch followed by rinsing and drying. Surface-parallel alignment was obtained either by rubbing the electrode surface with Kimwipes or by a 30° angle deposit of about 100 Å of SiO on the electrode surface.[21] A tilted parallel alignment (36° off the surface) was obtained by a 5° angle SiO deposit.[22] The liquid crystal tilt angle (θ) was measured by a technique similar to one reported recently,[23] in which we used a

differential capacitance measurement. The perpendicular alignment was made by bonding long alkyl chains onto an electrode surface coated with a thin layer of SiO_2. Various alignment modes in test cells (see Figure 1) were obtained by combinations of electrodes with these three basic alignment. The average tilt angle ($\bar{\theta}$) in these cells is assumed to be the average of the two surface angles measured independently in the basic alignment configurations. The electrode spacing of the cells was nominally 13 μm.

The dynamic scattering was measured in transmission, using unpolarized green light (centered at 525 nm) at normal incidence and a silicon photodiode detector with a 2° field of view. The scattering versus voltage curves are from slow-scan measurements with 100 Hz (sinusoidal) signals. Repetitive electrical pulses of two seconds on and ten seconds off were used to measure response times, which are defined as follows: delay time is the time between the application of signal and 10% scattering; rise time is the time to go from 10% to 90% scattering; decay time is the time between removal of this signal and return to 10% scattering. The microscopic pictures of the scattering were taken using a Zeiss standard WL polarizing microscope with one polarizer. The polarization direction was adjusted to be parallel to the direction of the surface-parallel component of liquid crystal alignment at the incident electrode surface.

RESULTS AND DISCUSSION

Scattering Versus Voltage Curves

Light transmission as a function of applied voltage (100 Hz) was obtained for cells with each of the nine alignment configurations illustrated in Figure 1. Typical scattering curves (where % scattering = 100 - % transmission) are shown in Figure 2 for the TBATMS salt dopant and in Figure 3 for the DBF/TFM redox dopant system. The dynamic scattering threshold voltage (V_{th}) is obtained by extrapolating the steep rise in scattering back to zero. It agrees, within experimental error, with the threshold voltages observed with the microscope for formation of hydrodynamic domains. The threshold is strongly dependent on the initial surface alignment and V_{th} increases sharply as the average surface tilt angle ($\bar{\theta}$) increases, as discussed below. There appears to be no substantial effect of the 90° twist on the V_{th} values. The scattering curves for parallel or tilted alignment, without a twist, (curves A, B, and E) show a wide voltage range in which the scattering increases steadily with applied voltage above the initial rise near V_{th}. In a display device this type of response can be used to obtain a good gray scale range of scattering intensity. The scattering curves with large average tilt angles such as the surface-perpendicular or splay alignments (curves G, H, and I) show a field realignment effect[24] below the scattering threshold. They go to high scattering levels just above threshold and have a much narrower range of

increased scattering at higher voltages. This shows that cells with large tilt angles are less suitable for gray scale displays, with a multiplexed input signal. The twisted nematic cells (curves C, D, and F) show unique type of scattering curve in which a maximum scattering level is reached prior to $2V_{th}$ and then the scattering level decreases slightly with increasing applied voltage. On the basis of microscope pictures (discussed below), this appears to be related to the strong tendency of the twisted cells to maintain regular hydrodynamic flow patterns at high voltages instead of going into a more random dynamic scattering mode.

Effect of Tilt Angle on Threshold Voltage

Duplicate threshold measurements were made on each of two or more cells for each of the nine configurations and average V_{th} values were obtained for each dopant system. These values are given in Figure 4, in which it is shown that V_{th} increases linearly as $\cos\bar{\theta}$ goes from 1.0 (surface-parallel) to zero (surface-perpendicular). The $\cos\bar{\theta}$ is a factor that is proportional to the average surface-parallel component of length of a liquid crystal molecule, i.e., it is proportional to the projected length of the molecule on the cell surface. The straight line relationship between V_{th} and $\cos\bar{\theta}$ is shown for each dopant in Figure 4. The DBF/TFM dopant system has lower V_{th} values due to its higher conductivity anisotropy in this liquid crystal.[9] We have observed, qualitatively, similar V_{th} vs $\cos\bar{\theta}$ relationships for two other liquid crystals

that have more negative values of dielectric anisotropy, but the effect on V_{th} is smaller in magnitude as their $\Delta\varepsilon$ becomes more negative. In the present ester liquid crystal, where $\Delta\varepsilon = -0.12$, the ratio of thresholds for the surface-perpendicular and surface-parallel alignments, $(V_{th}^{S-\perp}/V_{th}^{S-\parallel})$, is about 1.7. Another ester liquid crystal with $\Delta\varepsilon = -0.26$ shows the threshold ratio of ∿1.3. N-p-(Methoxybenzylidene)-p-n-butylaniline (MBBA), whose $\Delta\varepsilon = -0.53$, shows the threshold ratio of only ∿1.1. Nevertheless, the V_{th} for dynamic scattering appears to be partially dependent upon the magnitude of the surface-parallel component of the initial liquid crystal alignment. Although field alignment of the liquid crystals in surface-perpendicular cells begins far below the scattering threshold, even MBBA is not fully realigned to a surface-parallel condition at the V_{th} for scattering.[25] Only the center part of the cell at V_{th} has an alignment that is nearly parallel to the surface, and there is a tilted alignment region between the center part of the cell and the perpendicular alignment at each surface. The increase of V_{th} with the initial surface tilt ($\bar{\theta}$) is probably mainly because the conductivity anisotropy is less effective in producing turbulence when the liquid crystal is partly tilted in the direction of the applied field, than when the liquid crystal is perpendicular to it. This is also consistent with observations that dynamic scattering in positive dielectric anisotropy materials occurs with surface-parallel but not with surface-perpendicular alignment.[26,27]

The critical frequencies (i.e., dynamic scattering cut-off frequency) of these liquid crystal samples are high enough so that theoretically[23] our ac thresholds would be the same as dc thresholds in the TBATMS-doped samples and only slightly higher than dc values for the DBF/TFM samples. (Experimentally, the dc dynamic scattering thresholds are in fact substantially lower due to charge injection effects.[12,13]) Theoretical calculations[17-19] on the effect of the tilt angle ($\bar{\theta}$) on the dc threshold voltage for hydrodynamic motion have been made considering only the surface-parallel ($\bar{\theta} = 0°$) and the surface-perpendicular ($\bar{\theta} = 90°$) cases. These calculations predict that the surface-perpendicular alignment has a lower V_{th} than the surface-parallel alignment for liquid crystals such as MBBA and p-azoxyanisole. Calculations[18] using the the Helfrich equations for MBBA predict that $(V_{th}^{S-\perp}/V_{th}^{S-\parallel}) = 0.86$. The two-dimensional model of Penz and Ford[19] predicts $V_{th}^{S-\parallel}$ more accurately for MBBA, but not $V_{th}^{S-\perp}$, resulting in a predicted $V_{th}^{S-\perp}/V_{th}^{S-\parallel}$ of less than 0.7. As noted above, we find that MBBA shows a $(V_{th}^{S-\perp}/V_{th}^{S-\parallel}) \simeq 1.1$. Our results regarding this ratio are similar to recent results of Barnik et al.,[29] who report that a MBBA-like material has $(V_{th}^{S-\perp}/V_{th}^{S-\parallel}) \approx 1.4$, and that the ratio increases with less negative values of $\Delta\varepsilon$. It should also be noted that Gruler[18] used the Helfrich equations to predict that $V_{th}^{S-\perp}/V_{th}^{S-\parallel}$ ratios >1 for MBBA-like liquid crystals of small negative dielectric anisotropy, e.g., he calculated a ratio of ~1.4

for a liquid crystal with $\Delta\varepsilon \approx -0.12$, while we find a ratio of $\sim$1.7 for our ester.

Response Times

Response time measurements were made on the same sets of duplicate cells used for the tilt angle measurements. The average values are shown in Figure 5 for the two dopant systems. Note that a logarithmic time scale is used to compress the data for a graphic format. The actual thickness of each cell was not measured and there are probably enough variations from the nominal 13 μm cell thickness to cause some inaccuracies in the relative response times, which are approximately proportional to the square of the thickness. The decay times are approximately the same for all the cells with surface-parallel alignment ($\bar{\theta} = 0°$ in modes A, B, C, and D) with or without a twisted configuration. However, much longer decay times are shown for all other configurations in which $\bar{\theta} > 0$ ($\bar{\theta}$ between 36° and 90° for cells E, F, G, H, and I). This is in agreement with previous observations[30] that dynamic scattering from short pulses decayed faster in cells with surface-parallel compared to surface-perpendicular alignment. The delay and rise times are considerably longer when $\bar{\theta} = 90°$ than for other alignments, and there appears to be some increase in delay and rise times in the $\bar{\theta} = 36°$ to 63° range as compared to $\bar{\theta} = 0°$. These delay and rise time effects are probably related to the fact that with a fixed applied signal of 30 V the $V_{applied}/V_{th}$ ratio decreases as $\bar{\theta}$ increases. Alignment

configuration F (twisted tilted) shows somewhat anomalous results of slow response times compared to the simple tilted alignment (E), although both F and E have $\bar{\theta} = 36°$ and have the same average V_{th} values.

Microscopic Flow Patterns

Microscope pictures of domains and dynamic scattering are shown in Figure 6, with comparisons for the nine alignments at the same $V_{applied}/V_{th}$ ratios with the TBATMS-doped liquid crystal. The pictures are taken with polarized light parallel to the parallel alignment direction on the incident electrode. Similar results are observed (but not shown) for the same liquid crystal doped with the DBF/TFM mixture. At low voltages the hydrodynamic flow patterns correspond to Williams-type[31] domains. The domain patterns for parallel[32] and twisted parallel[33] alignments have been observed previously. Each alignment shows a characteristic-type of low voltage pattern. The twisted nematic alignments (C, D, and F) show the most regular patterns, which persist at higher V/V_{th} values than patterns with other alignments. The persistence of these fairly regular domain patterns instead of a more random turbulence may be related to the lower levels of scattering in the C, D, and F cells compared to other alignments in the $2V_{th}$ to $4V_{th}$ range, as shown in Figures 2 and 3. The splay (G,H) and particularly the perpendicular alignment (I) show the least regular patterns and they go into random turbulence at lower V/V_{th} values. The surface-perpendicular cells appear to have virtually no regular domain patterns just slightly above V_{th}.

ACKNOWLEDGMENT

We are indebted to the Directorate of Chemical Sciences, Air Force Office of Scientific Research, Contract F44620-72-C-0075 for partial financial support of this research.

References

1. Heilmeier, G. H., Zanoni, L. A., and Barton, L.A., Appl. Phys. Lett., 13, 46 (1968).
2. Margerum, J. D. and Miller, L. J. (A review article, in press, J. Colloid and Interface Science.)
3. Heilmeier, G. H., Zanoni, L. A., and Barton, L. A., Proc. IEEE 56, 1162 (1968).
4. Heilmeier, G. H., Zanoni, L. A., and Barton, L. A., IEEE Trans. Electron Devices ED-17, 22 (1970).
5. de Gennes, P. G., Comments Solid State Phys. 3, 35 (1971).
6. Koelmans, H. and van Boxtel, A. M., Mol. Cryst. Liq. Cryst., 12, 185 (1971); Phys. Lett. 32A, 32 (1970).
7. Matsumoto, S., Kawamoto, M., and Tsukada, T., Chem. Lett. 1973, 837.
8. Aldrich, R. E. and Lauer, R. B., IEEE Conference Records of 1972 Conference on Display Devices, October 11-12, 1972.
9. Margerum, J. D., Lim, H. S., Braatz, P. O., and Lackner, A. M., paper K-1 at 6th International Liq. Cryst. Conf., Kent, Ohio, Aug. 1972 (submitted for publication).
10. Wargocki, F. E., and Lord, Jr., A. E., J. Appl. Phys. 44, 831 (1973).
11. Elliott, G., Harvey, E., and Williams, M. G., Electronics Lett. 9, 399 (1973).
12. Lim, H. S. and Margerum, J.D., J. Electrochem. Soc. 123, 837 (1976).
13. Lim, H. S. and Margerum, J. D., Appl. Phys. Lett. 28, 378 (1976).

14. Baise, A. I., Teucher, I., and Labes, M. M., Appl. Phys. Lett. 21, 142 (1972).

15. Creagh, L. T., and Kmetz, A. R., J. Electron. Mat. 1, 350 (1972).

16. Creagh, L. T., Kmetz, A. R., and Reynolds, R. A., IEEE Trans. Electron Devices ED-18, 672 (1971).

17. Helfrich, W., J. Chem. Phys. 51, 4092 (1969).

18. Gruler, H., Mol. Cryst. Liq. Cryst., 27, 31 (1974).

19. Penz, P. A., and Ford, G. W., (a) Phys. Review A, 6, 414 (1973), (b) ibid., 6, 1676 (1972).

20. Ronseau, K., Farrington, G. C., and Dolphin, D., J. Org. Chem. 37, 3968 (1972).

21. Guyon, E., Pieranski, P., and Boix, M., Lett. Appl. Eng. Sci., 1, 19 (1973).

22. Janning, J. L., Appl. Phys. Lett. 21, 173 (1972).

23. Myerhofer, D., J. Appl. Phys., 46, 5084 (1975).

24. Schiekel, M. F., and Fahrenschon, K., Appl. Phys. Lett., 19, 391 (1971).

25. Ohtsu, M., Akahne, T., and Tako, T., Japan J. Appl. Phys., 13, 621 (1974).

26. Baise, A. E., and Labes, M. M., J. Chem. Phys., 59, 551 (1973).

27. Penz, P. A., Mol. Cryst. Liq. Cryst., 23, 1 (1973).

28. Dubois-Violetti, E., et al., Phys. Rev. Lett., 25, 1642 (1970).

29. Barnik, M. I., Blinov, L. M., Grabenkin, M. F., Pikin, S. A., and Chigrinov, V. G., Zh. Eksp. Teor. Fiz., 69, 1080 (1975).

30. Aftergut, S., and Cole, H. S., 1972 SID International Symposium Digest of Technical Papers, June 1972, San Francisco, Calif. p. 92.

31. Williams, R., J. Chem. Phys. 39, 384 (1963).

32. Helfrich, W., Mol. Cryst. Liq. Cryst., 21, 187 (1973).

33. Wright, J. J., and Dawson, J. F., Phys. Lett., 43A, 145 (1973).

Figure Captions

Fig. 1. Alignment modes of the liquid crystal in the test cells.

Fig. 2. Scattering vs voltage curves with various alignments. Dopant: 0.1% TBATMS. Resistivity: $\sim 2 \times 10^8$ Ω-cm. 13 μm thick cells.

Fig. 3. Scattering vs voltage curves with various alignments. Dopant: 0.5% each of DBF and TFM. Resistivity: $\sim 1.8 \times 10^9$ Ω-cm. 13 μm thick cells.

Fig. 4. Effect of surface tilt angle on the threshold voltage of dynamic scattering.

⊙ : 0.1% TBATMS, $(\sigma_{\parallel}/\sigma_{\perp}) = 1.23$

⊡ : 0.5% each of DBF and TFM, $(\sigma_{\parallel}/\sigma_{\perp}) = 1.34$

Fig. 5. Response times of the test cells with various alignments. Nominal electrode separation: 12.7 μm.

A: 0.1% TBATMS

B: 0.5% each of DBF and TFM.

Fig. 6. Microscopic pictures of dynamic scattering patterns with various alignment modes. Dopant: 0.1% TBATMS. (View is normal to electrode surfaces, with incident

CODE (NAME)	DIAGRAM	SURFACE ALIGNMENT	ALIGNMENT TECHNIQUE	TILT ANGLES $\bar{\theta}$	
A		//	RUBBING	0°	0°
(PARALLEL)		//	RUBBING	0°	
B	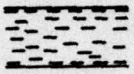	//	30° - SiO	0°	0°
(PARALLEL)		//	30° - SiO	0°	
C	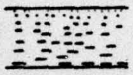	90° //	RUBBING	0°	0°
(TWISTED PARALLEL)		//	RUBBING	0°	
D	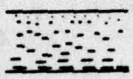	90° //	30° - SiO	0°	0°
(TWISTED PARALLEL)		//	30° - SiO	0°	
E	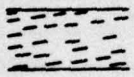	TILTED	5° - SiO	36°	36°
TILTED		TILTED	5° - SiO	36°	
F		90° TWIST-TILTED	5° - SiO	36°	36°
(TWISTED TILTED)		TILTED	5° - SiO	36°	
G		⊥	CHEMICAL	90°	45°
(SPLAY)		//	30° - SiO	0°	
H		⊥	CHEMICAL	90°	63°
(TILTED SPLAY)		TILTED	5° - SiO	36°	
I		⊥	CHEMICAL	90°	90°
(PERPENDICULAR)		⊥	CHEMICAL	90°	

Fig. 1. Alignment modes of the liquid crystal in the test cells.

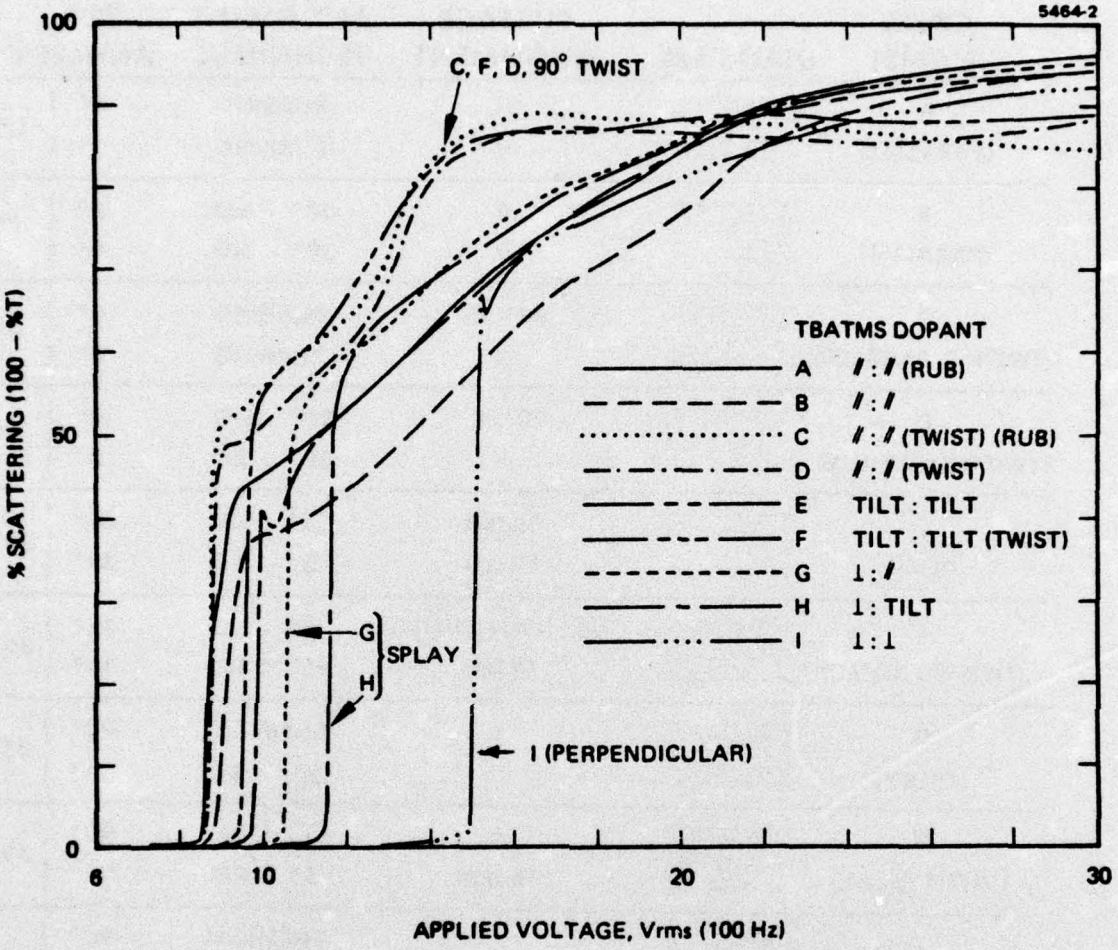

Fig. 2. Scattering vs voltage curves with various alignments. Dopant: 0.1% TBATMS. Resistivity: $\sim 2 \times 10^8$ Ω-cm. 13 μm thick cells.

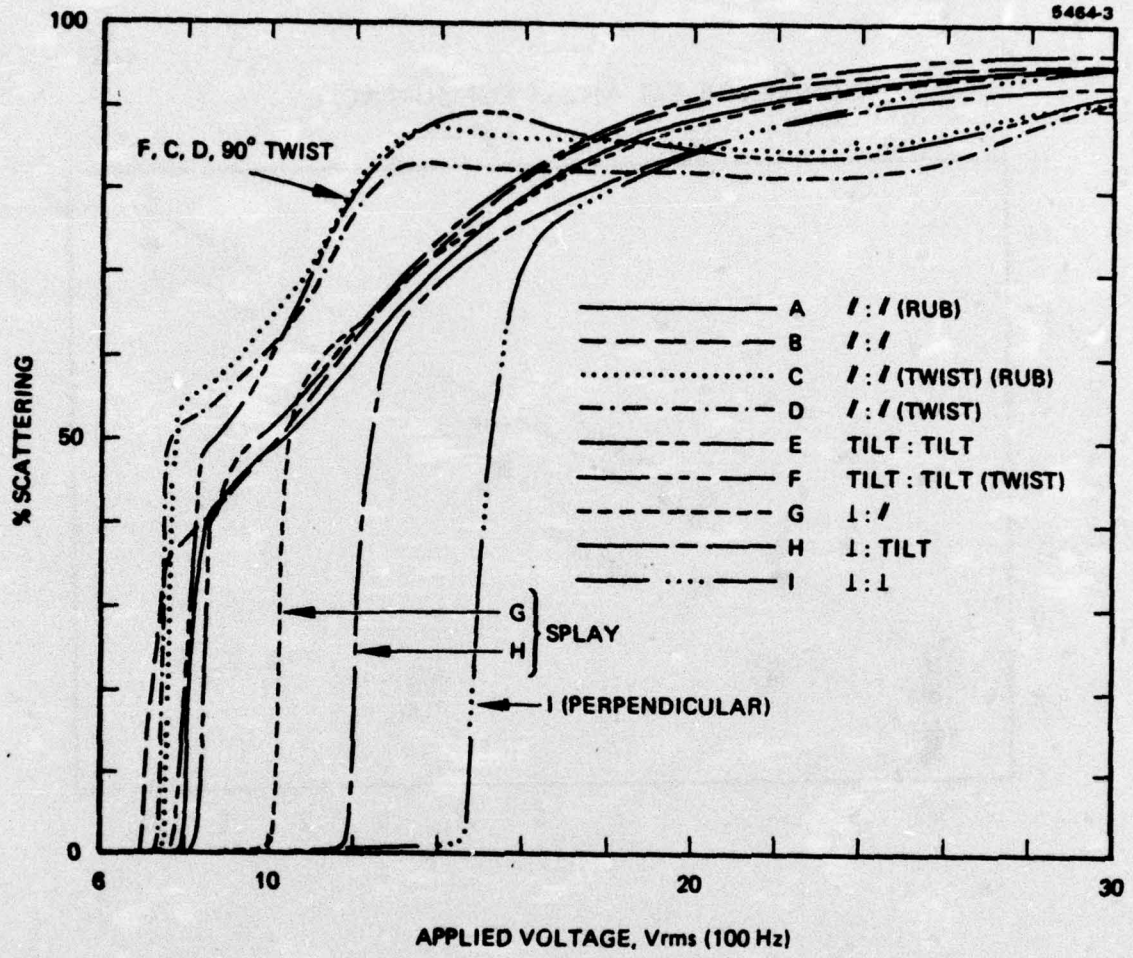

Fig. 3. Scattering vs voltage curves with various alignments. Dopant: 0.5% each of DBF and TFM. Resistivity: $\sim 1.8 \times 10^9$ Ω-cm. 13 μm thick cells.

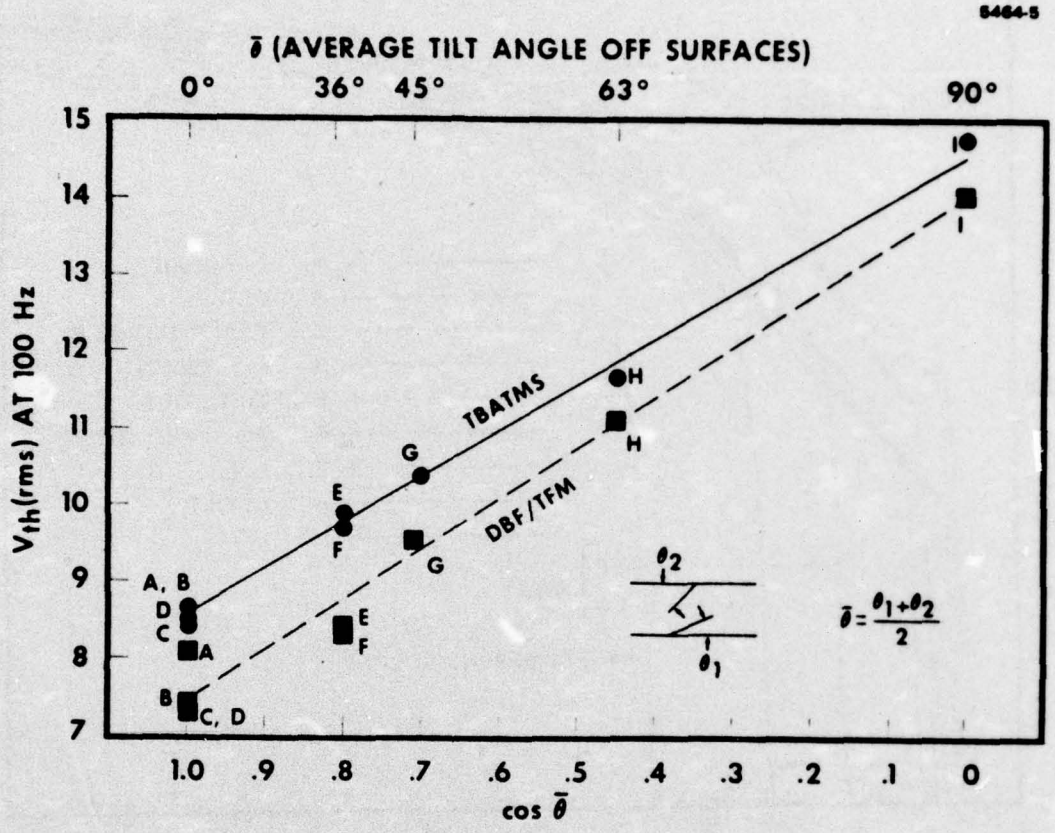

Fig. 4. Effect of surface tilt angle on the threshold voltage of dynamic scattering.

⊙: 0.1% TBATMS $(\sigma_{\parallel}/\sigma_{\perp}) = 1.23$.

⊡: 0.5% each of DBF and TFM $(\sigma_{\parallel}/\sigma_{\perp}) = 1.34$.

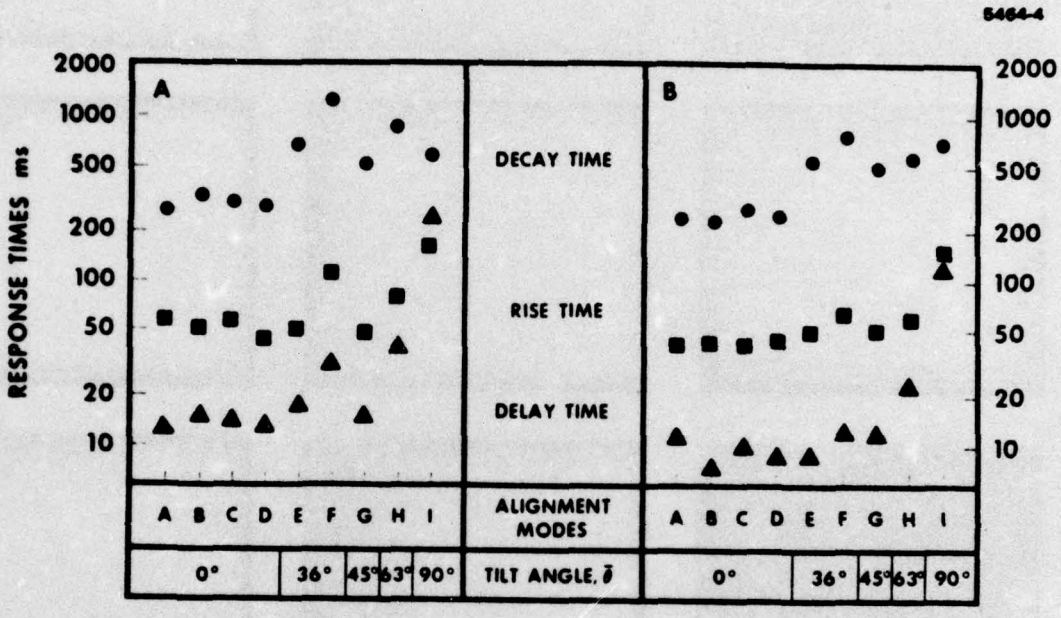

Fig. 5. Response times of the test cells with various alignments. Nominal electrode separation: 12.7 μm. A: 0.1% TBATMS. B: 0.5% each of DBF and TFM.

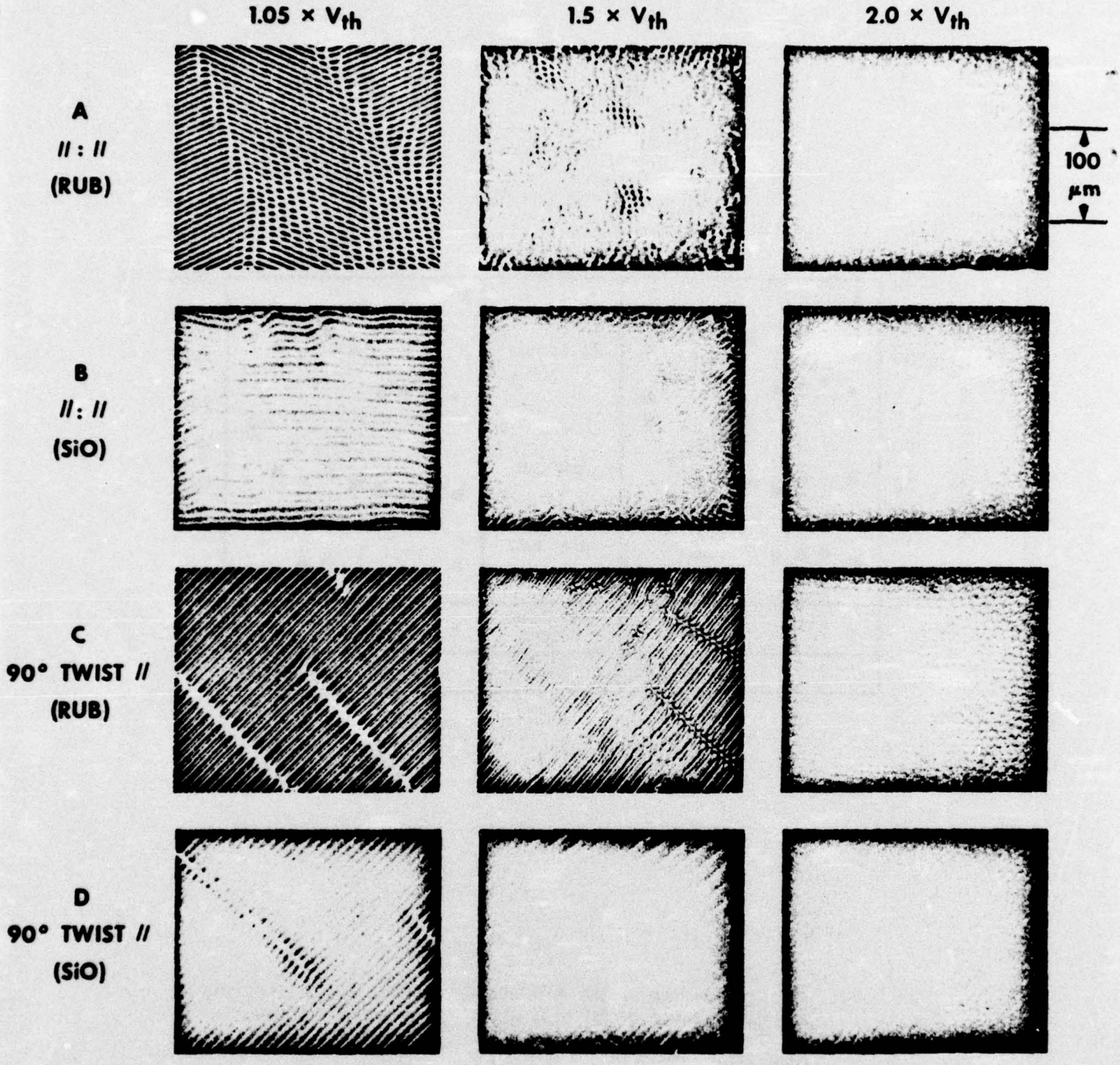

Fig. 6. Microscopic pictures of dynamic scattering patterns with various alignment modes. Dopant: 0.1% TBATMS. (View is normal to electrode surfaces, with incident light polarized parallel to the surface-parallel alignment direction.)

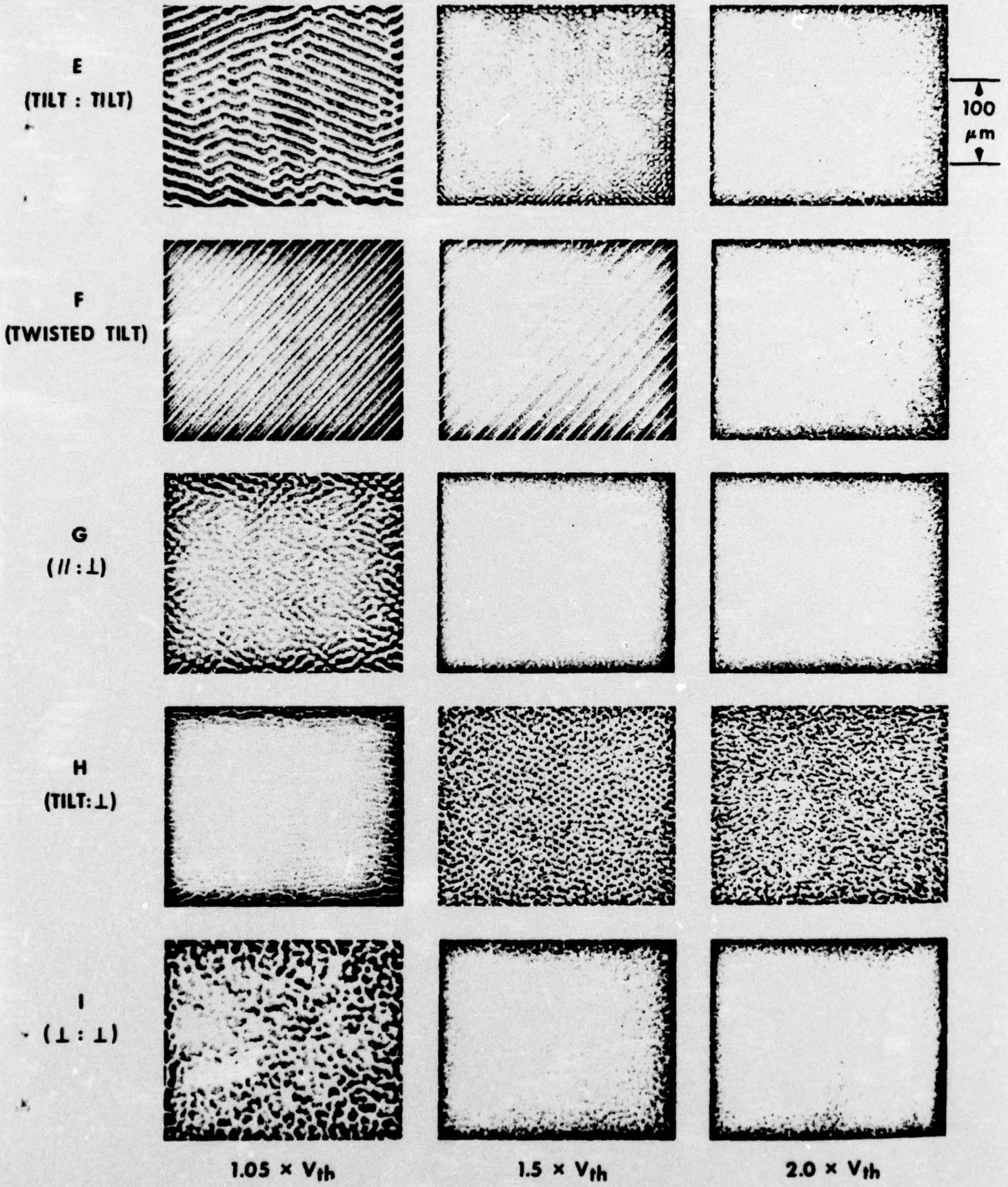

Fig. 6. Continued.

APPENDIX F

Preprint

"Electrochemical Properties of Dopants and the
DC Dynamic Scattering of a Nematic Liquid Crystal"

by H. S. Lim, J. D. Margerum and A. Graube

Submitted for publication in the Journal of the Electrochemical Society

(To be presented at the 150th meeting of the
Electrochemical Society, Las Vegas, Nevada, October 1976.)

ELECTROCHEMICAL PROPERTIES OF DOPANTS AND THE DC DYNAMIC SCATTERING OF A NEMATIC LIQUID CRYSTAL

H. S. Lim,* J. D. Margerum, and A. Graube
Hughes Research Laboratories
Malibu, California 90265

ABSTRACT

Flow of liquid crystal from one electrode to the other is observed during dynamic scattering of a phenyl benzoate nematic liquid crystal. The direction of the flow depends upon the electrochemical properties of dopants. The flow is from cathode to anode when the dopant is an electron acceptor and vice versa when the dopant is a donor. A redox dopant gives distinctively different dc dynamic scattering patterns from a salt dopant and does not give the Williams domain pattern observed with a salt dopant. Charge conduction mechanisms through the liquid crystal are discussed in terms of the electrochemical properties of the liquid crystal component and the dopants.

---

*Electrochemical Society Active Member.

Key words: redox dopant, salt dopant, charge injection, electrohydrodynamic motion, dynamic scattering.

Dopants are commonly used to improve the properties of nematic liquid crystals (LC) for dynamic scattering (DS) displays.[1] The conductivity anisotropy[2-4] of a LC depends very much on the dopants which are used. The ac threshold voltage and scattering level of dynamic scattering of LC's are strongly affected by the conductivity anisotropy,[3,4] giving a lower threshold voltage and higher scattering as the anisotropy becomes larger. The conductivity anisotropy depends on the structure of the dopants as well as the liquid crystal material itself.[4] The dc-DS characteristics also depend on the electrochemical properties of the dopant; redox dopants consisting of electron acceptors, or donors, or a combination of both, give a low threshold voltage[5,6] and a high scattering level.[6] A combination of an electron acceptor and a donor gives good electrochemical stability[6-8] for long-term dc-DS of liquid crystals. Redox dopants which can be reduced and oxidized much easier than the LC compounds minimize the participation of the LC compounds in the electrochemical reactions which are responsible for their decomposition.[6,9]

In a recent preliminary report,[9] we showed that the charge injection and LC flow direction as well as the localization and type of scattering patterns in a dc-activated LC depend upon the dopants which are used. Earlier, Heilmeier et al.,[10] reported that in anisylidene-p-aminophenylacetate the DS is initiated from the negative electrode and is propagated to the positive electrode. However, they used

geometrically dissimilar electrodes and they did not specify the dopants responsible for the observed conductivity and DS of their Schiff base. Lacroix and Tobazeon[11] carried out studies on N-(p-methoxybenzylidene)-p-n-butylaniline (MBBA) in a special cell in which the electrodes were coated with anion permeable membranes. They observed that the LC motion started at the negative (anion injecting) electrode and spread toward the positive (collector) electrode, giving a "finger" type flow pattern followed by a turbulent region spreading toward the collector.

In the present paper we report studies on the hydrodynamic motion of LC and mechanism of charge transport through the LC during DS in terms of electrochemical property of dopants as well as electrochemistry of the LC compounds and dopants.

Experimental

The LC used is a phenyl benzoate mixture designated as HRL-2N10. It is a four-component mixture of p-butylphenyl p-toluate, p-butoxyphenyl p-butoxybenzoate, p-butoxyphenyl p-hexyloxybenzoate and p-butoxyphenyl p-octyloxybenzoate in a weight ratio of 15:5:9:9, respectively. It has a nematic range of about 20° to 55°, a dielectric anisotropy of $\Delta\varepsilon = -0.12$ (25°C, 500 Hz) and a birefringence of $\Delta n = 0.14$ (25°, 545 nm). Before adding dopants, the LC is highly resistive, with a resistivity greater than 10^{11} ohm-cm at 100 Hz. The dopants used include electrochemically inactive salts such as tetrabutylammonium perchlorate (TBAP) and tetrabutylammonium trifluoromethanesulfonate (TBATMS); electron acceptors such as

7,7',8,8'-tetracyanoquinodimethane (TCNQ) and (2,4,7-trinitro-9-fluorenylidene)malononitrile (TFM); and electron donors such as di-n-butylferrocene (DBF) and tetrathiofulvalene (TTF). The acceptor and donor dopants are called "redox" dopants throughout the paper. TBATMS was prepared[12] by reaction of trifluoromethanesulfonic acid and tetrabutylammonium bromide. The crude product was recrystallized from water. Other dopants were commercially available materials which were purified either by recrystallization or by vacuum distillation.

Two different types of test cells are used for the microscopic study. Schematic diagrams of type A and B cells are shown in Figure 1. The purpose of the type B cell is to allow enough space so that the liquid crystal can move from one electrode to the other without generating a compensating flow because of the spatial restriction in the case of the type A cell. The electrode separations (S) were varied from 180 μm to 600 μm and the thickness of the liquid crystal layer (d) from 25 μm to 200 μm. The liquid crystal is aligned either perpendicular or parallel to the electric field and parallel to the surface of the glass substrates by a rubbing technique unless stated otherwise. The microstructure of the DS is observed from a direction perpendicular to the direction of the applied electric field using a Zeiss standard WL polarizing microscope.

Electrochemical studies of the LC components and dopants were carried out in acetonitrile (ACN) or dimethylformamide (DMF) using TBAP as supporting electrolyte. Techniques used were

cyclic voltammetry and polarography using platinum or mercury electrodes. Potentials were measured against a saturated calomel electrode (SCE).

Results and Discussions

Both cathodic and anodic reactions of the LC components were totally irreversible. Oxidations occur at potentials more positive than approximately 1.7 V (versus SCE) and reductions occur at potentials more negative than ca. -2.2 V, as shown in Table I. Primary reaction products of both cathodic and anodic processes would probably be radical ions[13,14] of the LC esters, which would be unstable in the experimental conditions. Electrode reactions of the redox dopants are all reversible. The formal reduction potentials of the dopants are listed in Table II. Low redox potentials of the dopants indicate that the electron acceptors such as TFM and TCNQ and donors such as DBF and TTF are expected to dominate cathodic and anodic processes, respectively, in the LC if they are present in sufficient concentrations.

The dominating effects of the electrochemical properties of dopants on the electrohydrodynamics of the LC have been observed during the microscopic study of DS with applied dc fields. The characteristic microscopic patterns of DS with various types of dopants are shown in Figures 2 and 3. Salt dopants and redox dopants show distinctly different DS patterns. When the dopant is salt-type and the liquid crystal alignment is perpendicular to the electric field, the scattering pattern has a

line structure which is asymmetric with respect to the polarity of the field but otherwise similar to that previously observed by Chang[15] with MBBA subjected to an ac signal. (When the alignment is parallel to the electric field, the line structure is spatially very irregular; otherwise, the appearance is similar to the perpendicular case.) Thin flow lines of liquid crystal are initiated from both electrodes visibly at the same time and propagated toward the opposite electrodes. Dust particles move along the lines in the direction of the propagation, indicating that the lines are caused by liquid crystal flow. These particles continue to move back and forth along the finger-type flow lines and there appears to be little or no net flow of liquid crystal from one electrode to the other, even with type B cells in which room for net flow is provided. This observation is consistent with earlier observations on Williams domain patterns.[16]

When the dopant is a redox-type, i.e., an electron acceptor or an electron donor, the general appearance of the scattering pattern is quite different from that observed with the salt dopants. Turbulent motions of liquid crystal are observed at lower voltages, without formation of the regular line structure discussed above. The turbulence is initiated from one electrode and propagated to the other at a visible rate. Except at very high voltages, the turbulence does not reach the opposite electrode and remains localized near the electrode where it was initiated (Figures 2 and 3). A surprising observation is that the

turbulence is initiated from the cathode when the dopant is an electron donor and from the positive when the dopant is an electron acceptor, i.e., the turbulence is observed at the opposite electrode of expected charge injection by the dopants.

The flow of LC under the influence of the applied dc field is in fact in the direction corresponding to the direction of expected unipolar charge injection by the dopant if such injection takes place. Net flow of LC in type B cell is observed by following the movement of dust particles. Figure 4 shows an example of microscopic flow patterns with a donor dopant (DBF). As indicated by arrows in the figure, average dust particles move from the backside of the charge injection electrode toward the opposite electrode, travel across the electrode boundary and come back to the starting point by the periphery of the electrodes where the electrical field is weak. The direction of the flow is always from the anode to the cathode when the dopant is a donor and from the cathode to the anode when the dopant is an acceptor. The dopant-dependent flow of LC is confirmed by another independent method using a test cell which is shown schematically in Figure 5. The field is applied across two metal screen electrodes and a net liquid flow in a given direction introduces a pressure which changes the height of the liquid crystal in the capillaries. When voltage is applied to the cell, the LC column is displaced from the anode side to the cathode side when the dopant is an electron donor and vice versa when the dopant is an acceptor. When the dopant is either

a salt or an equimolar mixture of the donor (DBF) and the acceptor (TFM), the displacement is much smaller than previous cases.

The dopant-dependent flow of LC under the influence of the dc field clearly indicates that the electrochemical property of the dopants plays the dominant role in the electrohydrodynamics. The observation is consistent with the charge conduction mechanism (Figure 6a) that when the dopant is an electron acceptor, negative charge injection occurs at the cathode ($A + e \rightarrow A^-$), the charge migrates to the anode in the form of a space charge[11] to be neutralized at the anode ($A^- \rightarrow A + e$) and vice versa when the dopant is a donor (Figure 6b). The LC flow is caused by the flow of ions through it. The alternative mechanisms diagrammed in Figures 6c-f meet the electroneutrality condition but do not explain the net flow of the LC.

When the redox dopant is a mixture of an electron acceptor and a donor, the direction of the net flow of LC depends on relative amounts of each component. Microscopic patterns show that the electrohydrodynamic behavior is a combination of those of an acceptor and a donor rather than those of a salt dopant with a flow line structure. The patterns contain regions of turbulence which are similar to those with an acceptor dopant and regions which are similar to those with a donor dopant (Figure 3). The charge conduction mechanism appears to involve regions where the mechanism shown in Figure 6a operates and other regions where the mechanism shown in Figure 6b operates.

These two different regions are randomly distributed throughout the conduction area.

When the dopant is a salt, the charge conduction mechanism is probably as shown in Figure 7a. The LC components are reduced at the cathode to give a radical anion ($LC + e \rightarrow LC^-$) and oxidized at the anode to give a radical cation ($LC \rightarrow LC^+ + e$) At the same time, channels of cation and anion space charge regions are formed during the charge migrations to the opposite electrodes and the charge is neutralized at the opposite electrodes by reverse reactions. An alternate mechanism (Figure 7b) which includes a reaction of the cation and anion in the bulk of LC does not explain the flow lines of LC which are observed with the salt dopant.

The microscopic patterns shown in Figures 2 and 3 (no scattering is observed with salt dopants at 30 V and 40 V, respectively) indicate that the redox dopants give lower threshold voltage of DS than the salt dopants. Turbulent patterns of LC with redox dopants also indicate the same dopants will cause higher scattering of light than the line structure of LC with salt dopants. These observations are consistent with the observations[6] in a conventional 13 μm thick display cell in which the LC is sandwiched between two flat transparent electrodes.

Our observations[6] of long dc operational lifetimes of LC with redox dopants as compared to short lifetimes with salt dopants are also consistent with the present charge conduction

mechanism. The short operational lifetime with a salt dopant is probably due to the formation of LC radical ions which are unstable, while in the presence of redox dopants such LC radical ions are not formed.

Conclusions

1. Discretely different dc-activated hydrodynamic instabilities are observed with a redox dopant than with a salt dopant in the same ester liquid crystal. At voltages just above the threshold the liquid crystal with salt dopants shows a flow pattern with periodically arrayed flow channels, while the liquid crystal with redox dopants shows turbulence motion.

2. The direction of liquid crystal flow during dc dynamic scattering depends on the electrochemical property of the redox dopants.

3. The electrochemical properties of the liquid crystal compounds and redox dopants, and the direction of liquid crystal flow are consistent with a charge transport mechanism involving unipolar injection. Positive charge is injected by electrochemical reaction of dopants at the anode when the dopant is a donor, and negative charge is injected at the cathode when the dopant is an acceptor, to form a space charge. The space charge migrates to the opposite electrode to be neutrallized by the reverse electrochemical reaction.

4. When the dopant is a redox-type, dynamic scattering appears to be initiated and localized (at low voltages) at the opposite electrode of charge injection.

5. The higher dc scattering levels[6] of the present liquid crystal with redox dopants than with salt dopants appear to be due to the distinctively different hydrodynamic instability patterns.

Acknowledgment

We are indebted to the Directorate of Chemical Sciences, Air Force Office of Scientific Research, Contract F44620-72-C-0075 for partial financial support of this research. We also wish to thank Mr. Michael J. Little for helpful discussions on the experimental setup and Dr. Leroy J. Miller and Mr. John E. Jensen for the synthesis of the liquid crystal materials.

References

1. G. H. Heilmeier, L. A. Zanoni, and L. A. Baron, IEEE Trans. Elec. Dev., ED-17, 22 (1970).
2. R. chang, in "Liquid Crystals and Ordered Fluids," Vol. 2, J. F. Johnson and R. S. Porter, Editors, p. 367, Plenum Publishing Corp. (1974).
3. M. I. Barnik, L. M. Blinov, M. F. Grebenkin, S. A. Pikin, and V. G. Chigrinov, Phys. Lett., 51A, 175 (1975); Zh. Eksp. Teor. Fiz., 69, 1080 (1975).
4. J. D. Margerum, H. S. Lim, P. O. Braatz, and A. M. Lackner, Sixth International Liquid Crystal Conf., Kent, Ohio, August 1976.
5. A. I. Baise, J. Teucher, and M. M. Labes, Appl. Phys. Lett., 21, 142 (1972).
6. H. S. Lim and J. D. Margerum, Appl. Phys. Lett., 28, 478 (1976).
7. Y. Ohnishi and M. Ozutsumi, Appl. Phys. Lett., 24, 213 (1974).
8. S. Barret, F. Gaspard, R. Hernio, and F. Mondon, J. Appl. Phys., 47, 2375 (1976).
9. H. S. Lim and J. D. Margerum, J. Electrochem. Soc., 123, 837 (1976).
10. G. H. Heilmeier, L. A. Zanoni, and L. A. Barton, Proc. IEEE, 56, 1162 (1968).
11. J. C. Lacroix and R. Tobazeon, Appl. Phys. Lett., 20, 251 (1972).
12. K. Rousseau, G. C. Farrington, and D. Dolphin, J. Org. Chem., 3968 (1972).

13. A. Lomax, R. Hirasawa, and A. J. Bard, J. Electrochem. Soc., 119, 1679 (1972).

14. A. Denat and B. Gosse, Chem. Phys. Lett., 22, 91 (1973).

15. R. chang, J. Appl. Phys., 44, 1885 (1973).

16. P. A. Penz, Phys. Rev. Lett., 24, 1405 (1970); Phys. Rev. A, 10, 1300 (1974).

Figure Captions

Fig. 1. Schematic drawings of test cells.

Fig. 2. Photographs of the microscopic patterns of DS using type A cells. Crossed polarizers are used with one polarizer parallel to the direction of LC alignment. d = 51 μm.
(A) 0.03%, $\rho \sim 4 \times 10^8$ Ω-cm; (B) saturacted, $\rho \sim 10^{10}$ Ω-cm; (C) 0.5%, $\rho \sim 10^{10}$ Ω-cm; and (D) 1%, $\rho \sim 10^{10}$ Ω-cm.

Fig. 3. Photographs of the microscopic patterns of DS using type B cells. Crossed polarizers are used with one polarizer parallel to the direction of LC alignment. d = 51 μm.
0.02% TBAP, $\rho \sim 2 \times 10^9$ Ω-cm; 0.2% TFM, $\rho \sim 10^{10}$ Ω-cm; saturated TCNQ, $\rho \sim 10^{10}$ Ω-cm; 0.5% TTF, $\rho \sim 9 \times 10^{10}$ Ω-cm; 0.2% DBF, $\rho \sim 10^{10}$ Ω-cm; and 0.1% DBF-TFM, $\rho \sim 10^{10}$ Ω-cm.

Fig. 4. Flow pattern of LC in a type B cell.

Fig. 5. Liquid crystal flow detection cell.

Fig. 6. Charge conduction mechanisms through LC when the dopant is a redox type.

Fig. 7. Charge conduction mechanisms through LC when the dopant is a salt.

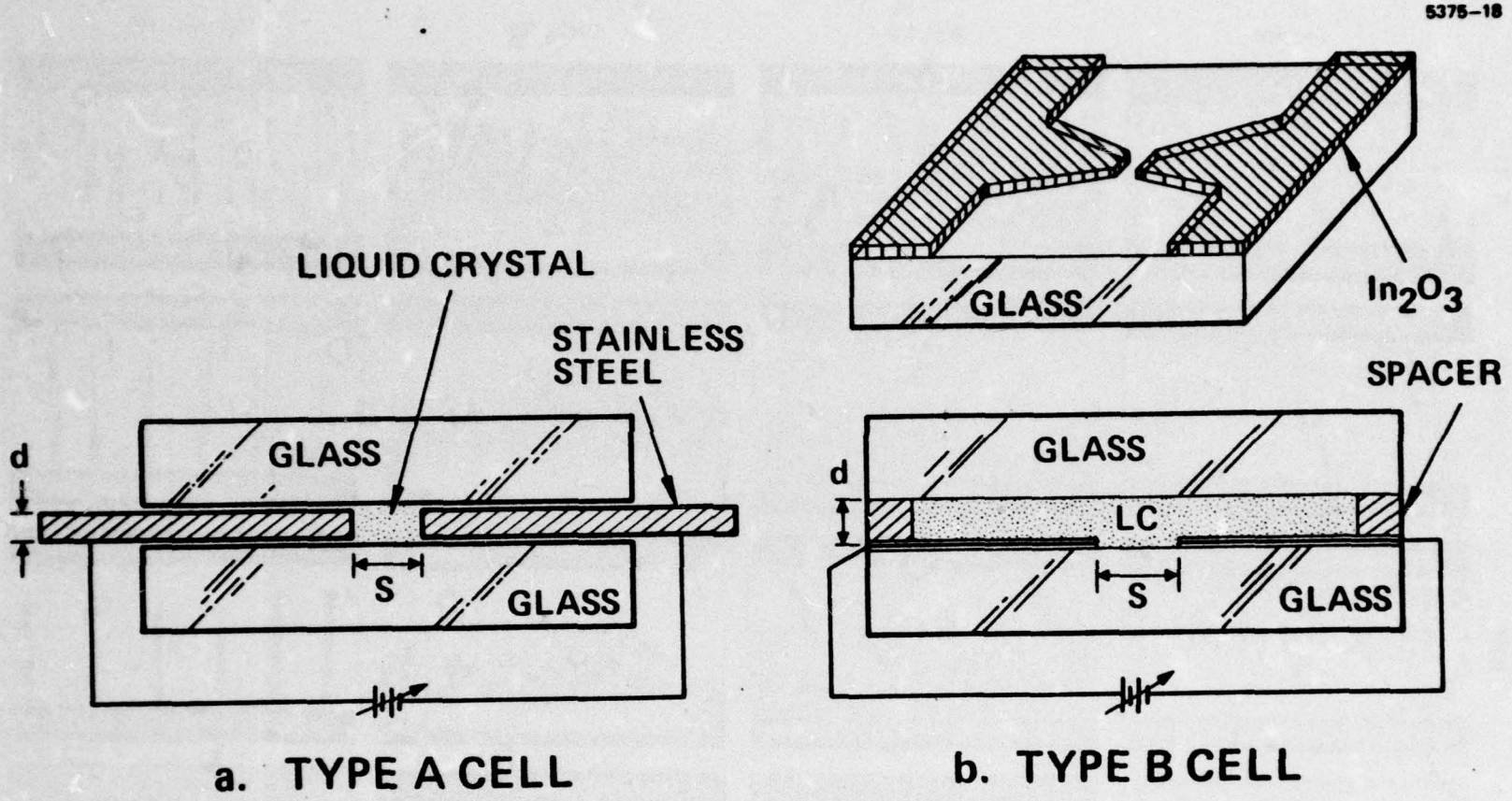

Fig. 1. Schematic drawings of test cells.

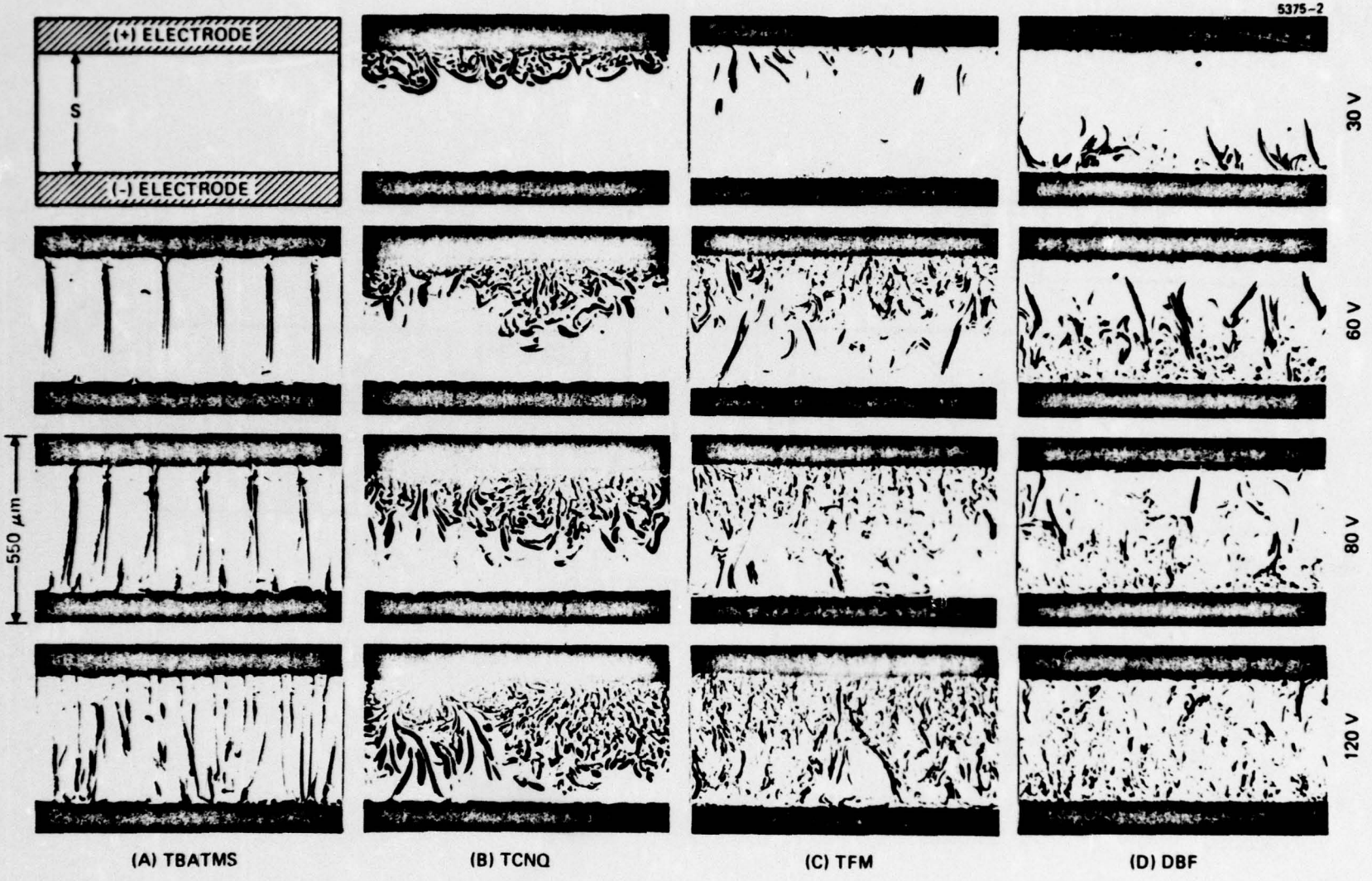

Fig. 2. Photographs of the microscopic patterns of DS using type A cells. Crossed polarizers are used with one polarizer parallel to the direction of LC alignment. D = 51 µm. (A) 0.03%, $\rho \sim 4 \times 10^8$ Ω-cm; (B) saturated, $\rho \sim 10^{10}$ Ω-cm; (C) 0.5%, $\rho \sim 10^{10}$ Ω-cm; and (D) 1%, $\rho \sim 10^{10}$ Ω-cm.

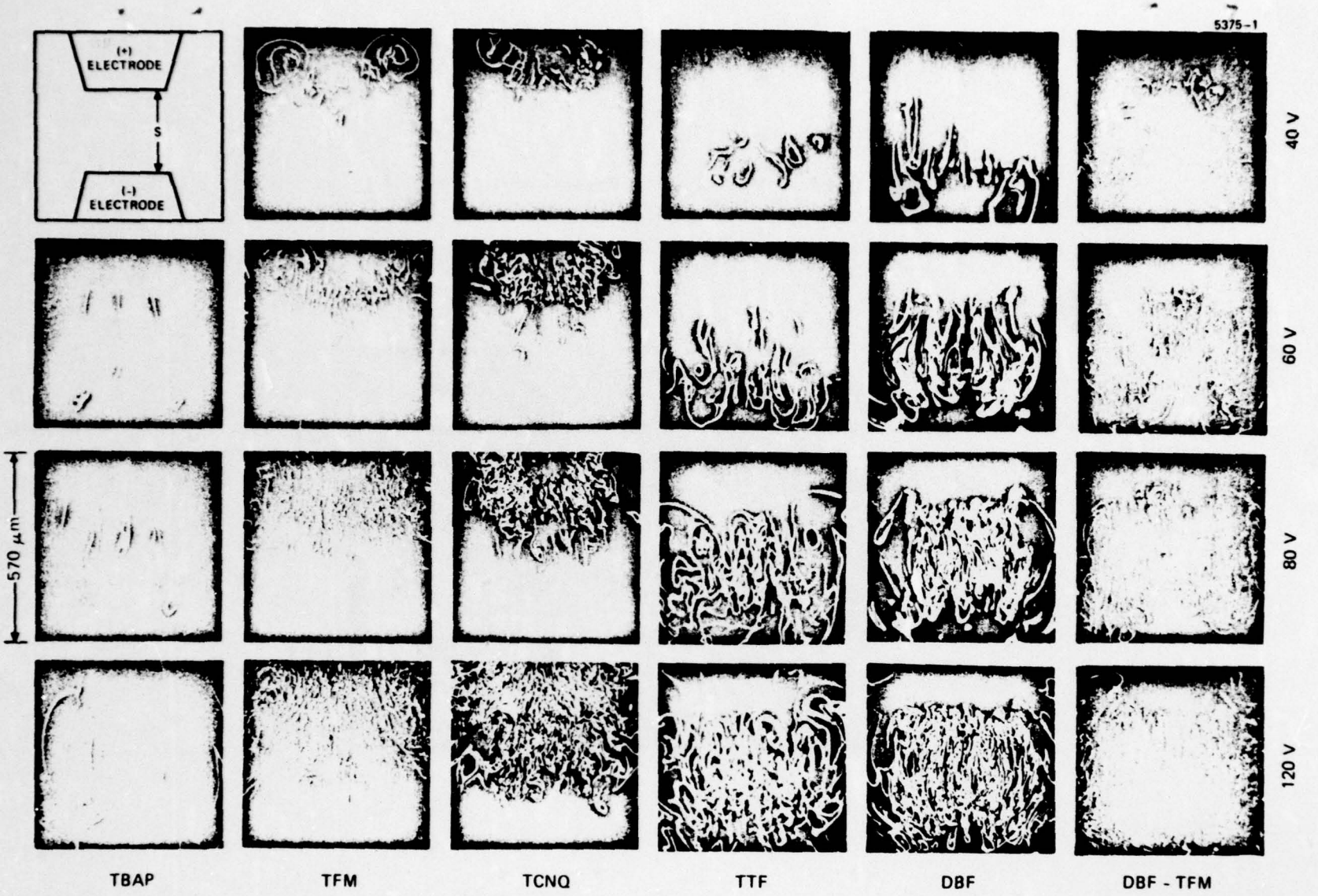

Fig. 3. Photographs of the microscopic patterns of DS using type B cells. Crossed polarizers are used with one polarizer parallel to the direction of LC alignment. d = 51 μm. 0.02% TBAP, $\rho \sim 2 \times 10^9$ Ω-cm; 0.2% TFM, $\rho \sim 10^{10}$ Ω-cm; saturated TCNQ, $\rho \sim 10^{10}$ Ω-cm; 0.5% TTF, $\rho \sim 9 \times 10^{10}$ Ω-cm; 0.2% DBF, $\rho \sim 10^{10}$ Ω-cm; and 0.1% DBF-TFM, $\rho \sim 10^{10}$ Ω-cm.

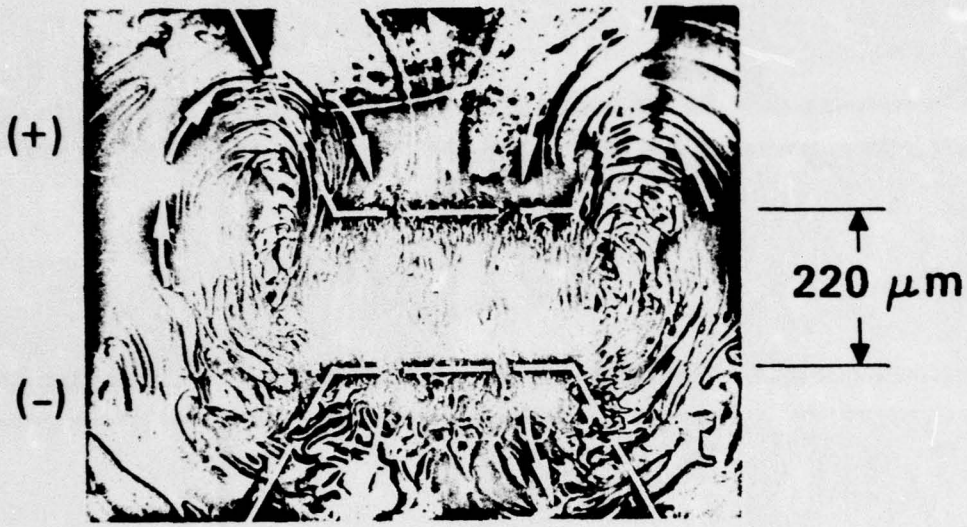

Fig. 4. Flow pattern of LC in a type B cell.

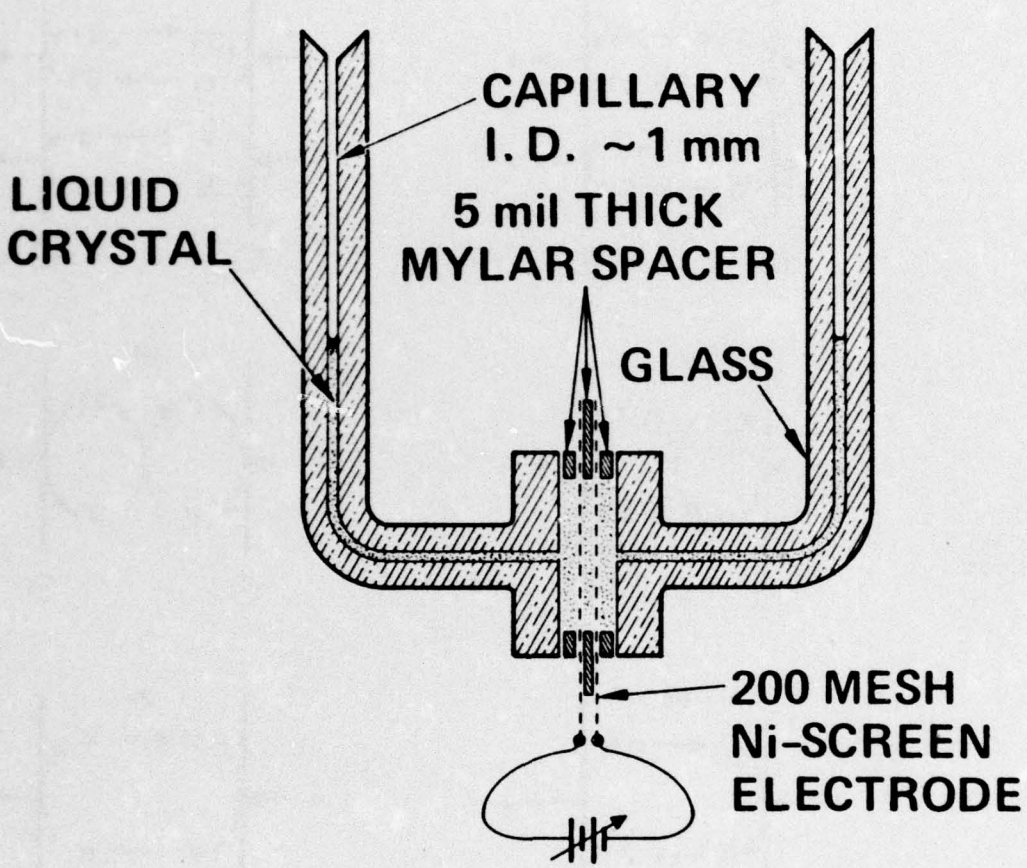

Fig. 5. Liquid crystal flow detection cell.

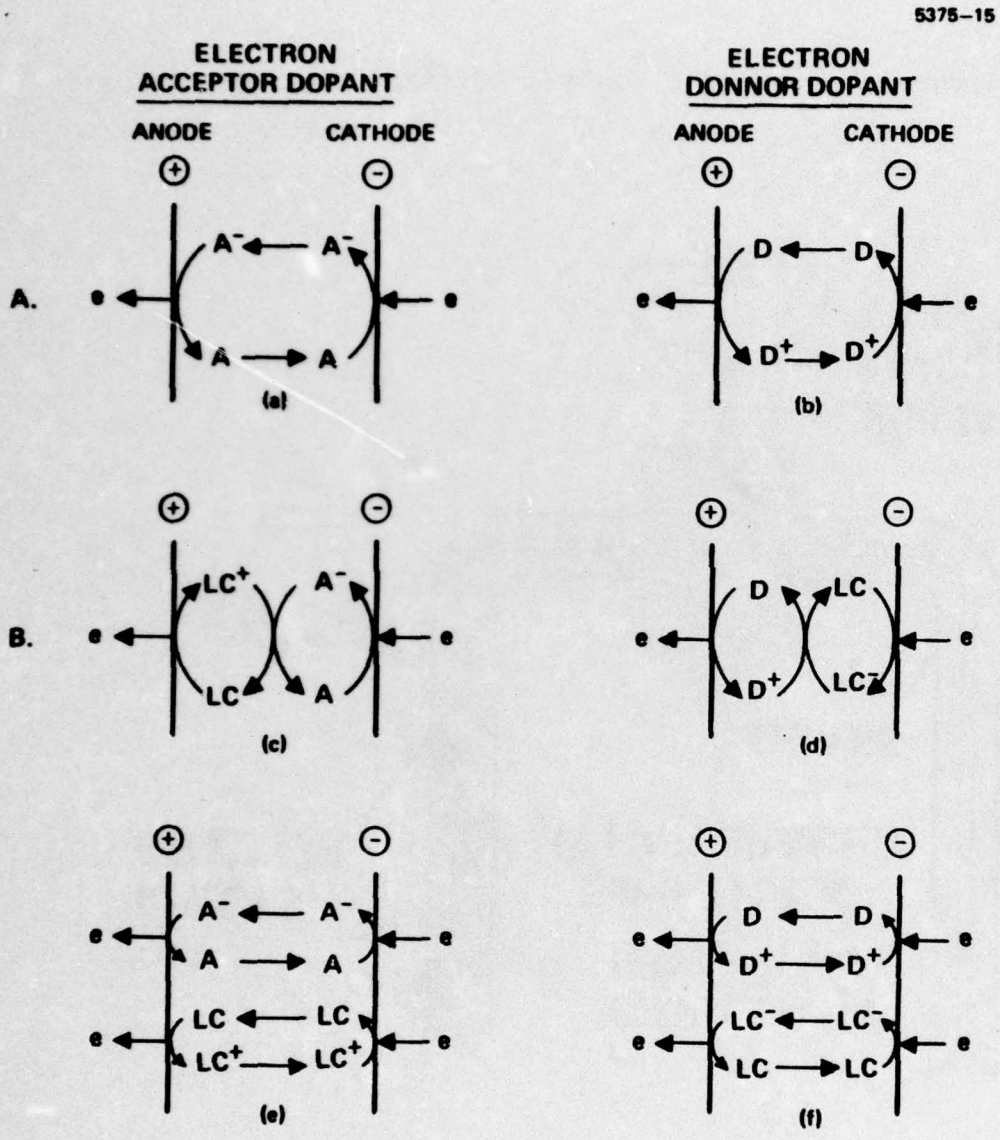

Fig. 6. Charge conduction mechanisms through LC when the dopant is a redox type.

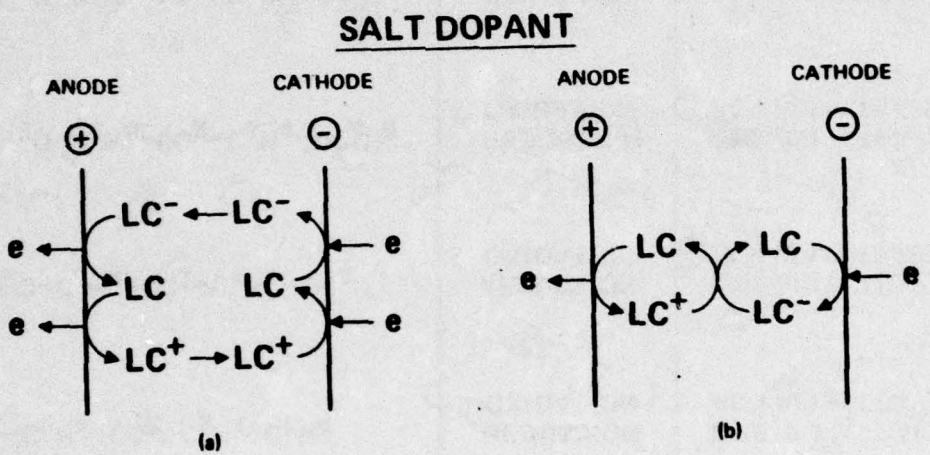

Fig. 7. Charge conduction mechanisms through LC when the dopant is a salt.

Table I. Decomposition potentials for liquid crystal components.

5375-12

COMPOUNDS	REACTION	SOLVENTS[a]	POTENTIALS* V versus S C E
p–CH_3–C_6H_4–CO_2–C_6H_4–C_4H_9	REDUCTION OXIDATION	DMF (0.1 M TBAP) ACN (0.1 M TBAP)	–2.2 +2.0
p–C_4H_9O–C_6H_4–CO_2–C_6H_4–OC_4H_9	REDUCTION OXIDATION	DMF (0.1 M TBAP) ACN (0.1 M TBAP)	–2.3 +1.7
p–$C_6H_{13}O$–C_6H_4–CO_2–C_6H_4–OC_4H_9	REDUCTION OXIDATION	DMF (0.1 M TBAP) ACN (0.1 M TBAP)	–2.3 +1.7
p–$C_8H_{17}O$–C_6H_4–CO_2–C_6H_4–OC_4H_9	REDUCTION OXIDATION	DMF (0.1 M TBAP) ACN (0.1 M TBAP)	–2.3 +1.7

*PEAK POTENTIALS BY CYCLIC VOLTAMMETRY

Table II. Formal reduction potentials of dopants.

5375-13

REDOX COUPLES	SOLVENTS	POTENTIALS V versus S C E
$TTF^{+} + e = TTF$	ACN (0.1 M TBAP)	+0.30
$DBF^{+} + e = DBF$	ACN (0.1 M TBAP)	+0.32
$TFM + e = TFM\cdot^{-}$	ACN (0.1 M TBAP)	+0.03
$TCNQ + e = TCNQ\cdot^{-}$	ACN (0.1 M TBAP)	+0.20
	ACN (0.1 M TEAP*)	+0.19‡

*TETRAETHYLAMMONIUM PERCHLORATE

‡C.K. Mann and K.K. Barnes, "Electrochemical Reactions in Nonaqueous Systems," Marcel Dekker Inc., N.Y. 1970, pp. 335–343.